Understanding bainite formation in steels

Ravi, Ashwath

DOI
10.4233/uuid:d3bc68cd-76de-4d5c-b6b4-c739e36323ae

Publication date
2019

Document Version
Final published version

Citation (APA)
Ravi, A. (2019). *Understanding bainite formation in steels*. [Dissertation (TU Delft), Delft University of Technology]. https://doi.org/10.4233/uuid:d3bc68cd-76de-4d5c-b6b4-c739e36323ae

Understanding bainite formation in steels

Understanding bainite formation in steels

Proefschrift

ter verkrijging van de graad van doctor
aan de Technische Universiteit Delft,
op gezag van de Rector Magnificus prof. dr. ir. T.H.J.J. van der Hagen,
voorzitter van het College voor Promoties,
in het openbaar te verdedigen op
woensdag 16 oktober 2019 om 10:00 uur

door

Ashwath Maniam RAVI

Master of Science,
Universidade de Aveiro, Portugal,
geboren te Palo Alto, Verenigde Staten van Amerika

Dit proefschrift is goedgekeurd door de

Promotoren:	Prof. dr. M.J. Santofimia
	Prof. dr. ir. J. Sietsma

Samenstelling promotiecommissie bestaat uit:

Rector Magnificus,	voorzitter
Prof. dr. M.J. Santofimia,	Technische Universiteit Delft, *promotor*
Prof. dr. ir. J. Sietsma,	Technische Universiteit Delft, *promotor*
Onafhankelijke leden:	
Prof. dr. A. Borgenstam,	Kungliga Tekniska högskolan, Zweden
Prof. dr. S. Godet,	Université libre de Bruxelles, België
Dr. M.C. Somani,	Oulun yliopisto, Finland
Dr. S.M.C. van Bohemen,	TATA Steel, Nederland
Prof. dr. ir. L.A.I. Kestens,	Technische Universiteit Delft
Prof. dr. ir. J.L. Herder,	Technische Universiteit Delft, *reservelid*

Keywords: Steel; Bainite; Kinetics; Nucleation; Heat treatments

Printed by: Ipskamp Printing

Front & Back: Designed by Ashwath

ISBN 978-94-028-1712-6

An electronic version of this dissertation is available at
`http://repository.tudelft.nl/`.

To the most important people in my life

Contents

Summary

Bainite formation is one of the most interesting and scientifically challenging puzzles in the field of steel metallurgy. The complexity of austenite to bainite transformation mechanism has piqued the interest of many researchers. Bainite is a key microstructural constituent in several modern day advanced high strength steels. With the growing importance of advanced high strength steels in the recent years to cater towards the material needs of our society, in terms of a better fuel economy and lower CO_2 emission, the pursuit of understanding the fundamentals of bainite formation in steels has further intensified. This societal relevance combined with the scientific challenges in understanding the mechanism of bainite formation serves as the motivation for this doctoral thesis.

Currently, two competing theories have been proposed by the scientific community regarding the mechanism of bainite formation. One theory suggests that the bainite growth occurs via diffusionless and displacive mechanism where the rate of bainite formation is determined by the nucleation rate of individual bainitic sub-units. The other theory argues that bainite growth is a diffusional process where the rate of bainite formation is controlled by the diffusion kinetics of carbon from bainite into austenite. In this work, the kinetics of bainite formation is investigated and analysed in detail based on the former theory. According to this theory, bainite formation in steels begins at pre-existing interfaces such as austenite grain boundaries. Nucleation and growth of bainitic sub-units at these interfaces lead to new bainite/austenite interfaces. Bainite formation continues via further nucleation of new bainitic sub-units at the these interfaces, resulting in the overall bainite microstructure. The fundamental theme of the research activities carried out in this work is to understand the underlying physical factors which influence bainite nucleation. These studies not only provide insight into the kinetics of bainite formation but also aim to understand the strengths and weaknesses of the nucleation based theory on bainite formation.

The rate of bainite formation in steels at any given moment in time is mainly dependent on the surrounding austenite fraction as well as on the nature of the interfaces present within the austenite matrix. As bainite formation progresses, the nature of the residual austenite surrounding the bainite changes due to variation in several parameters such as carbon content of the austenite, density of available interfaces within the austenite matrix for bainite nucleation, volume fraction of austenite and the dislocation density near the bainite/austenite interfaces. In this work, a novel physically-based approach, which accounts for the variation of these parameters, is developed to describe the kinetics of bainite formation (see Chapter 3). The kinetic description is validated using experimentally obtained kinetic data. In addition to understanding the instantaneous rate of bainite formation as a function of bainite evolution, the effect of martensite/austenite interfaces (in Chapter

4), ferrite/austenite interfaces (in Chapter 5) and cementite/austenite interfaces (in Chapter 6) on the rate of bainite formation is studied with the help of customised set of heat treatment experiments. Along with austenite grain boundaries, these interfaces can serve as pre-existing interfaces for bainite formation depending on the initial austenite condition. The experiments are carried out in a dilatometer and the resulting microstructures are characterised using optical microscopy and scanning electron microscopy. Additionally, in Chapter 5, electron back scatter diffraction studies and atom probe tomography experiments are used to further understand the influence of ferrite/austenite interfaces on bainite formation.

Based on the results obtained from these studies, several conclusions regarding the mechanism and kinetics of bainite formation (discussed in detail in Chapter 7) can be derived. Firstly, the overall rate of bainite formation can be described in terms of the sum of the rate of bainite formation as a result of bainite nucleation at pre-existing interfaces and the rate of bainite formation due to nucleation at bainite/austenite interfaces. The mechanisms of bainite formation at either of these interfaces are similar although the activation energy for bainite nucleation is dependent on the interface at which the nucleation occurs. Secondly, studies reveal that the progress of bainite formation within the austenite matrix becomes increasingly slow as the bainite fraction increases, due to an increase in the activation energy for bainite nucleation at bainite/austenite interfaces. These results highlight the importance of understanding the role of interfaces during bainite formation. Furthermore, studies related to the effect of pre-existing interfaces on the rate of bainite formation show that the overall time required for bainite formation depends heavily on the rate of bainite nucleation at the pre-existing interfaces. Experimental results suggest that, depending on the type of interfaces available prior to bainite formation, the time required for the bainite formation to begin as well as the instantaneous rate of bainite formation as a function of bainite evolution can be controlled.

The results obtained in this doctoral thesis provide significant insight into the effect of various parameters which control the rate of bainite formation in steels. Furthermore, based on the comparison of the experimental results with the mechanism of bainite formation as suggested by the diffusionless and displacive theory, it is observed that the kinetics of bainite formation can be described well using this theory. However, certain factors related to the cessation of bainite growth and limitation of bainite nucleation, such as stored energy and carbon redistribution during bainite formation, are yet to be understood completely. Thus, developing a predictive kinetic model to describe bainite formation kinetics based on the diffusionless and displacive mechanism still remains an open issue. However, the results obtained in this work contribute to the basic physical description of such a model and thus add to the groundwork laid down in the quest to unravel the mystery behind the mechanism of bainite formation. From a technological perspective, the results also open up new avenues for designing efficient heat treatment routes for the development of multi-phase advanced high strength steels involving bainitic microstructures.

Samenvatting

Bainietformatie is een van de meest interessante en wetenschappelijk uitdagende puzzels op het gebied van staalmetallurgie. De complexiteit van het transformatiemechanisme van austeniet naar bainiet heeft de interesse van veel onderzoekers gewekt. Bainiet is een belangrijk microstructureel bestanddeel in verschillende moderne geavanceerde hoogsterkte staalsoorten. Met het groeiende belang van geavanceerde hoogsterkte staalsoorten in de afgelopen jaren om tegemoet te komen aan de materiële behoeften van onze samenleving, in termen van een beter energiezuinigheid en een lagere CO_2-uitstoot, is het streven naar een beter begrip van de fundamenten van de bainietvorming in staal verder toegenomen. Deze maatschappelijke relevantie in combinatie met de wetenschappelijke uitdagingen in het begrijpen van het mechanisme van bainietvorming vormt de motivatie voor deze promotiethesis.

Momenteel zijn er twee concurrerende theorieën voorgesteld door de wetenschappelijke gemeenschap met betrekking tot het mechanisme van bainietvorming. Eén theorie suggereert dat de groei van bainiet gebeurt via een diffusievrij en displacive mechanisme waarbij de snelheid van bainietvorming wordt bepaald door de nucleatiesnelheid van individuele bainitaire subeenheden. De andere theorie stelt dat bainietgroei een diffusieproces is waarbij de snelheid van bainietvorming wordt gecontroleerd door de diffusiekinetiek van koolstof van bainiet naar austeniet. In dit werk wordt de kinetiek van bainietvorming in detail onderzocht en geanalyseerd op basis van de eerste theorie. Volgens deze theorie begint bainietvorming in staal bij reeds bestaande interfaces zoals austenietkorrelgrenzen. Nucleatie en groei van bainitaire subeenheden bij deze interfaces leiden tot nieuwe bainiet/austeniet interfaces. De vorming van bainiet gaat door via verdere nucleatie van nieuwe bainitaire subeenheden bij deze interfaces, wat resulteert in de algemene bainietmicrostructuur. Het fundamentele thema van de onderzoeksactiviteiten die in dit werk worden uitgevoerd, is het begrijpen van de onderliggende fysische factoren die de bainietnucleatie beïnvloeden. Deze studies geven niet alleen inzicht in de kinetiek van bainietvorming, maar ook in de sterke en zwakke punten van de nucleatie gebaseerde theorie over bainietvorming.

De snelheid van bainietvorming in staal op een bepaald moment in de tijd is voornamelijk afhankelijk van de omringende austenietfractie en de aard van de interfaces die aanwezig zijn in de austenietmatrix. Naarmate de bainietvorming vordert, verandert de aard van het resterende austeniet rond het bainiet door variatie in verschillende parameters zoals het koolstofgehalte van het austeniet, de dichtheid van de beschikbare interfaces binnen de austenietmatrix voor bainietnucleutatie, de volumefractie van austeniet en de dislocatiedichtheid in de buurt van de bainiet/austeniet interfaces. In dit werk wordt een nieuwe fysisch-gebaseerde benadering, die rekening houdt met de variatie van deze parameters, ontwikkeld om de kinetiek van bainietvorming te beschrijven (zie Hoofdstuk 3). De kinetische

beschrijving wordt gevalideerd met behulp van experimenteel verkregen kinetische gegevens. Naast inzicht in de momentane snelheid van bainietvorming als functie van de evolutie van bainiet, wordt het effect van martensiet/austeniet interfaces (in Hoofdstuk 4), ferriet/austeniet interfaces (in Hoofdstuk 5) en cementiet/austeniet interfaces (in Hoofdstuk 5) op de snelheid van bainietvorming bestudeerd met behulp van warmtebehandelingsexperimenten op maat. Samen met austenietkorrelbegrenzingen kunnen deze interfaces dienen als reeds bestaande interfaces voor bainietvorming, afhankelijk van de initiële austenietconditie. De experimenten worden uitgevoerd in een dilatometer en de resulterende microstructuren worden gekarakteriseerd met behulp van optische microscopie en scanning elektronenmicroscopie. Daarnaast worden in Hoofdstuk 5, electron back scatter diffractie studies en atoom sondetomografie experimenten gebruikt om de invloed van ferriet/austeniet interfaces op de vorming van bainiet verder te begrijpen.

Op basis van de resultaten van deze studies kunnen verschillende conclusies worden getrokken met betrekking tot het mechanisme en de kinetica van bainietvorming (in detail besproken in Hoofdstuk 7). Ten eerste kan de algemene snelheid van bainietvorming worden beschreven in termen van de som van de snelheid van bainietvorming als gevolg van bainietnucleutatie bij bestaande interfaces en de snelheid van bainietvorming als gevolg van nucleatie bij bainiet/austeniet interfaces. De mechanismen van bainietvorming bij een van deze interfaces zijn vergelijkbaar, hoewel de activeringsenergie voor bainietnucleutatie afhankelijk is van de interface waarop de nucleatie optreedt. Ten tweede blijkt uit studies dat de voortgang van de bainietvorming binnen de austenietmatrix steeds langzamer verloopt naarmate de bainietfractie toeneemt, als gevolg van een toename van de activeringsenergie voor bainiet-nucleutatie bij bainiet/austeniet interfaces. Deze resultaten benadrukken het belang van het begrijpen van de rol van interfaces tijdens de vorming van bainiet. Bovendien studies met betrekking tot het effect van reeds bestaande interfaces op de snelheid van bainietvorming tonen aan dat de totale tijd die nodig is voor bainietvorming sterk afhankelijk is van de mate van bainietkernisering op de reeds bestaande interfaces. Experimentele resultaten suggereren dat, afhankelijk van het type interfaces beschikbaar voor de vorming van bainiet, de tijd die nodig is voor de vorming van bainiet om te beginnen, alsmede de momentane snelheid van de vorming van bainiet als functie van de evolutie van bainiet kan worden gecontroleerd.

De resultaten van dit proefschrift geven een belangrijk inzicht in het effect van verschillende parameters die de snelheid van de bainietvorming in staal bepalen. Bovendien, gebaseerd op de vergelijking van de experimentele resultaten met het mechanisme van bainietvorming zoals gesuggereerd door de diffusievrije en displacive theorie, wordt opgemerkt dat de kinetiek van de bainietvorming goed beschreven kan worden met deze theorie. Bepaalde factoren die verband houden met de stopzetting van de groei van bainiet en de beperking van de nucleatie van bainiet, zoals opgeslagen energie en de herverdeling van koolstof tijdens de vorming van bainiet, zijn echter nog niet volledig begrepen. De ontwikkeling van een voorspellend kinetisch model om de kinetiek van de bainietvorming te beschrijven op basis van het diffusievrije en displacive mechanisme blijft dus nog steeds een open vraag. De resultaten van dit werk dragen echter bij tot de fysische basisbeschrijving van een

dergelijk model en dragen zo bij tot de basis van de zoektocht om het mysterie achter het mechanisme van bainietvorming te ontrafelen. Vanuit technologisch oogpunt openen de resultaten ook nieuwe wegen voor het ontwerpen van efficiënte warmtebehandelingsroutes voor de ontwikkeling van meerfasige geavanceerde hoogsterkte staalsoorten met behulp van bainitaire microstructuren.

1

Introduction

Nature and nature's laws lay hid in the night;
God said 'Let Newton be!' and all was light.

Alexander Pope

It did not last: the devil shouting 'Ho.
Let Einstein be!' restore the status quo.

Sir John Collings Squire

1

The curiosity of the human mind to understand nature and utilise its resources has led to several major discoveries and inventions over the course of history. In the 13^{th} century BC, blacksmiths discovered that iron becomes harder when left in charcoal furnaces. The discovery of this carbon infused iron, or commonly referred to as steel, is a seminal moment in time. Since its discovery, steel is the most widely used and the most widely studied material in the world [1]. Today, steel forms the "gold standard" against which many emerging materials are compared. Such overwhelming dominance enjoyed by steels is due to its adaptability [2]. Through their innumerable varieties of microstructures, steels have constantly managed to meet the requirements of the industry from 6^{th} century BC wootz steel in Damascus swords to advanced high strength steels in modern day applications..

However, like for all structural materials, increasing the strength of steel generally decreases its ductility [3]. In the quest to develop increasingly stronger and more ductile steels, scientists are pushing the boundaries of this inverse strength-ductility relationship. Over the years, studies have shown that multi-phase steel microstructures can address this issue [4, 5]. One of the main constituents of such microstructures is bainite [6–9]. Bainite microstructures typically consist of an assembly of bainitic ferrite laths which are separated by untransformed austenite, martensite or cementite [6, 10–12]. The thickness of the bainitic laths depends on the transformation temperature at which bainite forms [13]. Typically, as the transformation temperature decreases, the bainitic laths tend to become finer [11–13]. It is well established in the literature that the grain size refinement in metallic materials can lead to improved strength and toughness combinations [14–16]. The mechanism of bainite formation therefore can lead to very fine grained structures, thereby making bainitic microstructures a popular choice for materials for structural applications [12, 15].

The formation of bainite in steels is one of the most intensely researched topics in the field of metallurgy [6, 17–24]. Despite the importance of bainite among the modern-day steels, even a qualitative theory to explain the bainite formation still remains a subject of controversy due to the complexity of its formation mechanism [10, 11, 20]. Based on the microstructural and kinetic observations, two different “schools of thought” have been put forth to describe bainite formation [20, 25]. One “school of thought” argues that bainite formation is a diffusional process where carbon diffusion from bainitic ferrite into austenite plays an important role in bainite growth [26]. The competing theory suggests that the bainite reaction is a displacive and diffusionless transformation and nucleation of bainitic sub-units occurs via ther-

mally activated migration of pre-existing dislocations [17].

It is evident from the reports in the literature that a fundamental theory to elucidate the mechanism of bainite formation is still evolving. However, with the ever-growing significance of bainite in the field of structural steels, an in-depth understanding of the bainite kinetics is extremely important from an industrial point of view in order to select the right alloy and heat treatment conditions during production. Furthermore, from a scientific perspective, such an understanding would provide valuable insight into the complex bainite formation process.

In this work, the kinetics of bainite formation is studied in detail through the lens of the displacive theory of bainite formation. The research work described in this thesis mainly explores two fundamental and related questions regarding bainite formation and its kinetics.

1. How to describe the overall rate of austenite to bainite transformation kinetics using a physically based approach?

2. How does the rate of bainite formation in steels vary with varying initial austenite conditions?

Different kinetic models have been proposed in the literature to understand the kinetics of bainite formation based on the displacive mechanism. These models are briefly reviewed in Chapter 2. The existing nucleation-kinetics based models developed using the displacive mechanism of bainite formation have illustrated that they can adequately simulate the kinetics of bainite formation. However, these models use several empirical constants to estimate the overall rate of bainite formation [27]. Furthermore, a close examination of the published results suggests that these models still show a certain degree of miscalculation of kinetics.

In this work, a model is proposed to describe the kinetics of isothermal bainite formation by accurately predicting the degree of carbon enrichment of the austenite. The fitting parameters used in this model are physical entities related to nucleation, phase compositions and microstructural dimensions. The proposed model is described in detail in Chapter 3. The model is derived under the assumptions given by the displacive theory of bainite formation and draws inspiration from previously proposed models [28, 29].

The rate of bainite formation depends on the characteristics of the austenite matrix in which the bainite formation occurs. The chemical composition as well as the degree of transformation strain accommodated within the austenite matrix changes with increasing bainite fraction. Using the model proposed in this thesis,

the rate of bainite nucleation can be simulated accounting for the associated changes to the characteristics of the austenite matrix as a function of bainite evolution.

In addition to understanding the effect of the dynamically changing nature of the austenite matrix (during bainite formation) on the kinetics of bainite formation, the effect of the initial austenite condition on the overall rate of bainite formation is also studied in this work. The heat treatment route applied prior to bainite formation affects the characteristics of the austenite matrix available for bainite formation. For instance, the austenite matrix can be partially decomposed into other transformation products such as martensite or ferrite prior to bainite formation, or the austenite grain size can be varied. Studies have shown that the bainite formation in steels can proceed even in the presence of pre-existing martensite and below the M_s temperature of the steel (temperature at which austenite to martensite transformation formation begins) [30–33]. In Chapter 4, the formalism of the proposed kinetic model (in Chapter 3) is used to analyse the experimental results obtained for the kinetics of bainite formation below the M_s temperature. Such an analysis sheds light onto the role of prior martensite during bainite formation.

The effect of initial austenite condition on the rate of bainite nucleation is further analysed in this work using experimental studies. Already published results suggest that interfaces act as potential nucleation sites for bainite nucleation and the density of nucleation sites depends on the area of the interfaces. It must be noted that the partial austenite decomposition into ferrite and cementite before bainite formation leads to ferrite/austenite and cementite/austenite interfaces. In Chapter 5, the effect of ferrite/austenite interfaces on the rate of bainite formation in low-carbon steels is studied using dilatometer and scanning electron microscopy experiments. Additionally, in Chapter 5, electron back scatter diffraction studies and atom probe tomography experiments are used to determine the chemical composition in the vicinity of the austenite grain boundaries prior to bainite formation, aiming to investigate its effect on the rate of subsequent bainite formation in detail. In Chapter 6, the effect of cementite/austenite interfaces on the rate of bainite nucleation and bainite formation is studied using dilatometer experiments and DICTRA simulations in high carbon steels. The results described in Chapter 5 and Chapter 6 regarding the effect of interfaces on the rate of bainite formation can be used to propose strategies to accelerate bainite formation kinetics in steels.

The results obtained from the individual studies reported in this thesis are summarised and visualized in perspective in Chapter 7. The conducted studies provide significant insight into the mechanism of bainite nucleation and bainite formation

in steels. The model proposed in this work to simulate the rate of bainite formation can be used to understand bainite formation kinetics in a wide variety of steels and under different transformation conditions. Furthermore, results obtained can be exploited to design customised heat treatments in order to control the bainite formation in steels. In addition to these results, the displacive theory of bainite formation in its current form is critically analysed for its strengths and weaknesses in Chapter 7. Based on the combined results of this study, new lines of investigations are proposed in order to develop further in-depth understanding of the complex mechanism of bainite formation.

1

References

[1] J. Dossett, H. Boyer, *Practical Heat Treating* (A S M International, 2006).

[2] H. Bhadeshia, R. Honeycombe, *Steels: Microstructure and Properties* (Elsevier Ltd., 2006).

[3] H. Springer, M. Belde, D. Raabe, *Materials Science and Engineering: A* **582**, 235 (2013).

[4] J. Speer, F. Rizzo, D. Matlock, D. Edmonds, *Materials Research* **8**, 417 (2005).

[5] F. Caballero, H. Bhadeshia, K. Mawella, D. Jones, P. Brown, *Materials Science and Technology* **17**, 512 (2001).

[6] H. Bhadeshia, *Bainite in Steels: Transformations, Microstructure and Properties*, Matsci Series (IOM Communications, 2001).

[7] F. Caballero, H. Bhadeshia, *Current Opinion in Solid State and Materials Science* **8**, 251 (2004).

[8] H. Bhadeshia, *Proceedings of the Royal Society of London A: Mathematical, Physical and Engineering Sciences* **466**, 3 (2009).

[9] B. de Cooman, *Current Opinion in Solid State and Materials Science* **8**, 285 (2004).

[10] R. Hehemann, K. Kinsman, H. Aaronson, *Metallurgical Transactions* **3**, 1077 (1972).

[11] I. Timokhina, H. Beladi, X. Xiong, Y. Adachi, P. Hodgson, *Acta Materialia* **59**, 5511 (2011).

[12] C. Garcia-Mateo, F. G. Caballero, *ISIJ International* **45**, 1736 (2005).

[13] S. Singh, H. Bhadeshia, *Materials Science and Engineering: A* **245**, 72 (1998).

[14] R. Song, D. Ponge, D. Raabe, J. Speer, D. Matlock, *Materials Science and Engineering: A* **441**, 1 (2006).

[15] H. Bhadeshia, *Science and Technology of Advanced Materials* **14**, 014202 (2013).

[16] K. Nagai, *Canadian Metallurgical Quarterly* **44**, 187 (2005).

[17] H. Bhadeshia, D. Edmonds, *Acta Metallurgica* **28**, 1265 (1980).

[18] W. Reynolds Jr., H. Aaronson, G. Spanos, *Materials Transactions, JIM* **32**, 737 (1991).

[19] Z.-G. Yang, H.-S. Fang, *Current Opinion in Solid State and Materials Science* **9**, 277 (2005).

[20] L. Fielding, *Materials Science and Technology* **29**, 383 (2013).

[21] F. Caballero, M. Miller, C. Garcia-Mateo, J. Cornide, *Journal of Alloys and Compounds* **577, Supplement 1**, S626 (2013).

[22] H. Chen, S. van der Zwaag, *Acta Materialia* **72**, 1 (2014).

[23] K. Rakha, H. Beladi, I. Timokhina, X. Xiong, S. Kabra, K.-D. Liss, P. Hodgson, *Materials Science and Engineering: A* **589**, 303 (2014).

[24] I. Timokhina, K. Liss, D. Raabe, K. Rakha, H. Beladi, X. Xiong, P. Hodgson, *Journal of Applied Crystallography* **49**, 399 (2016).

[25] H. Chen, K. Zhu, L. Zhao, S. van der Zwaag, *Acta Materialia* **61**, 5458 (2013).

[26] M. Hillert, *Metallurgical and Materials Transactions A* **25**, 1957 (1994).

[27] M. Santofimia, F. Caballero, C. Capdevila, C. Garcia-Mateo, C. de Andres, *Materials Transactions* **47**, 1492 (2006).

[28] S. van Bohemen, J. Sietsma, *International Journal of Materials Research* **99**, 739 (2008).

[29] H. Bhadeshia, *Journal de Physique* **43**, 443 (1982).

[30] H. Vetters, J. Dong, H. Bornas, F. Hoffmann, H.-W. Zoch, *International Journal of Materials Research* **97**, 1432 (2006).

[31] H. Kawata, M. Takahashi, K. Hayashi, N. Sugiura, N. Yoshinaga, *THERMEC 2009* (Trans Tech Publications, 2010), vol. 638 of *Materials Science Forum*, pp. 3307–3312.

[32] A. Navarro-López, J. Sietsma, M. Santofimia, *Metallurgical and Materials Transactions A* **47**, 1028 (2016).

[33] W. Gong, Y. Tomota, S. Harjo, Y. Su, K. Aizawa, *Acta Materialia* **85**, 243 (2015).

2

Background

Both the kinetic and structural results obtained appear inconsistent with a growth model based on a diffusional ledge mechanism.

Bhadeshia and Edmonds, The bainite formation in silicon steel [1]

The authors criticize the inability of the solute drag-like effect to explain the upper/lower bainite and the lower bainite/martensite bays as well. This criticism is, of course, wholly irrelevant.

Liu et al., Discussion of The bainite formation in silicon steel [2]

We note that despite much work on bainite by many investigators, there is no convincing evidence for the existence of superledges in the bainite-austenite interface.

Bhadeshia and Edmonds, Reply to Discussion of The bainite formation in silicon steel [3]

Neither the authors' definition of lower bainite nor the difference, if any, between this definition and that usually accepted seemed clear.

Aaronson et al., Comments on Reply to Discussion of The bainite formation in silicon steel [4]

In summary, we reject the allegations and criticisms raised by Liu et al., and suggest that the conclusions reached in our original paper are correct.

Bhadeshia and Edmonds, Reply to Comments on Reply to 'Discussion of 'The bainite formation in silicon steel [5]

2

Davenport and Bain published their work on "*Transformation of Austenite at Constant Subcritical Temperatures*" [6] in 1930. In their work on austenite decomposition of steel, they identified a microstructure which was an 'acicular, dark etching aggregate'. In earlier articles, Robertson [7] and Hultgren [8] had reported similar microstructures. These microstructures were observed to form at temperatures above the athermal martensite formation temperature (M_s) but below temperatures where pearlite was formed. In recognition to the work done by Bain, these microstructures were later referred to as Bainite [9]. Since then, the research work done in the field of bainite formation is immense. In this chapter, the existing knowledge on the mechanism and kinetics of bainite formation is discussed in depth.

2.1. Microstructural evolution of bainite

The microstructure of bainite mainly consists of sheaves (or plates) of ferrite (typically referred to as bainitic ferrite) intertwined with cementite, retained austenite, or martensite [10]. A detailed Transmission Electron Microscopy (TEM) image depicting various microstructural constituents of a bainitic sheaf is shown in Figure 2.1 [11].

2.1.1. Bainitic ferrite

A bainitic sheaf is composed of a cluster of bainitic ferrite sub-units. The sub-units have a lath or plate morphology [12]. Typically, bainitic sub-units are about 0.2 µm thick and about 10 µm long [13]. It is important to point out that the terms 'bainite' and 'bainitic ferrite' are used interchangeably in this thesis, when referring to nucleation of bainite as well as bainite/austenite (α_b/γ) interfaces. Such an interchangeable use can be also commonly observed in several published works. During austenite to bainite transformation, bainitic sub-units first nucleate at austenite grain boundaries (γ/γ interfaces). This process is referred to as grain-boundary nucleation or grain-boundary bainite nucleation in this thesis. As bainite formation continues, bainitic sub-units nucleate at bainitic ferrite/austenite (α_b/γ) interfaces as well. This process is referred to as autocatalytic nucleation in this thesis since nucleation of bainite at α_b/γ interfaces leads to new α_b/γ interfaces which serve as nucleation sites for further bainite formation.

As mentioned in Chapter 1, two competing theories have been proposed in the literature to describe the mechanism of bainite formation. The displacive and diffusionless mechanism of bainite formation argues that growth of bainitic sub-units is accompanied by shape deformation of the transformed region [14, 15]. In order

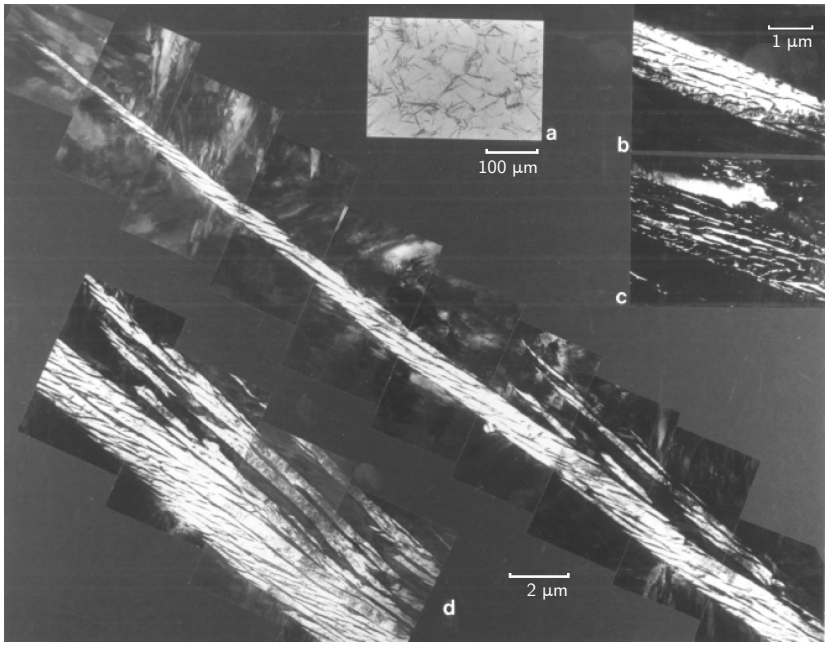

Figure 2.1: TEM image of a sheaf of upper bainite in a partially transformed Fe-0.43C-2Si-3Mn wt% alloy. (a) Light micrograph. (b) Bright field image of retained austenite between sub-units (bright regions - bainite sub-units, dark regions - retained austenite). (c) Dark field image of retained austenite between sub-units (bright regions - retained austenite, dark regions - bainite sub-units; scale similar to image (b)). (d) Montage showing structure of the sheaf (bright regions - bainite sub-units, dark regions - retained austenite). [11]

to minimise the strain energy associated with this shape change, bainitic sub-units adopt a thin lenticular plate-like structure [16]. The strain energy associated with bainite formation is further compensated by the plastic deformation of the surrounding austenite matrix. Atomic force measurements conducted by Swallow and Bhadeshia have pointed out the shape deformation and the plastic relaxation of austenite surrounding the bainitic sub-units [17]. Additionally, TEM studies have confirmed a relatively high dislocation density in the vicinity of α_b/γ interfaces, which can be attributed to the deformation of austenite during bainite growth [18]. Dislocations introduced due to the plastic relaxation of austenite hinder the growth of bainitic ferrite sub-units [13, 19]. This implies that the bainitic growth in the form of sheaves requires additional nucleation events. The displacive theory of bainite formation suggests that bainitic sheaf structure forms through autocatalytic nucleation of new bainitic sub-units at already formed α_b/γ interfaces.

The diffusional theory of bainite formation claims that bainite growth occurs via sympathetic nucleation and diffusional ledge-wise growth. Sympathetic nucleation is defined as "*the nucleation of a precipitate crystal at an interphase boundary of a crystal of the same phase when these crystals differ in composition from their matrix phase throughout the transformation process*" [10]. Such a nucleation mechanism combined with diffusional growth of bainite is considered to be responsible for the fine grain morphology of bainitic microstructures [10, 20]. Experimental evidence suggests that during bainitic growth within the austenite matrix, certain sections of the α_b/γ interfaces are coherent or semi-coherent while other sections are incoherent [15, 21]. Based on the diffusional mechanism of bainite formation, the plate-like growth of bainitic sub-units is attributed to the difference in growth rate between the incoherent interfaces and the coherent or semi-coherent interfaces, while the growth rate is mainly controlled by carbon diffusion [15, 22]. According to this view, the mechanism of bainite formation is considered to be similar to the mechanism of allotriomorphic ferrite formation which occurs at relatively higher temperatures [15, 22].

2.1.2. Cementite precipitation during bainite formation

Bainite formation in steels is accompanied by partitioning of carbon into the surrounding austenite matrix. When the carbon concentration in the austenite matrix exceeds the solubility limit given by the (extrapolated) $\gamma/\gamma + \theta$ phase boundary, cementite (usually indicated as θ) precipitates [11] (See Figure 2.2).

Depending on the bainite formation temperature and the alloy composition, the

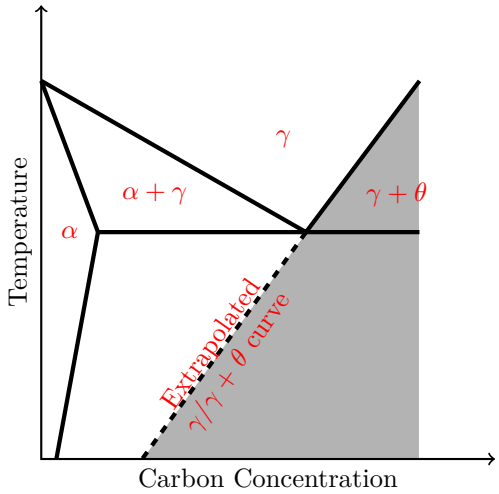

Figure 2.2: Schematic illustration representing the Fe-C phase diagram and the thermodynamic condition necessary for cementite precipitation [11]. The phase diagram indicates the most stable phase(s) at a given temperature and the carbon concentration in these phases. Based on this illustration, it can be seen that cementite precipitation occurs in austenite when the carbon concentration in austenite lies in the shaded region.

nature of the cementite precipitation varies. This results in two different types of bainite microstructures — Upper bainite and Lower bainite [11]. In the case of upper bainite, cementite precipitates in between bainitic ferrite sub-units as continuous or semi-continuous layers. In lower bainite, cementite precipitation occurs within the sub-units as well as between them [10]. Cementite precipitation between bainitic sub-units occurs by a similar process as described above in both upper and lower bainite. In case of lower bainite, cementite precipitation within the bainitic ferrite sub-units is similar to cementite formation during martensite tempering [11].

Cementite layers in upper bainite tend to be coarser than in lower bainite [11]. Upper bainite forms within the temperature range of 550 °C to 400 °C while lower bainite forms within the temperature range of 400 °C to 250 °C [13]. It should be noted that the temperatures mentioned here are typical temperature ranges given in the literature [11]. Actual temperatures at which bainite forms mainly depends on the composition of the steel.

The steel composition also influences kinetics of cementite precipitation during bainite formation. It has been well established that silicon has low solubility in cementite [23, 24]. Evidence suggests that the growth of cementite precipitates during bainite formation occurs under para-equilibrium conditions without the partitioning of substitutional solute atoms [25]. In silicon-containing steels, cementite which

forms under para-equilibrium conditions traps the silicon as it grows. This slows down the kinetics of cementite precipitation from austenite since the resulting free energy change of the reaction is reduced [26]. The cementite can only form with partitioning of silicon which can take a very long time depending on the prevailing thermal conditions [26, 27]. Therefore, in silicon-containing steels, carbon partitioning into austenite along with sluggish cementite precipitation kinetics from austenite results in carbon enrichment of austenite during bainite formation. This increases the stability of the austenite surrounding the bainitic ferrite and these stable austenite regions can be retained at low temperatures. This implies that silicon-containing steels can lead to bainitic ferrite/austenite microstructures with negligible amount of cementite. Such microstructures are typically referred to as carbide-free bainite. Literature reports suggest that aluminium-containing steels can also form similar microstructures [11].

Experimental studies however indicate that silicon does not have the same impact if cementite precipitation occurs within bainitic ferrite sub-units, as would be case in lower bainite [28]. Driving force calculations by Kozeschnik and Bhadeshia for para-equilibrium cementite in ferrite suggest that the rate of cementite precipitation increases as the carbon concentration of ferrite increases [26]. As mentioned earlier, lower bainite mainly forms at relatively low temperatures. Low temperature bainite formation also leads to an increase in the dislocation density of bainitic ferrite. Under such circumstances, the carbon atoms are trapped within the dislocations rather than as cementite precipitates [29]. Annihilation of dislocations leads to release of carbon, which in turn facilitates cementite precipitation that can proceed within the bainitic ferrite regardless of presence of silicon.

2.1.3. Multi-phase bainite/austenite microstructures

Using the knowledge described in Sections 2.1.1 and 2.1.2, researchers have developed an exciting class of steels called Carbide-Free Bainitic (CFB) Steels. Edmonds et al. credit Hehemann and co-workers for developing the silicon containing CFB Steels [24]. Since then, several studies have made use of this concept to design steels which can meet the demands of the industry [24, 30–32].

Like in the case of any material, the properties exhibited by CFB steels is a direct result of its microstructure. The microstructure of these steels is composed of bainitic ferrite plates which are separated by thin films of retained austenite. In some cases, martensite may also be present. As discussed in Section 2.1.1, the ultra-fine nature of bainitic ferrite contributes to increased strength and toughness.

Studies have shown that the thickness of bainitic ferrite subunits can be less than 100 nm [33]. The bainite in such steels is usually formed at very low temperatures (around 200 °C) [34]. Furthermore, the presence of thin films of retained austenite between the ferrite plates retards crack propagation and also toughens the material. Retained austenite also reduces the effect of the penetration of steel by hydrogen [35]. Typical alloying elements of CFB steels include silicon, manganese, aluminium, nickel, chromium, molybdenum and vanadium.

2.2. Bainite growth and incomplete reaction phenomenon

During isothermal treatments in certain steels, the austenite to bainite transformation ceases well before austenite achieves the equilibrium composition as dictated by the phase diagram. Even after extended holding of the steel at the transformation temperature, complete transformation to bainite does not occur and a fraction of austenite remains untransformed [11]. This phenomenon is called the "Incomplete Reaction Phenomenon". Figure 2.3 gives the evolution of bainite fraction as a function of time during isothermal bainite formation treatment in two different steels. Steel 1 (Fe-0.2C-3Mn in wt%) does not show any incomplete reaction phenomenon and the austenite is completely decomposed into bainite during isothermal treatment, while in case of Steel 2 (Fe-0.2C-3Mn-2Si in wt%), the incomplete reaction phenomenon is observed. The three main theories put forth to describe this phenomenon are briefly described below.

2.2.1. T_0 and $T_0^{'}$ theory

One of the theories proposed in the literature to describe the incomplete reaction phenomenon during bainite formation is the T_0 theory. This theory is based on the proposition that austenite to bainite formation in steels is a displacive and diffusionless process. According to this view, the driving force for diffusionless growth of bainite at a particular transformation temperature exists only if the Gibbs free energy of austenite (G_γ) is greater than the Gibbs free energy of (bainitic) ferrite (G_α) for the same composition (Figure 2.4). It must be noted that G_γ decreases with increasing carbon concentration of austenite. As mentioned earlier, bainite formation is accompanied by carbon partitioning and can lead to carbon enrichment of austenite. Under such conditions, the driving force for diffusionless growth of bainite decreases as bainite formation continues. The bainite growth stops when the carbon concentration of austenite is such that G_γ is equal to G_α. In Figure 2.4, the T_0 curve gives the upper limit of the carbon concentration in austenite for a

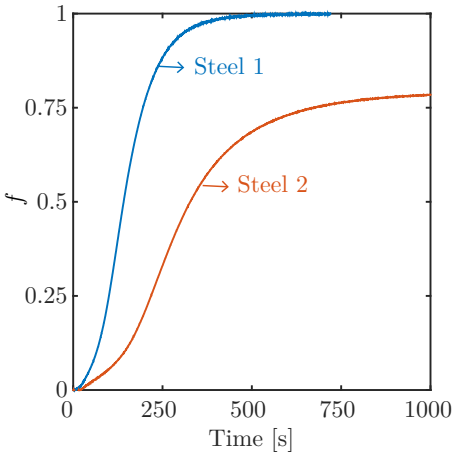

Figure 2.3: Bainite evolution in two different steels during in-house experiments at 380 °C after complete austenitization at 1000 °C for 5 min. The chemical composition of Steel 1 is Fe-0.2C-3Mn (in wt%) and of Steel 2 Fe-0.2C-3Mn-2Si (in wt%). Si containing steels typically shows incomplete reaction phenomenon.

given bainite formation temperature above which the driving force for diffusionless growth of bainite is unavailable ($G_\gamma \leq G_\alpha$). It should be noted that the T_0 curve does not consider the non-chemical free-energy contributions such as interfacial energy and strain energy [16]. Therefore, a modified curve known as the $T_0^{'}$ curve which also accounts for the stored energy due to bainite transformation, usually considered to be about 400 J mol^{-1} [36], was developed based on the studies by Le Houllier et al. [37] as well as Bhadeshia and Edmonds [16] (Figure 2.4). Several studies argue that the $T_0^{'}$ curve gives valuable insight with regard to predictability of bainite transformation [12, 31, 38, 39].

2.2.2. Solute drag theory

Using the principles of the diffusional theory of bainite formation, researchers have proposed the incomplete reaction phenomenon to be a result of a "solute drag-like effect" [40–42]. Substitutional atoms are known to segregate to interfaces during diffusional growth of ferrite and consequently have a drag effect on the grain boundary motion [43]. However, at temperatures at which bainite formation occurs, the diffusion rate of substitutional atoms is extremely sluggish [11]. It must be noted that the rate of bainite growth is mainly controlled by carbon diffusion according to the diffusional theory of bainite formation [22]. Despite the low diffusion rate of substitutional atoms, researchers argue that a "solute drag-like effect" can still

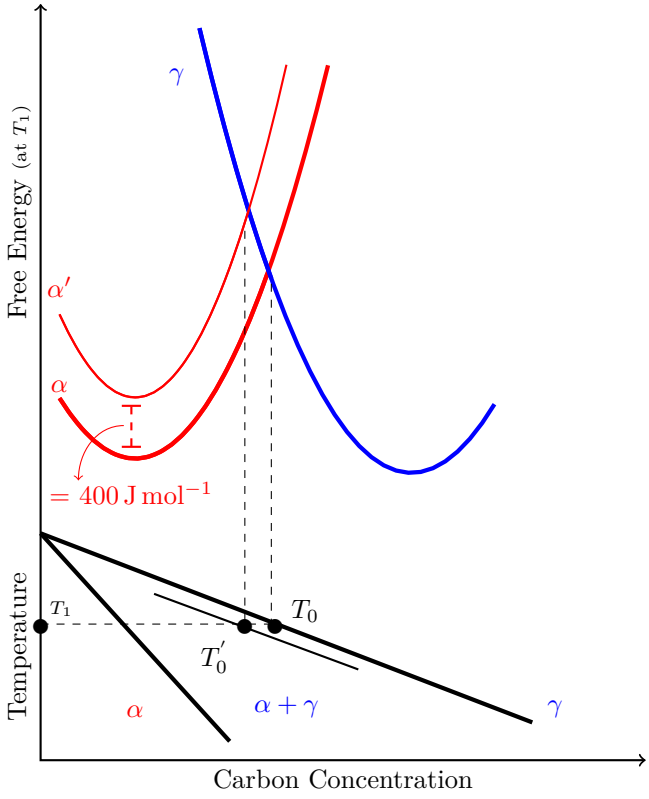

Figure 2.4: Schematic representation of the $T_0^{'}$ theory [11] illustrates that the diffusionless transformation of austenite to bainite at a given temperature can proceed only if the carbon concentration of austenite is below the thermodynamic limit given by the $T_0^{'}$ curve. The top section of the figure shows the variation in Gibbs energy of ferrite (α) and austenite (γ) phases as a function of carbon concentration at a given temperature, T_1. The bottom half of the figure gives a schematic of the phase diagram and the $T_0^{'}$ curve calculated based on the Gibbs energy variation at different temperatures. The stored energy due to bainite formation is typically calculated to be $400\,\mathrm{J\,mol^{-1}}$ [36].

be in play during bainite formation where substitutional atoms with a strong attraction with carbon can decrease the activity of carbon in the austenite in the immediate vicinity of austenite/bainite interfaces, leading to transformation stasis and incomplete reaction phenomenon [40, 42, 44].

Researchers have argued that the incomplete reaction is not a characteristic of all bainite transformations. Reynolds et al. investigated the generality of incomplete transformation to bainite in Fe-C-X (where X = Mn, Si, Ni, or Cu) alloys and carbon content varied between 0.1 wt% and 0.4 wt% [41]. They conclude that the incomplete reaction phenomenon occurs only in Fe-0.1C-Mn steel and not in other steels [41]. They further argue that since the incomplete reaction is only observed in the presence of certain alloying elements, it is a result of a solute drag-like effect due to segregation of these elements (mainly manganese, molybdenum and chromium) [41]. These studies question the validity of the $T_0^{'}$ concept. However, it should be noted that in the experiments conducted by Reynolds et al., carbide precipitation was observed as well [41] which directly influences the carbon concentration of austenite. It must be noted that according to the $T_0^{'}$ concept, the incomplete reaction phenomenon occurs only if carbon concentration of austenite is higher than a certain thermodynamic limit.

Recently, Chen et al. [45, 46] used a new approach called Gibbs Energy Balance (GEB) model which provides a physical understanding of the solute drag effect on the interface mobility and incomplete reaction phenomenon during bainite formation. Gibbs Energy Balance model suggests that the incomplete reaction phenomenon during isothermal bainite formation is marked by the transition of bainitic growth mode from a fast mode to a sluggish mode [45]. At the moment of this transition, the chemical driving force for bainite formation is balanced by the energy dissipated by the segregation of alloying elements to the migrating interfaces [45].

2.2.3. WB_s theory

WB_s theory was proposed by Hillert et al. as a thermodynamic description to define the growth limit of Widmanstatten ferrite and bainitic ferritic. Unlike the $T_0^{'}$ theory and the solute drag theory, WB_s theory does not make any *a priori* assumption regarding the mechanism of bainite formation [47]. Experimental evidence shows that during incomplete bainite formation phenomenon the carbon concentration in the austenite matrix does not reach the equilibrium value as predicted thermodynamically [40]. WB_s theory suggests that this effect is due to acicular growth of bainitic ferrite. Hillert measured the lengthening rate of acicular ferrite in Fe-C

binary alloys and observed that, if the measured lengthening rate is extrapolated to zero velocity, the carbon concentration in austenite matrix is lower than the expected equilibrium concentration [40, 47]. Based on these results, WB_s theory argues that the incomplete reaction phenomenon is a result of the morphology of the bainitic microstructures and the mechanism of bainite growth must be similar to the mechanism of acicular ferrite growth [47].

2.3. Kinetics of bainite formation

Understanding of the kinetics of bainite formation in steels is important for designing efficient heat treatments to develop bainitic microstructures as well as to develop deeper insight into the mechanism of bainite formation [48–53]. The isothermal bainite formation kinetics mainly depends on the composition of the steel and the temperature at which bainite formation occurs [48, 50–52]. Bainite formation in steels can also be affected by the nature of the initial austenite condition [53, 54]. Studies show that one of the strategies to control the rate of bainite formation is through the formation of a small fraction of martensite prior to bainite formation [55–61]. Several reports show that quenching of samples to a temperature below the M_s temperature followed by isothermal holding above the M_s temperature leads to an acceleration of bainite formation when compared to transformation without any martensite formation [55, 57–60]. However, the mechanism behind this acceleration is disputed. Kawata et al. [57] suggest that the acceleration of bainite kinetics is due to the faster nucleation of bainitic sub-units from martensite/austenite interfaces. Vetters et al. [56] argue that the initial pre-quenching alters the conditions within the austenite matrix for easier austenite to bainite transformation. On the other hand, Sourmail and Smanio [62], point out in their study that although the overall heat treatment time for austenite decomposition is reduced, they observe no detectable change in the instantaneous rate of bainite formation due to the presence of martensite.

Studies have also been carried out to understand the effect of prior martensite on isothermal holding below M_s temperatures [56, 63, 64]. Certain literature evidence not only shows that bainite formation can occur during the isothermal holding below the M_s temperature [56, 63, 65] but also that the prior martensite formation can have a strong accelerating effect on bainite formation [56]. However, other studies seem to indicate that the isothermal transformation product during holding below M_s temperature may not be bainite [66, 67].

Experimental studies have also been carried out to understand the effect of prior

ferrite formation on subsequent bainite formation kinetics. Some studies suggest that prior ferrite formation retard any subsequent bainite formation while others suggest that it can stimulate bainite formation [68, 69].

Prior austenite grain size, which is controlled by the austenitization temperature and the austenitization time, is also found to affect the kinetics of bainite formation [52]. However, its effect is debated. Some studies show that decreasing the austenite grain size can accelerate the bainite formation kinetics [11, 70, 71] while other studies show the contrary [72, 73]. Such results have been related to the evolution of bainite microstructures within the austenite grain during bainite formation [74]. Microstructural studies suggest that bainite formation begins at austenite grain boundaries [74]. However, a detailed understanding regarding the exact role of the austenite grain boundaries on bainite nucleation based on experimental evidence is extremely scarce in the current literature.

In summary, available literature suggests that the role of the applied heat treatment prior to bainite formation on the kinetics of austenite to bainite transformation is not yet fully understood, especially if partial austenite decomposition occurs prior to bainite formation. Such an understanding is vital for multiple reasons:

- for a deeper qualitative insight into various factors affecting bainite formation.
- to design new and efficient heat treatment routes for accelerated bainite formation in steels.
- to (eventually) design a predictive tool to evaluate the evolution of bainite formation based on the applied heat treatment in multi-phase steels.

2.3.1. Nucleation kinetics based models

Using the observed experimental results, both “schools of thought” (the displacive and diffusionless approach as well as the diffusional approach) have proposed different models to predict the transformation kinetics based on their own assumptions of bainite formation [49, 51, 69, 75–78].

Santofimia et al. [39] reviewed and evaluated several kinetic models which are based on the displacive theory of bainite transformation. Their review provides an insight into the framework of various kinetic models. With the help of their review as well as by analysing additional various models, it can be identified that most of the existing models which assume a displacive mechanism for bainite formation share several common features. These features are discussed below.

1. The time required for nucleation of bainitic ferrite is considered to be much longer than the time for its growth. Therefore, bainite formation is mainly controlled by the rate at which successive nucleation events take place. The rate of bainite formation is directly proportional to the nucleation rate. Santofimia et al. [39] commented that the models mostly vary only in the manner in which the nucleation rate is calculated. According to the original overall transformation kinetics theory for bainite formation developed by Bhadeshia [48], the nucleation rate of bainite, $\mathrm{d}N/\mathrm{d}t$, can be expressed in the form of

$$\frac{\mathrm{d}N}{\mathrm{d}t} = N_{T_h} \exp\left(\frac{-Q}{kT}\right) \tag{2.1}$$

where N_{T_h} is a pre-exponential factor, Q is the activation energy for bainite nucleation, k is the Boltzmann constant and T is the transformation temperature. Equation 2.1 has been used as the basis for the calculation of nucleation rate by most nucleation-based models to express the bainite kinetics [39, 51, 75–78]. However, Van Bohemen and Sietsma pointed out that the pre-exponential factor used in the calculation of nucleation is usually treated as an empirical constant rather than as a physical parameter [77]. The use of empirical constants could lead to improper calculation of the nucleation rate [77].

2. The displacive mechanism of bainite nucleation suggests that the initial formation of bainite leads to an increase in the density of nucleation sites. This is the effect of autocatalysis. This autocatalytic nucleation is accounted for using an autocatalytic parameter [75, 77, 78]. This parameter is analogous to the autocatalytic factor used to describe the kinetics of isothermal martensite transformation [79–81]. The autocatalytic parameter is an empirical dimensionless coefficient [75, 76]. Also, the physical significance of the values obtained for the autocatalytic parameter is still unclear. In their review, Santofimia et al. argue that the autocatalytic nucleation is not properly accounted for in these models and needs better treatment [39]. Some models describe the autocatalytic nucleation using other means, such as a geometrical conception of the transformation [76] or using an austenite grain volume [82]. However, they still use empirical constants with no clear physical meaning to calculate the grain-boundary nucleation kinetics [39, 82].

3. According to the displacive theory of bainite formation, the formation of bainite from austenite is accompanied by partitioning of carbon into the sur-

rounding austenite matrix [14]. This leads to carbon enrichment of austenite during the transformation and eventually leads to cementite precipitation [14]. In the presence of certain alloying elements like silicon and aluminium, cementite precipitation is sluggish [26]. The maximum volume fraction of bainite is usually calculated using the $T_0^{'}$ theory (Section 2.2.1) where the carbon concentration in bainite is assumed to be equal to the para-equilibrium carbon concentration in ferrite [11]. Although such a calculation can give a good estimate of the maximum volume fraction of bainite, it may not be accurate since this calculation implicitly assumes that overlapping reactions are suppressed during the transformation of austenite to bainite. However, any overlapping reactions such as precipitation of cementite along with bainite formation lead to a decrease in the degree of carbon enrichment of austenite, consequently promoting further bainite formation [39]. This might lead to an underestimation of the maximum volume fraction bainite. Santofimia et al. [39] conclude that most models fail to predict the kinetics of bainite formation in lean silicon steels where the models do not account for cementite precipitation, which can however occur simultaneously with bainitic ferrite formation. A unified model to predict a bainite kinetics regardless of the degree of carbon enrichment is therefore necessary.

In order to tackle the problem of predicting the kinetics of bainite formation in lean silicon steels, Van Bohemen and Sietsma [77] developed a kinetic model based on nucleation kinetics. This model was developed using concepts from the displacive theory of bainite and martensite formation. The treatment of nucleation rate was much more rigorous compared to previous models where several empirical constants were used. Since this model does not predict the incomplete reaction phenomenon which is exhibited for high silicon steels, Van Bohemen and Hanlon [78] proposed a modified version of the Van Bohemen and Sietsma model [77] for this purpose.

However, Van Bohemen and Sietsma model [77] as well as Van Bohemen and Hanlon model [78] do not account for all possibilities by which a bainite reaction can terminate. It has been suggested that the displacive formation of bainite can proceed if and only if the following conditions are satisfied [36]:

$$\Delta G^{\gamma\rightarrow\alpha} < -G_{SB}; \quad \text{where} \quad \Delta G^{\gamma\rightarrow\alpha} = G^{\alpha} - G^{\gamma} \tag{2.2}$$

$$\Delta G_m < G_N; \quad \text{where} \quad \Delta G_m = G_m^{\alpha} - G_m^{\gamma} \tag{2.3}$$

Equation 2.2 and Equation 2.3 relate to the conditions necessary for bainite growth and nucleation respectively. In Equation 2.2, $\Delta G^{\gamma \rightarrow \alpha}$ represents the free energy change during bainite formation. G^{α} and G^{γ} give the ferrite free energy and austenite free energy respectively, when both the composition of ferrite and of austenite is equal to the composition of interest. G_{SB} is the stored energy of bainite. The maximum temperature below which diffusionless growth of bainite can occur, i.e. Equation 2.2 is satisfied, is called the $T_0^{'}$ temperature [11].

In Equation 2.3, ΔG_m is the maximum driving force for nucleation. It is the greatest possible reduction in free energy that can be achieved during formation of a ferrite nucleus such that the composition of surrounding austenite matrix remains unaffected. It is calculated using parallel tangent construction. G_m^{α} and G_m^{γ} give the ferrite free energy and austenite free energy when this condition of maximum free energy reduction is achieved. Equation 2.3 indicates that bainite nucleation can only occur when ΔG_m is less than a critical value G_N. This critical value G_N can be determined by the universal nucleation function [36, 39, 83] which is an empirical function and gives the variation of ΔG_m as a function of the highest temperature at which ferrite can form by a displacive mechanism, T_h. This function was developed based on data obtained from a vast array of steels [36, 83]. It was observed that the variation between ΔG_m and T_h can be fitted to a straight line which gives G_N as a function of temperature. [36, 83]. Additionally, it was observed that the universal nucleation function is independent of chemical composition of steel [36, 83]. Thus, it was extrapolated that ΔG_m must be smaller than G_N if bainite formation were to proceed regardless of steel composition. The temperature at which ΔG_m of a given steel is equal to G_N is the T_h temperature of that steel.

Both T_h and $T_0^{'}$ temperatures decrease with increasing carbon enrichment of austenite in the course of bainite formation. Generally, it is observed that the $T_0^{'}$ temperature decreases at a much higher rate with increasing carbon enrichment than the T_h temperature. When either T_h or $T_0^{'}$ temperature becomes equal to the isothermal transformation temperature, the bainite reaction will terminate and an incomplete reaction phenomenon will occur. The nucleation rate at this point would be equal to zero. A dependence of the nucleation rate on both T_h and $T_0^{'}$ temperatures is not considered in the Van Bohemen and Sietsma model [77] nor in the Van Bohemen and Hanlon model [78]. Its effects would not be significant in the prediction of bainite kinetics in lean silicon steels due to the negligible effective carbon enrichment of austenite during transformation. However, without such a dependence, in case of high silicon steels, the modelled nucleation rate at the end

of the transformation may not always reach zero. This signifies that the reaction could proceed even further which is physically impossible.

Based on the above discussion, it is evident that an improved physically based kinetic model is required to better understand the bainite nucleation kinetics. Such understanding would also provide deeper insight into the validity of the displacive and diffusionless theory of bainite formation. This will be the central theme of this thesis.

References

[1] H. Bhadeshia, D. Edmonds, *Metallurgical Transactions A* **10**, 895 (1979).

[2] S. Liu, W. Reynolds, H. Aaronson, H. Hu, G. Shiflet, *Metallurgical Transactions A* **16**, 457 (1985).

[3] H. Bhadeshia, D. Edmonds, *Metallurgical Transactions A* **16**, 466 (1985).

[4] H. Aaronson, W. Reynolds, H. Hu, S. Liu, *Metallurgical Transactions A* **20**, 324 (1989).

[5] H. Bhadeshia, D. Edmonds, *Metallurgical Transactions A* **20**, 330 (1989).

[6] E. Davenport, E. Bain, *Transactions of the Metallurgical Society of AIME* **90**, 117 (1930).

[7] J. Robertson, *Journal of Iron and Steel Institute* (1929).

[8] A. Hultgren, *A metallographic study on tungsten steels* (John Wiley and Sons, New York, 1929).

[9] H. Bhadeshia, *Metallurgical and Materials Transactions B* **41**, 701 (2010).

[10] Z.-G. Yang, H.-S. Fang, *Current Opinion in Solid State and Materials Science* **9**, 277 (2005).

[11] H. Bhadeshia, *Bainite in Steels: Transformations, Microstructure and Properties*, Matsci Series (IOM Communications, 2001).

[12] L. Fielding, *Materials Science and Technology* **29**, 383 (2013).

[13] H. Bhadeshia, R. Honeycombe, *Steels: Microstructure and Properties* (Elsevier Ltd., 2006).

[14] H. Bhadeshia, J. Christian, *Metallurgical Transactions A* **21**, 767 (1990).

[15] S. Singh, *Phase Transformations in Steels*, E. Pereloma, D. Edmonds, eds. (Woodhead Publishing, 2012), vol. 1 of *Woodhead Publishing Series in Metals and Surface Engineering*, pp. 385–416.

[16] H. Bhadeshia, D. Edmonds, *Acta Metallurgica* **28**, 1265 (1980).

[17] E. Swallow, H. Bhadeshia, *Materials Science and Technology* **12**, 121 (1996).

[18] F. Caballero, H.-W. Yen, M. Miller, J.-R. Yang, J. Cornide, C. Garcia-Mateo, *Acta Materialia* **59**, 6117 (2011).

[19] H. Bhadeshia, *Scripta Materialia* **70**, 12 (2014).

[20] H.-S. Fang, J.-B. Yang, Z.-G. Yang, B.-Z. Bai, *Scripta Materialia* **47**, 157 (2002).

[21] G. Miyamoto, N. Takayama, T. Furuhara, *Scripta Materialia* **60**, 1113 (2009).

[22] M. Hillert, *Metallurgical and Materials Transactions A* **25**, 1957 (1994).

[23] F. Caballero, H. Bhadeshia, *Current Opinion in Solid State and Materials Science* **8**, 251 (2004).

[24] D. Edmonds, D. Matlock, J. Speer, *Advanced Steels: The Recent Scenario in Steel Science and Technology* (Springer-Verlag Berlin Heidelberg and Metallurgical Industry Press, 2011), chap. Developments in High Strength Steels with Duplex Microstructures of Bainite or Martensite with Retained Austenite: Progress with Quenching and Partitioning Heat Treatment, pp. 241–254.

[25] H. Bhadeshia, M. Lord, L.-E. Svensson, *Joining & Welding Solutions to Industrial Problems, JWRI, Osaka University* (2003).

[26] E. Kozeschnik, H. Bhadeshia, *Materials Science and Technology* **24**, 343 (2008).

[27] N. Shaposhnikov, B. Mogutnov, *Russian Metallurgy* **2008**, 96 (2008).

[28] F. Caballero, M. Miller, C. Garcia-Mateo, *Materials Chemistry and Physics* **146**, 50 (2014).

[29] F. Caballero, M. Miller, S. Babu, C. Garcia-Mateo, *Acta Materialia* **55**, 381 (2007).

[30] F. Caballero, H. Bhadeshia, K. Mawella, D. Jones, P. Brown, *Materials Science and Technology* **18**, 279 (2002).

[31] F. Caballero, H. Bhadeshia, K. Mawella, D. Jones, P. Brown, *Materials Science and Technology* **17**, 512 (2001).

[32] H. Bhadeshia, *Materials Science Forum* **500 - 501**, 63 (2005).

[33] EP2310545 - Super bainite steels and methods of manufacture thereof, European Patent Office (2011).

[34] M. Peet, Transformation and tempering of low-temperature bainite, Ph.D. thesis, University of Cambridge (2010).

[35] H. Bhadeshia, *J. Phys. IV France* **07**, 367 (1997).

[36] H. Bhadeshia, *Acta Metallurgica* **29**, 1117 (1981).

[37] R. Le Houillier, G. Bégin, A. Dubé, *Metallurgical Transactions* **2**, 2645 (1971).

[38] H. Bhadeshia, D. Edmonds, *Metal Science* **17**, 411 (1983).

[39] M. Santofimia, F. Caballero, C. Capdevila, C. Garcia-Mateo, C. de Andres, *Materials Transactions* **47**, 1492 (2006).

[40] Y. Xia, G. Miyamoto, Z. Yang, C. Zhang, T. Furuhara, *Acta Materialia* **91**, 10 (2015).

[41] W. Reynolds, S. Liu, F. Li, S. Hartfield, H. Aaronson, *Metallurgical Transactions A* **21**, 1479 (1990).

[42] H. Aaronson, W. Reynolds, G. Purdy, *Metallurgical and Materials Transactions A* **35**, 1187 (2004).

[43] M. Hillert, B. Sundman, *Acta Metallurgica* **24**, 731 (1976).

[44] W. Reynolds, F. Li, C. Shui, H. Aaronson, *Metallurgical Transactions A* **21**, 1433 (1990).

[45] H. Chen, K. Zhu, L. Zhao, S. van der Zwaag, *Acta Materialia* **61**, 5458 (2013).

[46] H. Chen, S. van der Zwaag, *Acta Materialia* **72**, 1 (2014).

[47] M. Hillert, L. Höglund, J. Ågren, *Metallurgical and Materials Transactions A* **35**, 3693 (2004).

[48] H. Bhadeshia, *Journal de Physique* **43**, 443 (1982).

[49] D. Quidort, Y. Bréchet, *ISIJ International* **42**, 1010 (2002).

[50] D. Quidort, Y. Bréchet, *Scripta Materialia* **47**, 151 (2002).

[51] S. van Bohemen, *Metallurgical and Materials Transactions A* **41**, 285 (2010).

[52] C. Garcia-Mateo, F. Caballero, H. Bhadeshia, *ISIJ International* **43**, 1821 (2003).

[53] T. Sourmail, V. Smanio, *Acta Materialia* **61**, 2639 (2013).

[54] M. Umemoto, T. Furuhara, I. Tamura, *Acta Metallurgica* **34**, 2235 (1986).

[55] W. Steven, A. Haynes, *Journal of Iron and Steel Institute* (1956).

[56] H. Vetters, J. Dong, H. Bornas, F. Hoffmann, H.-W. Zoch, *International Journal of Materials Research* **97**, 1432 (2006).

[57] H. Kawata, M. Takahashi, K. Hayashi, N. Sugiura, N. Yoshinaga, *THERMEC 2009* (Trans Tech Publications, 2010), vol. 638 of *Materials Science Forum*, pp. 3307–3312.

[58] W. Gong, Y. Tomota, S. Harjo, Y. Su, K. Aizawa, *Acta Materialia* **85**, 243 (2015).

[59] M. Santofimia, S. van Bohemen, J. Sietsma, *Journal of the Southern African Institute of Mining and Metallurgy* **113**, 143 (2013).

[60] M. Santofimia, D. Hanlon, S. van Bohemen, L. Zhao, J. Sietsma, *Conference Proceedings International Symposium on New Developments in Advanced High-Strength Sheet Steels* (2013).

[61] S. van Bohemen, *Modern Bainitic Steels Workshop: From fundamentals to applications* (2012).

[62] T. Sourmail, V. Smanio, *Solid-Solid Phase Transformations in Inorganic Materials* (Trans Tech Publications, 2011), vol. 172 of *Solid State Phenomena*, pp. 821–826.

[63] S. Samanta, P. Biswas, S. Giri, S. Singh, S. Kundu, *Acta Materialia* **105**, 390 (2016).

[64] S. Samanta, P. Biswas, S. Singh, *Scripta Materialia* **136**, 132 (2017).

[65] A. Navarro-López, J. Hidalgo, J. Sietsma, M. Santofimia, *Materials Characterization* **128**, 248 (2017).

[66] J. Speer, B. de Cooman, D. Kim, *PRICM7* (Trans Tech Publications, 2010), vol. 654 of *Materials Science Forum*, pp. 98–101.

[67] M. Oka, H. Okamoto, *Metallurgical Transactions A* **19**, 447 (1988).

[68] K. Zhu, H. Chen, J.-P. Masse, O. Bouaziz, G. Gachet, *Acta Materialia* **61**, 6025 (2013).

[69] D. Quidort, Y. Bréchet, *Acta Materialia* **49**, 4161 (2001).

[70] M. Umemoto, K. Horiuchi, I. Tamura, *Transactions ISIJ* **22**, 854 (1982).

[71] S.-J. Lee, J.-S. Park, Y.-K. Lee, *Scripta Materialia* **59**, 87 (2008).

[72] F. Hu, P. Hodgson, K. Wu, *Materials Letters* **122**, 240 (2014).

[73] G. Xu, F. Liu, L. Wang, H. Hu, *Scripta Materialia* **68**, 833 (2013).

[74] A. Matsuzaki, H. Bhadeshia, *Materials Science and Technology* **15**, 518 (1999).

[75] G. Rees, H. Bhadeshia, *Materials Science and Technology* **8**, 985 (1992).

[76] M. Santofimia, F. Caballero, C. Capdevila, C. Garcia-Mateo, C. de Andres, *Materials Transactions* **47**, 2465 (2006).

[77] S. van Bohemen, J. Sietsma, *International Journal of Materials Research* **99**, 739 (2008).

[78] S. van Bohemen, D. Hanlon, *International Journal of Materials Research* **103**, 987 (2012).

[79] C. Magee, *Phase Transformation: Papers presented at a seminar of the American Society of Metals Oct 12 and 13, 1968* (1968).

[80] S. Pati, M. Cohen, *Acta Metallurgica* **17**, 189 (1969).

[81] S. van Bohemen, *Philosophical Magazine* **93**, 388 (2013).

[82] D. Gaude-Fugarolas, P. Jacques, *ISIJ International* **46**, 712 (2006).

[83] C. Garcia-Mateo, H. Bhadeshia, *Materials Science and Engineering: A* **378**, 289 (2004).

3

Modelling bainite formation kinetics in steels

A simple statement is bound to be untrue.
One that is not simple cannot be utilized.

Paul Valéry

As a model of a complex system becomes more complete,
it becomes less understandable

Bonini's Paradox

Parts of this chapter have been published in Acta Materialia **105** (2017) 155-164 [1] and Scripta Materialia **140** (2017) 82-86 [2].

The displacive theory for bainite formation assumes that the rate of bainite formation is driven by the rate of bainite nucleation [1, 3–9]. Most existing nucleation based models developed using the displacive mechanism of bainite formation use several empirical constants to account for the number density of grain-boundary nucleation sites and the number density of autocatalytic nucleation sites [5, 7]. However, the physical significance of the values obtained for the empirical constants, as discussed in Chapter 2, is still unclear [10].

Furthermore, most existing models do not properly account for the carbon enrichment which accompanies bainite formation in steels (Chapter 2). This results in an underestimation of the maximum volume fraction of bainite and consequently leads to an improper prediction of the bainite formation kinetics.

In this work, a model to predict the kinetics of isothermal bainite formation, accounting for the degree of carbon enrichment of austenite, is proposed. In an attempt to better treat the autocatalytic nucleation, a physically based approach considering the difference in the activation energy for grain-boundary nucleation and for autocatalytic nucleation is proposed here. The model is derived under the assumptions given by the displacive theory of bainite formation and draws inspiration from previously proposed models [5, 8].

3.1. The model

3.1.1. Nucleation rate

Bainitic ferrite sub-units may nucleate either at austenite grain boundaries (γ/γ interfaces) or at bainitic ferrite/austenite (α_b/γ) interfaces, the latter being autocatalytic bainite nucleation. The total nucleation rate during bainite formation from a fully austenitic phase, $\mathrm{d}N/\mathrm{d}t$, can be given as

$$\frac{\mathrm{d}N}{\mathrm{d}t} = \left(\frac{\mathrm{d}N}{\mathrm{d}t}\right)_G + \left(\frac{\mathrm{d}N}{\mathrm{d}t}\right)_A \tag{3.1}$$

where $(\mathrm{d}N/\mathrm{d}t)_G$ is the nucleation rate per unit volume due to nucleation at austenite grain boundaries and $(\mathrm{d}N/\mathrm{d}t)_A$ is the nucleation rate per unit volume due to autocatalytic nucleation.

It is generally accepted that bainite nucleation is a thermally activated process [11]. The nucleation rate is usually expressed as an exponential function of the temperature [7]. Using this approach, the nucleation rate due to grain-boundary nucleation can be written as

$$\left(\frac{\mathrm{d}N}{\mathrm{d}t}\right)_G = \frac{kT}{h} N_{tG} \exp\left(-\frac{Q_G^*}{kT}\right) \tag{3.2}$$

where k is the Boltzmann constant, h is the Planck constant, N_{tG} is the number density of potential grain-boundary nucleation sites, Q_G^* is the activation energy for grain-boundary nucleation and T is the transformation temperature.

The autocatalytic nucleation is accounted for in [5–7] with the help of an autocatalytic parameter. This parameter is analogous to the autocatalytic factor used to describe the kinetics of isothermal martensite transformation in [12, 13]. The autocatalytic parameter typically is treated as an empirical dimensionless coefficient [4, 7]. However, like grain-boundary nucleation, it can be postulated that autocatalytic nucleation is also a thermally activated nucleation event, its nucleation rate may also be expressed similarly as Equation 3.2, by

$$\left(\frac{\mathrm{d}N}{\mathrm{d}t}\right)_A = \frac{kT}{h} N_{tA} \exp\left(-\frac{Q_A^*}{kT}\right) \tag{3.3}$$

N_{tA} is the number density of potential autocatalytic nucleation sites and Q_A^* is the activation energy for autocatalytic nucleation. Q_A^* will be different from Q_G^* due to the different type of interface at which the nucleation takes place. Q_A^* can be mathematically related to Q_G^* by

$$Q_A^* = Q_G^* - \Delta Q^* \tag{3.4}$$

where ΔQ^* is the difference between the activation energy for grain-boundary nucleation and autocatalytic nucleation. It should be noted that the value of ΔQ^* could either be positive or negative and depends on local physical conditions in the vicinity of γ/γ interfaces and α/γ interfaces, such as local carbon concentration and dislocation density. No assumptions regarding the value of ΔQ^* are made during the development of the model.

Such an interpretation for the autocatalytic nucleation rate forms the physical basis for the autocatalytic parameter, as will be shown later.

3.1.2. Potential nucleation sites

The nucleation rate in Equation 3.2 and Equation 3.3 is expressed with a Boltzmann factor which gives the probability of successful nucleation events. In order to estimate this probability, it is important to quantify the number density of potential nucleation sites. Van Bohemen and Sietsma [5] calculated the total number density

of potential nucleation sites initially present in austenite (before bainite formation begins) using the principles of martensite formation. Magee's work [13] on athermal martensite nucleation suggests that the total number of martensitic plates per unit volume, N_m, that form during martensite formation at a particular temperature can be expressed as

$$N_m = \frac{m}{\bar{V}}(M_s - T) \tag{3.5}$$

where $\bar{V}$ is the average volume of a martensitic plate and M_s is the martensite start temperature. Since it can be postulated that each nucleation event would lead to the formation of a martensitic plate, m is the proportionality constant between the number density of martensite nucleation events and the degree of undercooling, $(M_s - T)$. Furthermore, at a given undercooling, the number density of potential martensitic type (i.e., bainitic in this case) nucleation sites can be expressed using an equation similar to Equation 3.5. With this assumption, the number density of potential nucleation sites for grain-boundary nucleation during bainite formation can be given by

$$N_{tG} = \frac{b_G}{V_b}(T_h - T) \tag{3.6}$$

where V_b is the volume of a bainitic ferrite sub-unit. The b_G parameter acts as a proportionality constant between the number density of nucleation sites and the degree of undercooling with respect to the T_h temperature. This parameter is analogous to the fitting parameter, α, in the Koistinen and Marburger equation [14] as well as to the parameter m, suggested in the work of Magee (Equation 3.5) [13].

It must be noted that Equation 3.6 gives the density of potential nucleation sites while Equation 3.5 gives the number density of nucleation events. This is because bainite nucleation requires thermal activation [8, 15], while athermal martensite nucleation does not need thermal activation. Therefore, during athermal martensite formation, the potential nucleation sites have a relatively high probability of nucleating into martensitic plates and thus, the density of potential nucleation sites can be assumed to be equal to the number density of nucleation events. It should be noted that in Equation 3.2 and Equation 3.3, the exponential term gives the probability of successful nucleation events. During bainite formation, this probability of successful nucleation is much lower due to the requirement of thermal activation and consequently, the number density of bainitic nucleation events will be much lower than the number density of potential bainitic nucleation sites at any given time.

Equation 3.6 in combination with Equation 3.2 gives the actual number density of successful grain-boundary nucleation events during bainite formation.

Van Bohemen and Sietsma [5] point out that one of the key differences between martensite nucleation and bainite nucleation is that the density of pre-existing defects for martensite nucleation is independent of the prior austenitization while the number density of γ/γ interfaces plays an important role in bainite nucleation. Therefore, with the help of Van Bohemen and Sietsma [5] approach, the b_G parameter can be given in relation to m if the effect of γ/γ interfaces is included. The density of available γ/γ interfaces depends on the fraction of remaining available austenite and the grain size of austenite. Thus, the b_G parameter can be written as

$$b_G = \frac{Z\delta}{d} f_\gamma m \tag{3.7}$$

where Z is a geometrical factor, δ is the effective thickness of an austenite boundary, d is the prior austenite grain size and f_γ is the volume fraction of remaining available austenite.

The factor $Z\delta/d$ accounts for the austenite grain boundary area per unit volume. For spherical austenite grains, Z would to be equal to 6. Van Bohemen and Sietsma proposed that δ is the effective thickness of the austenite grain boundary which is defined here as the atomic layers of a grain in the grain boundary region which can be involved in grain-boundary nucleation. It is assumed that only a few of the outermost atomic layers in a grain participate in the nucleation process and therefore δ is considered to be equal to 1 nm, equivalent to 2 atomic layers in each grain.

The remaining available austenite, f_γ, is defined in this work as the remaining fraction of austenite in which bainite formation can occur. This may not be equal to the total fraction of remaining austenite due to the "incomplete reaction phenomenon" exhibited during bainite formation [16]. Further description of f_γ is given in section 3.1.4. However, it is self-evident that f_γ decreases as bainite formation progresses. Thus, with the help of Equation 3.6 and Equation 3.7, N_{tG} as a function of volume fraction of bainite, f, at a given temperature may be schematically represented according to Figure 3.1.

The number density of potential autocatalytic nucleation sites can be derived similarly. Equivalent to Equation 3.6, it is written as

$$N_{tA} = \frac{b_A}{V_b}(T_h - T) \tag{3.8}$$

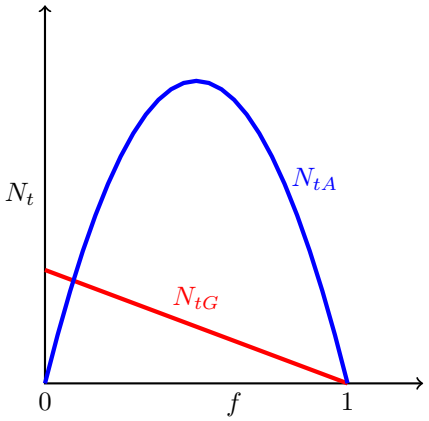

Figure 3.1: Schematic representation of potential grain-boundary nucleation sites (N_{tG}) and autocatalytic nucleation sites (N_{tA}) as function of volume fraction of bainite (f) at a given temperature.

where b_A is a parameter for autocatalytic nucleation during bainite formation.

The b_A parameter is different compared to the b_G parameter since the density of potential autocatalytic nucleation sites depends on the density of available α_b/γ interfaces which depends on both the fraction of bainite formed and the fraction of remaining available austenite. Assuming that nucleation events are random, the number density of potential autocatalytic nucleation sites can be assumed to be proportional to the surface area of the α_b/γ interface (Figure 3.1).

The density of available α_b/γ interfaces indirectly depends on the density of γ/γ interfaces since grain-boundary nucleation is a precursor for autocatalytic nucleation. If the austenite grain size is small, there are relatively many grain-boundary nucleation events due to relatively high density of γ/γ interface area. Grain-boundary nucleation events lead to the creation of α_b/γ interfaces and therefore the kinetics of grain-boundary nucleation events influences the rate at which α_b/γ interfaces form. Assuming that the volume of bainitic ferrite sub-units is constant during bainite formation at a constant temperature, a greater number of grain-boundary nucleation events leads to higher density of α_b/γ interfaces within a given time. Thus, the b_A parameter also depends on the number density of γ/γ interfaces (given by $Z\delta/d$) and it can be written as a function of m by

$$b_A = \frac{Z\delta}{d} m f_\gamma f = b_G f \tag{3.9}$$

where f is the volume fraction of bainite formed.

The number density of potential nucleation sites is also affected by the size

of the bainitic sub-units. As the size of the sub-units decreases, the density of potential nucleation sites increases. Additionally, the size of the sub-units affects the remaining available austenite in which subsequent nucleation can take place.

Such size effects are incorporated into the model in two ways. Firstly, the number density of potential grain-boundary and autocatalytic nucleation sites are calculated per unit volume of bainite formed (Equation 3.6 and Equation 3.8). Most of the existing kinetic models for bainite formation developed using the displacive mechanism of bainite formation use a fitting parameter to define the number density of potential nucleation sites [7]. Van Bohemen and Sietsma argue that this could lead to an imprecise treatment of the potential nucleation sites [5]. Considering the number density of potential nucleation sites as a function of the volume of the bainitic sub-unit is a physically more rigorous approach. Furthermore, it reduces the number of fitting parameters required for the model as shown in [5]. Secondly, the number densities of potential grain-boundary and autocatalytic nucleation sites are calculated as a function of volume fraction of bainite formed, f. Since the volume fraction of bainite formed due to each nucleation event depends on the size of the bainitic sub-unit, such a formulation automatically includes the size effects of bainitic sub-units on the remaining available austenite.

3.1.3. Carbon enrichment

Bainite formation in steels can be accompanied by carbon enrichment of the surrounding austenite as discussed in Chapter 2. This results in slower transformation since the effective activation energy increases and the effective undercooling decreases. In order to account for the effect of carbon enrichment, the following assumptions are made.

Firstly, mass balance of carbon applies and therefore, the carbon content in austenite, X_γ, can be expressed as a function of fraction of bainite formed, f, and bulk carbon content $\bar{X}$, according to

$$X_\gamma = \frac{(\bar{X} - fX_b)}{(1-f)}. \tag{3.10}$$

where X_b accounts for carbon that does not participate in the carbon enrichment of austenite. This implies that X_b accounts for carbon in bainitic ferrite, in any carbides present as well as any carbon that has been lost to carbon trapping at defects and dislocations in bainitic ferrite. Although an exact definition for bainite is still being debated, bainite can be viewed as an aggregate of bainitic ferrite and

carbides [17]. Therefore, X_b can be assumed to reflect carbon in bainite. Equations similar to Equation 3.10 have been used in earlier studies to account for carbon concentration in austenite during bainite formation. According to Bhadeshia and Edmonds [18], the variation of carbon content of austenite may be given as

$$X_\gamma = \bar{X} + f\frac{(\bar{X} - S)}{(1 - f)} \tag{3.11}$$

where S is the fraction of carbon trapped in bainite either in solid solution ($S = 0.03$ wt%) or in the form of carbides (S depends on the bainite formation temperature). The term S is equivalent to the term X_b that is used in the current model. Since in a generalised model it is difficult to presume the degree of carbon enrichment or carbide precipitation, an unknown value X_b is used rather than *a priori* chosen value.

In addition to assumption of mass balance, it is assumed that the degree of undercooling for bainite nucleation decreases linearly as the carbon concentration in austenite increases during bainite formation. This assumption is in line with thermodynamic calculations as given by Thermo-Calc. Based on this assumption and Equation 3.10, T_h which gives the critical temperature for bainite nucleation can be expressed as

$$T_h = T_{h\bar{X}} - C_1\frac{f(\bar{X} - X_b)}{(1 - f)}. \tag{3.12}$$

$T_{h\bar{X}}$ is the T_h temperature at the beginning of the transformation ($f = 0$, $X_\gamma = \bar{X}$) and C_1 is a proportionality constant relating T_h and carbon content.

Under the assumption of a displacive mechanism for bainite formation, the nucleation of bainitic ferrite is considered to occur by spontaneous dissociation of dislocations with an activation energy inversely proportional to the magnitude of the driving force [7]. Thus, the activation energy can be expressed as a function of the driving force which in turn is a function of the undercooling [19]. This implies that the activation energy for grain-boundary nucleation, Q^*_G, can be given as

$$Q^*_G = Q^*_{G\bar{X}} + K_\Gamma C_1\frac{f(\bar{X} - X_b)}{(1 - f)} \tag{3.13}$$

where $Q^*_{G\bar{X}}$ is the activation energy for grain-boundary nucleation at the start of the transformation ($f = 0$; $X_\gamma = \bar{X}$) and the K_Γ parameter is the proportionality constant relating activation energy for bainite nucleation and temperature.

Using Equation 3.4, the activation energy for autocatalytic nucleation, Q^*_A, is

expressed in terms of ΔQ^*. Bainite nucleation is an interfacial process and thus depends on the chemistry and the morphological characteristics of the interface at which it takes place. These aspects depend on the type of the interface [20, 21]. This suggests that the activation energy required for grain-boundary nucleation can be expected to be different compared to the activation energy required for autocatalytic nucleation. Furthermore, bainitic growth is a displacive process and leads to plastic deformation of the surrounding austenite matrix [3, 11, 22]. This implies that the dislocation density around the bainite/austenite interfaces may vary as the bainitic growth continues to form sheaves. Therefore, the activation energies of autocatalytic nucleation and of grain-boundary nucleation will increase with increasing bainite fraction at different rates. To account for these effects, it is assumed that the difference between the activation energies is a function of bainite fraction f and can be expressed as

$$\Delta Q^* = Q^*_G - Q^*_A = \Delta Q^*_{\bar{X}} + \phi f \tag{3.14}$$

where ϕ is the proportionality constant between ΔQ^* and f. $\Delta Q^*_{\bar{X}}$ is ΔQ^* at $f = 0$ ($X_\gamma = \bar{X}$).

3.1.4. Remaining available austenite

As seen in Equation 3.7 and Equation 3.9, the fraction of remaining available austenite, f_γ, is important to estimate the density of potential nucleation sites. f_γ is a fraction of the total untransformed austenite in which bainite formation can proceed. The fraction of austenite that can participate in the bainite reaction is usually smaller than the total austenite fraction since the carbon enrichment of austenite leads to decrease in driving force for bainite nucleation and bainite growth. The driving force for bainite nucleation is governed by the T_h temperature and is already accounted for using Equation 3.12. The driving force for bainite growth also affects subsequent bainite nucleation since the cessation of bainite growth would imply no further increase of the density of potential nucleation sites as new α_b/γ interfaces will not be created. Consequently, the remainder of austenite would be unavailable for bainite formation. This unavailable fraction of austenite needs to be subtracted when calculating the overall nucleation rate. In this work, this unavailable austenite, $(f_\gamma)_u$, is defined as the eventual fraction of austenite in which bainite growth cannot occur due to its stabilisation by means of carbon enrichment. It should be noted that $(f_\gamma)_u$ depends on the fraction of bainite formed and the degree of carbon enrichment.

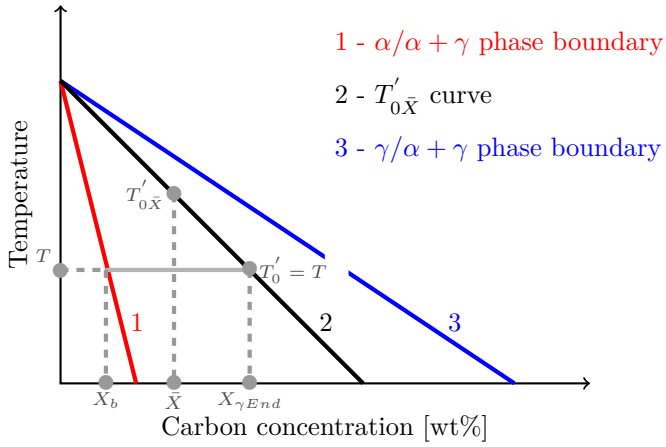

Figure 3.2: Schematic diagram representing the variation in $T_0^{'}$ as a function of carbon concentration of austenite. $T_{0\bar{X}}^{'}$ is the $T_0^{'}$ temperature at the the start of bainite formation process. Carbon enrichment of austenite due to bainite formation reduces the $T_0^{'}$.

Based on the above discussion, it is evident that $(f_\gamma)_u$ is the austenite fraction remaining when driving force for bainite growth is zero. As discussed in Chapter 2, $T_0^{'}$ temperature determines the driving force for bainite growth. Similar to the T_h temperature, the $T_0^{'}$ temperature decreases with increasing carbon enrichment of austenite as a result of bainite formation. Using Thermo-Calc calculations, the decrease of $T_0^{'}$ temperature can be expressed similar to Equation 3.12 as

$$T_0^{'} = T_{0\bar{X}}^{'} - C_2 \frac{f(\bar{X} - X_b)}{(1-f)} \tag{3.15}$$

where $T_{0\bar{X}}^{'}$ is the $T_0^{'}$ temperature at the beginning of the transformation ($f = 0$, $X_\gamma = \bar{X}$) and C_2 is a proportionality constant relating $T_0^{'}$ and carbon content. Figure 3.2 gives the variation of $T_0^{'}$ temperature as a function of carbon concentration of austenite which increases as bainite formation progresses. It can be postulated that the driving force for bainite growth becomes zero and the residual austenite becomes completely stable to bainite formation when $T_0^{'}$ is equal to bainite formation temperature. With the help of the variation of $T_0^{'}$ temperature as a function of carbon concentration of austenite, the fraction of unavailable austenite, $(f_\gamma)_u$, at a given point during transformation can be expressed as a function of remaining austenite fraction and the changes in $T_0^{'}$ temperature due to carbon enrichment, by

$$(f_\gamma)_u = (1-f)\left(\frac{T_{0\bar{X}}^{'} - T_0^{'}}{T_{0\bar{X}}^{'} - T}\right) \tag{3.16}$$

The remaining available fraction of austenite, f_γ, at a given point during transformation can be expressed as

$$f_\gamma = 1 - f - (f_\gamma)_u \tag{3.17}$$

With the help of Equation 3.16 and Equation 3.17, f_γ can be given as

$$f_\gamma = (1-f)\left(\frac{T_0^{'} - T}{T_{0\bar{X}}^{'} - T}\right) \tag{3.18}$$

Considering the lever rule, it can be seen from Figure 3.2 that for a given X_b value, bainite formation proceeds only if carbon concentration of austenite is below a certain limit.

3.1.5. Kinetic equation of the model

With the help of Equations 3.1-3.18, the framework of the proposed kinetic model is given here. The overall nucleation rate can be given as

$$\frac{\mathrm{d}N}{\mathrm{d}t} = (1-f)\left(\frac{T_0^{'} - T}{T_{0\bar{X}}^{'} - T}\right)\left[1 + \exp\left(\frac{\Delta Q^*}{kT}\right) f\right]\kappa \tag{3.19}$$

where κ is

$$\kappa = \frac{kT}{h}\frac{Z\delta}{d}\frac{m}{V_b}(T_h - T)\exp\left(-\frac{Q_G^*}{kT}\right) \tag{3.20}$$

T_h, Q_G^* and $T_0^{'}$ can be tracked using Equation 3.12, Equation 3.13 and Equation 3.15 respectively.

The physically relevant parameters X_b, $Q_{G\bar{X}}^*$ (Equation 3.13), $\Delta Q_{\bar{X}}^*$ (Equation 3.14) and ϕ (Equation 3.14) are the fitting parameters in this model. Literature suggests that $Q_{G\bar{X}}^*$ is generally in the range of 150 kJ mol^{-1}–200 kJ mol^{-1} [5]. Since each fitting parameter used in this model can be related to a physical entity, the values can be evaluated for their physical significance (see Section 3.3.2).

The constants $T_{h\bar{X}}$, $T_{0\bar{X}}^{'}$, C_1 and C_2 are calculated using Thermo-Calc. K_Γ and m are calculated using empirical methods proposed by Van Bohemen in [19] and [23], respectively.

With the help of Equation 3.19, the rate of bainite formation can be calculated using

$$\frac{\mathrm{d}f}{\mathrm{d}t} = \frac{\mathrm{d}N}{\mathrm{d}t} V_b \tag{3.21}$$

Equation 3.19 is very similar to the expression of nucleation rate proposed in early works, such as [4, 8, 9]. However, one of the major differences is that most of the empirical constants have been replaced with physical parameters, especially the autocatalytic parameter. Earlier models of bainite kinetics based on the displacive theory account for autocatalytic nucleation using the factor $(1 + \beta f)$ where β is the autocatalytic parameter. Comparing this with Equation 3.19, it can be seen that

$$\beta = \exp\left(\frac{\Delta Q^*}{kT}\right) \tag{3.22}$$

With the use of ΔQ^*, the acceleration of bainite kinetics due to autocatalysis can be interpreted in terms of difference in activation energy for grain-boundary nucleation and autocatalytic nucleation. The carbon-enrichment dependent parameters have also been treated in such a way that bainite kinetics can be estimated regardless of the chemical composition of the steel.

Most studies treat β as an empirical dimensionless fitting constant [5–9]. This suggests that, based on Equation 3.4 and Equation 3.22, the activation energy for grain-boundary nucleation and autocatalytic nucleation increase at the same rate with increasing bainite fraction. However, in this work, it is assumed that ΔQ^* depends on the bainite fraction (Equation 3.14) due to the differences in the type of interface at which grain-boundary bainite nucleation and autocatalytic nucleation takes place. In Section 3.3.2, the effect of bainite fraction on ΔQ^* and its implication in modelling the bainite formation kinetics in steels is discussed.

3.2. Experiments

Experimental data published in the literature [6, 24] as well as kinetic data obtained using dilatometer experiments during in-house experiments were used to test and validate the proposed model. The kinetic data obtained from steels with various C, Si and Mn contents were used. The chemical compositions of the steels are given in Table 3.1. The experimental data for bainite formation kinetics in Steel S1 and Steel S2 was obtained from [24] and [6]. In case of Steel S3, the bainite formation experiments were carried out in-house with the help of a Bähr DIL805A/D dilatometer. Specimens were first austenitised at 1000 °C for 5 min and then isothermally held

Table 3.1: Chemical compositions of steels used for study (values in wt%).

Steel	C	Mn	Si	Cr	Al	Reference
S1	0.53	0.69		0.28	0.03	[24]
S2	0.3	2.4	1.8			[6]
S3	0.2	3				This work

Table 3.2: Values for the constants used in relating experimental observations with the bainite formation model.

	Steel S1	Steel S2	Steel S3	Source
$T_{h\bar{X}}$ [K]	876	872	878	Thermo-Calc
C_1 [K/at.fr.]	2629	2926	2762	Thermo-Calc
$T_{0\bar{X}}$ [K]	784	822	831	Thermo-Calc
C_2 [K/at.fr.]	7197	7354	7164	Thermo-Calc
K_Γ [J mol^{-1} K]	164	139	173	[19]
m [K^{-1}]	0.016	0.018	0.018	[23]

at different temperatures ranging between 380 °C and 450 °C for 1 h. All heating steps were carried out at a heating rate of 5 °C/s while all cooling steps were carried out at a rate of −40 °C/s. The bainite fraction formed as a function of time was determined based on the obtained dilatometer data.

3.3. Results and discussion

3.3.1. Comparison with experimental data

One of the main objectives of this work is to develop a unified model to predict isothermal transformation kinetics accounting for the degree of carbon enrichment of austenite. The values for various constants used to test the model are given in Table 3.2. They were obtained using Thermo-Calc as well as different empirical equations, as mentioned in Section 3.1.5. The prior austenite grain size in case of Steel S1 was 140 µm [24] while the prior austenite grain size in case of Steel S2 was 22 µm [6]. The prior austenite grain size after austenitization at 1000 °C of Steel S3 was estimated to be 50 µm.

The experimental as well as calculated kinetics of the three different steels used in this study are given in Figure 3.3. Figure 3.3 shows that the model correlates well with the experimentally obtained kinetics. It should be noted that the experimental kinetics for Steel S3 was obtained using dilatometer experiments and over 7000 data points were recorded during the isothermal step where bainite formation occurs. Since the purpose of Figure 3.3 is to highlight the good correlation between the model

and the experimental data, only a few, but a representative set, of the experimentally obtained data points is shown.

3.3.2. Model fitting parameters

Carbon content in bainite

Carbon content in bainite, X_b, is an extremely important parameter. X_b, which is assumed to be a constant during the transformation, gives a measure of the carbon redistribution during the bainite formation. It influences the transformation significantly by affecting the values of T_h (Equation 3.12), $T_0^{'}$ (Equation 3.15), activation energy (Equation 3.13), maximum volume fraction of bainite and the degree of carbide precipitation.

From Equations 3.12, 3.13 and 3.15, it can be seen that the influence of X_b on the rate of bainite formation depends on the volume fraction of bainite, f. As f increases, the influence of X_b also increases. This implies that X_b plays a greater role during bainite formation than at the start of the transformation.

As discussed earlier, X_b reflects both the carbon in bainitic ferrite and the carbon in the carbides. If carbon is partitioned from bainitic ferrite into austenite according to a ferrite-austenite equilibrium (as given by the phase diagram), X_b would be equal to the solid solubility of carbon in ferrite. As the degree of carbide precipitation increases, the value of X_b becomes higher. Additionally, the value of X_b is higher if the dislocation density of bainitic ferrite increases or the degree of supersaturation of bainitic ferrite increases. It should be noted that the probability of carbon trapping within dislocations increases with increasing dislocation density. The maximum value for X_b would be $\bar{X}$. When $X_b = \bar{X}$, X_γ is equal to $\bar{X}$ for any bainite fraction. Using the lever rule (Figure 3.2), it can be noticed that 100 % bainite formation would occur in this case.

Due to the importance of X_b, the fit values obtained for X_b must be validated properly. The carbide precipitation in Steel S1 and Steel S3 is not suppressed because of the insignificant concentrations of silicon and aluminium. This is likely to result in negligible carbon enrichment of austenite and, as the experimental data suggests, the transformation continues until all austenite is transformed. Based on the experimental data, the model yields that X_b is equal to the bulk carbon content of the steel at all temperatures for the Steel S1 and Steel S3. According to the displacive nature of bainite formation, isothermal bainite formation can proceed if and only if the T_h and $T_0^{'}$ temperatures are greater than the isothermal transformation temperature [15]. Equation 3.12 indicates that, since X_b is equal to the bulk car-

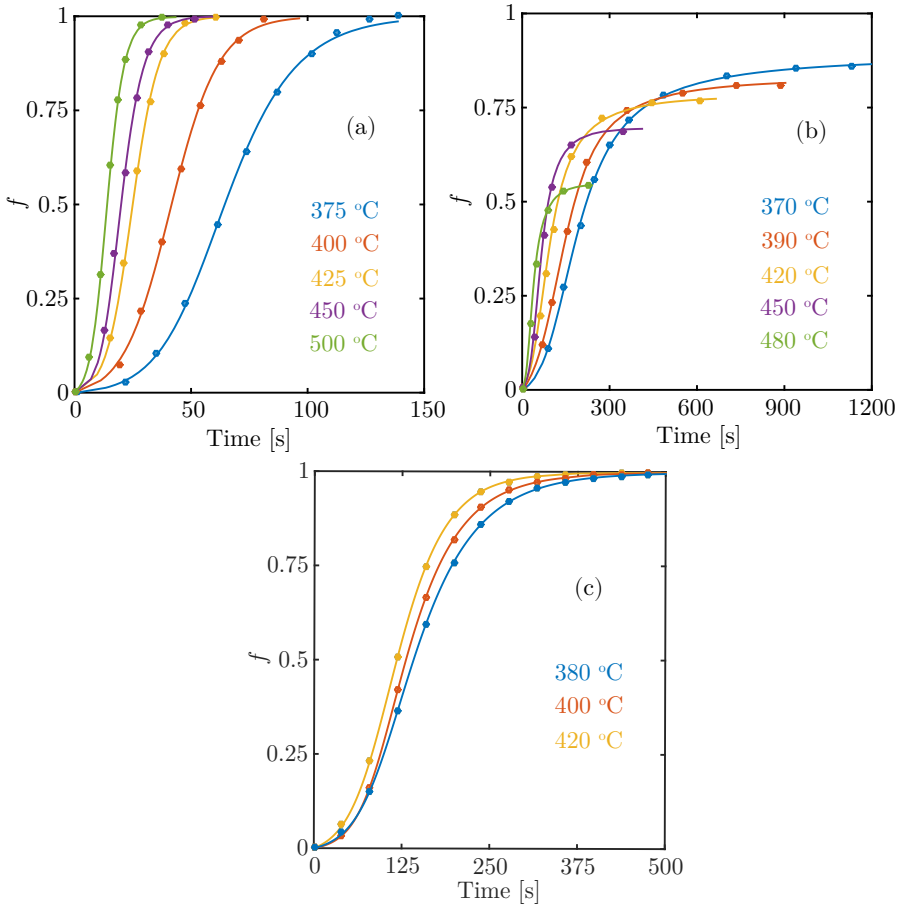

Figure 3.3: Experimental (markers) and calculated kinetics (solid lines) of bainite formation at different bainite formation temperatures (various colours) in (a) Steel S1 (from [24]), (b) Steel S2 (from [6]) and (c) Steel S3.

Table 3.3: X_b values obtained for Steel S2 ($\bar{X}$ = 0.3 wt%). The calculated standard error of the X_b values is less than 0.01 wt%.

T (in °C)	X_b (in wt%)
370	0.222
390	0.198
420	0.190
450	0.168
480	0.127

bon content of the steel, the T_h temperature does not decrease in the course of the transformation. Similarly, $T_0^{'}$ also does not decrease, which is accounted for using Equation 3.15. Thus, T_h and $T_0^{'}$ temperatures are always greater than the isothermal transformation temperature and the bainite reaction terminates only when the austenite is consumed entirely.

Since X_b also accounts for the carbon in carbides, the value of X_b can be used as an indicator for the degree of carbide precipitation. A high X_b value suggests that the driving force for carbide precipitation during bainite formation is high. In case of Steel S1 and S3, this is kinetically achievable in the absence of silicon.

Unlike Steel S1 and S3, Steel S2 is a high silicon steel and exhibits the incomplete reaction phenomenon due to the suppression of carbide precipitation (Figure 3.3). As expected, the model indicates that the X_b value is much lower than the bulk carbon concentration of the steel. The X_b values obtained for different isothermal transformations are given in Table 3.3, where, it can be observed that the X_b value increases with decreasing isothermal transformation temperature. Similar trend is reported in Van Bohemen and Hanlon [6]. Such a trend is either due to the increase in the driving force for carbide precipitation as temperature decreases, as expected thermodynamically or due to increase in dislocation density of bainitic ferrite, which has been shown in published experimental studies [25].

Figure 3.4 gives the comparison between experimentally obtained values and calculated values for carbon content in austenite in Steel S2. The experimentally observed values were obtained using XRD technique [6] which estimated the carbon content in retained austenite. It should be noted that the modelled values shown in Figure 3.4 give the carbon concentration in austenite at the moment the bainite formation ceases at the isothermal bainite formation temperature while the experimentally obtained values are obtained at room temperature after completing the overall heat treatment. Figure 3.4 shows that the experimental and modelled values for carbon concentration in austenite increase with decreasing isothermal

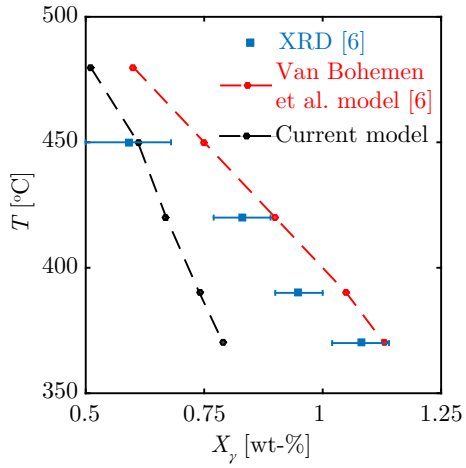

Figure 3.4: Carbon concentration in austenite at the end of the bainite formation at various bainite formation temperatures in Steel S2. In case of the modelled values obtained in this work, the calculated standard error is less than 0.01 wt%.

temperature. Such a trend is obvious considering that the volume fraction of bainite increases as the bainite formation temperature decreases (see Figure 3.3(b)) which leads higher degree of carbon partitioning from bainite to austenite.

Figure 3.4 also shows that the modelled values for carbon concentration in austenite at the end of the transformation are lower than the experimentally observed values [6], especially when bainite formation occurs at relatively low transformation temperatures. Additionally, the difference between the experimentally obtained values and the modelled values increases as the bainite formation temperature decreases. This can be explained by the mechanism of bainite formation in consideration with the volume fraction of bainite formed and the partitioning kinetics of carbon from bainitic ferrite to austenite. If bainitic ferrite is supersaturated in carbon at the moment when bainite formation ceases, the carbon partitioning can continue from bainite into surrounding austenite even after bainite formation terminates. This can lead to an increase in the carbon concentration of austenite. However, such an increase of carbon concentration of austenite depends on volume fraction of bainite formed as well as the degree of supersaturation of bainite. At higher bainite formation temperatures, both the volume fraction of bainite formed (see Figure 3.3) as well as X_b (see Table 3.3), a measure of carbon supersaturation of bainite, is lower. Furthermore, the rate of carbon diffusion is higher at higher temperatures. This implies that, the amount of carbon available for continued carbon

partitioning after the termination of bainite formation is lower at higher temperature. Additionally, the available carbon diffuses at faster rate. Therefore, it can be argued that degree of carbon partitioning after bainite formation is lower at higher temperatures. This results in the difference between experimentally obtained values and the modelled values seen in Figure 3.4. Moreover, the untransformed austenite at the end of the bainite reaction may further transform into martensite while cooling to room temperature. This is also reported in [6]. This results in further increase in the average carbon concentration of the retained austenite. Thus, the values calculated by the model give the carbon concentration in austenite can be expected to be lower than the experimentally observed values.

The obtained X_b values indicate that the T_h and $T_0^{'}$ temperatures decrease in the course of transformation. The model suggests that the bainite reaction stops when the $T_0^{'}$ temperature reaches the isothermal transformation temperature.

Initial grain-boundary and autocatalytic activation energies

As discussed in Section 3.1.5, the activation energy for grain-boundary nucleation at the start of the transformation ($f = 0$, $X_\gamma = \bar{X}$), $Q^*_{G\bar{X}}$, and the difference in activation energy for grain-boundary nucleation and autocatalytic nucleation at $f = 0$, $\Delta Q^*_{\bar{X}}$, are used as model parameters as well.

In Figure 3.5, $Q^*_{G\bar{X}}$, which was extracted from the fits, is plotted as a function of undercooling. Similarly, the activation energy for autocatalytic nucleation at the start of the transformation ($f = 0$, $X_\gamma = \bar{X}$), $Q^*_{A\bar{X}}$, (using Equation 3.4) is plotted as a function of undercooling in Figure 3.6. In both instances, the undercooling is with respect to the T_h temperature. It can be seen that both activation energies decrease linearly with undercooling. Also, similar results are reported by Van Bohemen and Sietsma [5]. However, they did not distinguish between the activation energy for grain boundary and autocatalytic nucleation and considered an equal activation energy for both types of nucleation.

Based on previously published research [7, 19], nucleation mechanism based on thermally activated migration of partial dislocations seems to provide a plausible explanation for the linear trend observed for activation energy vs. undercooling plots in Figure 3.5 and Figure 3.6. Such a dislocation motion assisted nucleation mechanism was proposed in the 1970s to explain the martensitic nucleation process [26, 27]. According to this mechanism, a nucleus is formed due to a stacking fault as result of dissociation of existing dislocations [26–28]. The stacking fault energy associated with the formation of a BCC nucleus in an FCC matrix is dependent on the change in chemical free energy due to the nucleation process, the strain energy

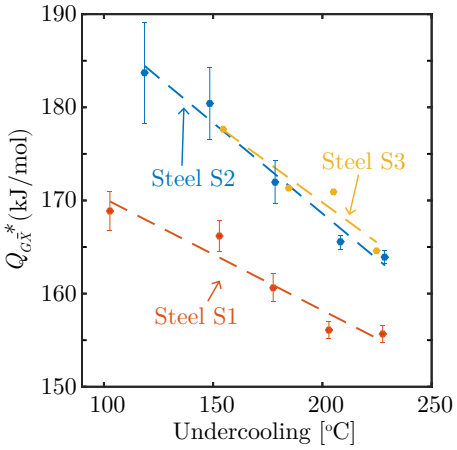

Figure 3.5: Grain-boundary activation energy at the start of transformation ($Q^*_{G\bar{X}}$) as a function of undercooling. The error bar gives the 95% confidence interval. In case the error bar is not visible, the margin of error is less than 0.15 kJ mol^{-1}.

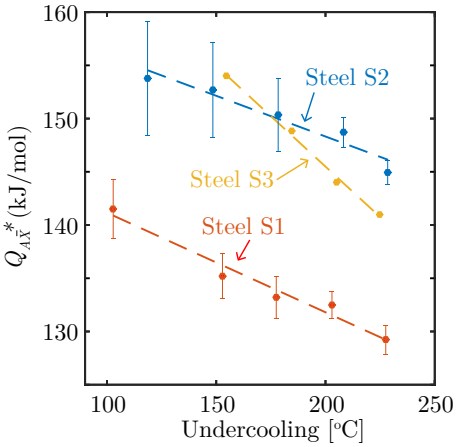

Figure 3.6: Activation energy for autocatalytic nucleation at the start of transformation ($Q^*_{A\bar{X}}$) as a function of undercooling. The error bar gives the 95% confidence interval. In case the error bar is not visible, the margin of error is less than 0.15 kJ mol^{-1}.

required to accommodate the nucleus within the matrix and the nucleus/matrix interfacial energy [28]. Olson and Cohen [28] suggest that the activation energy, G^*, for the propagation of partial dislocations with Burgers vector b and the subsequent formation of a nucleus can be expressed as

$$G^* \propto \left[\tau_\mu + \frac{\rho}{b} G_{st} + \frac{2\sigma}{n_p b}\right] v^* + \frac{\rho v^*}{b} \Delta G_{ch} \tag{3.23}$$

where τ_μ is the temperature independent resistance to dislocation motion, v^* is an activation volume, n_p is the number of close–packed planes participating in the faulting process and ρ is the spacing of the close–packed planes on which the faulting is assumed to occur. G_{st} gives the strain energy required to accommodate the nucleus within the matrix and σ the nucleus/matrix interfacial energy. ΔG_{ch} is the change in chemical free energy which is the difference between the free energy per unit volume of the nucleus and the free energy per unit volume of austenite. Literature evidence indicates that the above considerations can be extrapolated to bainite nucleation [5, 11, 29]. It can be seen from Equation 3.23 that the activation energy for nucleation assisted by dislocation migration is directly proportional to ΔG_{ch}. ΔG_{ch} depends on the degree of undercooling and it becomes more negative as undercooling increases which consequently would lower G^* based in Equation 3.23 [11, 28]. The trends observed in Figure 3.5 and Figure 3.6 are in line with the above theory.

It can be further postulated that the underlying mechanism of bainite nucleation is irrespective of the interface at which the nucleation takes places. This implies that both the activation energy for grain-boundary nucleation and the activation energy for autocatalytic nucleation would show similar trends as a function of undercooling. However, due to the differences in interfacial energy, the absolute values for the activation energies for grain-boundary nucleation and autocatalytic nucleation can be expected to be different (discussed further in Section 3.3.2). The obtained model fit values concur with the above discussion. The similarities between the trends obtained for activation energy values in this work and previously published research [7, 19] generates good confidence in the model fit parameters as well as in the model itself.

Literature also suggests that during bainite nucleation, carbon will partition from the BCC nucleus into FCC matrix [9, 11, 15]. Along with undercooling, this carbon partitioning during nucleation leads to an increase in the chemical free change. Therefore, it can be argued that carbon partitioning also leads to decrease in the overall activation energy. However, if both dislocation motion and carbon partition-

ing necessarily occur during nucleation, the total activation energy for nucleation may be the sum of the individual activation energies required for both processes.

The numerical values for activation energy obtained in Figure 3.5 and Figure 3.6 were compared with already published results. The reported values for overall activation energy for bainite formation lie in the range of 40 kJ mol^{-1}–200 kJ mol^{-1} [5, 30]. The activation energy values obtained in the current work (130 kJ mol^{-1}–185 kJ mol^{-1}) correlate well with these reported values.

Furthermore, the activation energy values for nucleation obtained in the current work were compared with reported activation energy values for various atomic processes [30]. The self-diffusion activation energy of Fe in α-Fe and in γ-Fe is around 250 kJ mol^{-1} and 285 kJ mol^{-1} respectively [30]. These values are much higher than the activation energy values obtained in the current work. However, the diffusion activation energy of carbon in γ-Fe is about 130 kJ mol^{-1} [30]. Comparing this value to the activation energy obtained in the current work, it can be suggested carbon diffusion in austenite plays a role in bainite nucleation. Also, assuming that the total activation energy for nucleation is the sum of activation energy for carbon partitioning and dislocation migration, the maximum expected activation energy contribution of the latter should be around 30 kJ mol^{-1}–40 kJ mol^{-1}.

Researchers have also studied the activation energy required for dislocation movement assisted nucleation in isothermal martensite formation [31]. These studies suggest that a temperature dependent activation energy value of 29 kJ mol^{-1}–145 kJ mol^{-1} can be expected for the migration of dislocations [31]. This range numerically compares well with the expected maximum activation energy of 30 kJ mol^{-1}–40 kJ mol^{-1} obtained in the current work. However, it must be noted that isothermal martensite formation occurs under conditions which are distinctly different from bainite formation. Therefore, numerical comparison of activation energy values must be done with caution. But, as explained above, the linearly decreasing trend observed for activation energy with undercooling is a compelling factor to consider thermally activated migration of partial dislocations as a mechanism for bainite nucleation.

Comparing Figure 3.5 and Figure 3.6, it can be noticed that the activation energy values for both mechanisms obtained for Steel S1 are lower than the values obtained for Steel S2 and Steel S3. Furthermore, activation energy values for Steel S2 and Steel S3 are similar to each other. It should be noted that Steel S2 and Steel S3 have higher Mn content than Steel S1. Also, Steel S2 is a silicon containing steel. Literature suggests that the activation energy depends on both composition-dependent and composition-independent factors [19, 28]. Other published experimental work

Table 3.4: Comparison of K_Γ parameter (values in $\mathrm{J\,mol^{-1}\,K}$) (Standard error of the modelled parameters provided in parentheses).

Steel	Empirical Value (Table 3.2)	Nucleation Mechanism	
		Grain Boundary	Auto-catalytic
Steel S1	164	120 (± 32)	94 (± 17)
Steel S2	139	194 (± 27)	76 (± 20)

also indicate that that the presence of Mn and Si in steel results in a slower rate of bainite formation [32]. This can also be seen by comparing the time scale for transformation in Figure 3.3. Such slower transformation kinetics can be attributed to the larger activation energy required for bainite formation as seen in Figure 3.5 and Figure 3.6.

The slopes of Figure 3.5 and Figure 3.6 provide the K_Γ parameter, which gives the relationship between activation energy and temperature. As discussed in Section 3.1.5, this parameter is used in the model to track the changes in activation energy due to carbon enrichment of austenite during bainite formation. The K_Γ parameter is a material parameter and depends on the chemical composition of the steel and its chemical free energy energy contribution per Kelvin [19]. Assuming that the chemical free energy contribution is the same for both mechanisms, the K_Γ parameter is considered to be equal for grain-boundary nucleation and autocatalytic nucleation. An empirical method proposed by Van Bohemen [19] is used to calculate its value which are compared with the slopes from Figure 3.5 and Figure 3.6 in Table 3.4

The fit values from Table 3.4 indicate that the K_Γ parameter for grain-boundary nucleation is not equal to the K_Γ parameter for autocatalytic nucleation. Furthermore, the values obtained from the fit do not correspond well with empirically calculated values. Therefore, further investigation into the K_Γ parameter needs to be carried out.

An initial analysis into the physical significance of the K_Γ parameter is discussed in [19]. Comparing [19] to the work published by Olson and Cohen on dislocation movement assisted nucleation [28], K_Γ can be given as

$$K_\Gamma = \rho v^* / b D_T \tag{3.24}$$

where D_T is the proportionality constant relating driving force and undercooling and ρ, b and v^* carry the same meanings as discussed in the case of Equation 3.23. v^* is called the activation volume and it is defined as the rate of change of activation

energy with respect to the applied stress [28]. In the context of nucleation assisted by dislocation movement, the applied stress originates from the available driving force for nucleation [11]. This suggests that the K_Γ parameter is proportional to the activation volume v^*. The difference in K_Γ values for grain-boundary nucleation and autocatalytic nucleation may be attributed to the difference in activation volume for the two nucleation processes. A deeper understanding regarding the role of activation volume in individual nucleation processes is necessary.

Difference in activation energy for grain-boundary and autocatalytic nucleation

Figure 3.5 and Figure 3.6 suggest that $Q^*_{A\bar{X}}$ is lower than $Q^*_{G\bar{X}}$. $\Delta Q^*_{\bar{X}}$ for Steel S1 is calculated to be in the range of $25\,\mathrm{kJ\,mol^{-1}}$–$30\,\mathrm{kJ\,mol^{-1}}$ while $\Delta Q^*_{\bar{X}}$ for Steel S2 is estimated to be in the range of $15\,\mathrm{kJ\,mol^{-1}}$–$30\,\mathrm{kJ\,mol^{-1}}$.

This difference in activation energies can be attributed to the difference in resistance offered to dislocation motion in case of grain-boundary and autocatalytic nucleation, since the interface at which respective nucleation events occur are different. Assuming that the shape of the nucleus formed during both grain-boundary and autocatalytic nucleation is the same, the strain energy contribution (G_{st} in Equation 3.23) to the fault energy would be the same in both cases. Also, since the degree of carbon enrichment at the start of the transformation ($f = 0$, $X_\gamma = \bar{X}$) is zero, the chemical free energy contribution (ΔG_{ch} in Equation 3.23) is equal for grain-boundary and autocatalytic nucleation processes. However, the interfacial energy contribution (σ in Equation 3.23) is influenced by the matrix which surrounds the nucleus. In case of grain-boundary nucleation at a γ/γ interface, the entire matrix which surrounds the nucleus is face-centered cubic (FCC), which results in the creation of α_b/γ interfaces between the nucleus and the matrix. However, in case of autocatalytic nucleation at an α_b/γ interface, both body-centered cubic (already formed bainitic ferrite sub-unit), and FCC (untransformed austenite surrounding the bainitic ferrite sub-unit) phases form the matrix in which the nucleus evolves. Nucleation then leads to the creation of both α_b/γ interfaces and α_b/α_b interfaces. Therefore, it can be established that, due to effects of interfacial energy contributions, the stacking fault energy of the nucleus formed at a γ/γ interface can be expected to be different from that of a nucleus formed at an α_b/γ interface; and consequently, the activation energy will also be different. Furthermore, the lower activation energy for autocatalytic nucleation may be due to the formation of low-energy interfaces during autocatalytic nucleation which could reduce the σ term in Equation 3.23. However, the role of 'prior' interfaces (like γ/γ interfaces) must also be taken into account while calculating the net interfacial energy. This depends on

the size and the orientation of the forming nucleus.

As mentioned previously, most studies use a constant β to account for autocatalytic nucleation during bainite formation. As given in Equation 3.22, β is dependent on the difference in the activation energy for grain-boundary and autocatalytic bainite nucleation. Assuming a constant β implies that this difference is constant during the transformation. This suggests that the activation energies for grain-boundary and autocatalytic nucleation increase at the same rate with increasing f. However, in this work, it is assumed that the activation energies for grain-boundary and autocatalytic nucleation increase at different rates with f (Equation 3.14). This assumption can be validated by analysing the obtained experimental data in detail.

Figure 3.7(a) gives the experimentally obtained bainite fraction, f, *vs* time in Steel S3 while Figure 3.7(b) gives the rate of bainite formation, $\mathrm{d}f/\mathrm{d}t$, as bainite formation progresses. Figure 3.7(c) shows experimentally obtained $(\mathrm{d}f/\mathrm{d}t)_v$ as a function of f in the same steel, where $(\mathrm{d}f/\mathrm{d}t)_v$ is the rate of bainite formation per unit volume of untransformed austenite (volume fraction available for bainite formation). It is given as

$$(\mathrm{d}f/\mathrm{d}t)_v = (\mathrm{d}f/\mathrm{d}t)/(1-f) \tag{3.25}$$

$(\mathrm{d}f/\mathrm{d}t)_v$ is an important parameter in understanding the bainite formation kinetics. The overall rate of bainite nucleation in steels mainly depends on the potency of bainite nucleation sites to form bainitic ferrite sub-units which is influenced by rate governing parameters such as bainite formation temperature and carbon concentration in austenite (Section 3.1) [4, 6, 7, 33]. $(\mathrm{d}f/\mathrm{d}t)_v$ gives a measure of this potency. Physically, it represents the rate at which nucleation sites within a unit volume of austenite can contribute to the overall nucleation rate. Numerically, $(\mathrm{d}f/\mathrm{d}t)_v$ can be determined using experimentally obtained $(\mathrm{d}f/\mathrm{d}t)$ data and the corresponding bainite fraction, f.

Using the proposed model in this work, $(\mathrm{d}f/\mathrm{d}t)_v$ can be given as

$$\left(\frac{\mathrm{d}f}{\mathrm{d}t}\right)_v \propto \left(1+\exp\left(\frac{\Delta Q^*}{kT}\right)f\right) \tag{3.26}$$

The proportionality factor in Equation 3.26 depends on the carbon content of austenite. As discussed in Section 3.3.2, the carbon content of austenite increases with increasing bainite fraction only if X_b is lower than $\bar{X}$. The results presented above show that X_b is almost equal to $\bar{X}$ due to carbide precipitation which accompanies bainite formation in Steel S1 and Steel S3. Therefore, the proportionality

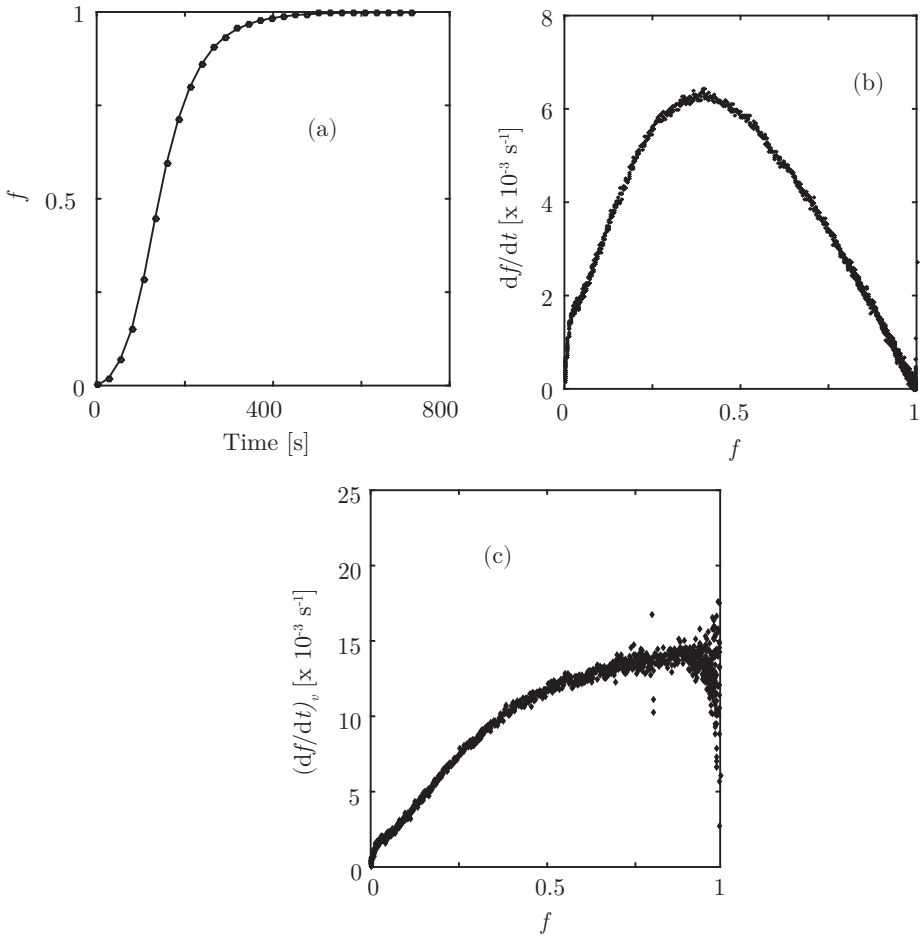

Figure 3.7: (a) Experimentally obtained bainite formation kinetics in Steel S3 at $T = 380\,^{\circ}\mathrm{C}$. (b) Corresponding $\mathrm{d}f/\mathrm{d}t$ *vs* f in Steel S3 at $T = 380\,^{\circ}\mathrm{C}$. (c) Corresponding $(\mathrm{d}f/\mathrm{d}t)_v$ *vs* f in Steel S3 at $T = 380\,^{\circ}\mathrm{C}$.

factor in Equation 3.26 remains a constant during bainite formation for Steel S1 and Steel S3. This implies that, in Steel S1 and S3, $(\mathrm{d}f/\mathrm{d}t)_v$ as a function of f depends only on ΔQ^* (Equation 3.26). As considered by previously published models [5–9], if ΔQ^* (or β based on Equation 3.22) is assumed to be a constant during transformation, $(\mathrm{d}f/\mathrm{d}t)_v$ would linearly increase with increasing bainite fraction based on Equation 3.26. However, experimentally obtained $(\mathrm{d}f/\mathrm{d}t)_v$ in Steel S3 (Figure 3.7(c)) shows a non-linear increase with increasing bainite fraction. This shows that ΔQ^* is not a constant which is considered in this work (Equation 3.14).

In order to further understand the effect of ΔQ^* on the kinetics of bainite formation, $(\mathrm{d}f/\mathrm{d}t)_v$ was calculated assuming varying ΔQ^* by numerically varying the value of ϕ. The dependence of ΔQ^* on ϕ is given by Equation 3.14. $(\mathrm{d}f/\mathrm{d}t)_v$ can be estimated in terms of ΔQ^* using Equations 3.19, 3.21 and 3.25. Figure 3.8 shows the $(\mathrm{d}f/\mathrm{d}t)_v$ trends as a function of bainite fraction by assuming four different ϕ values in Steel S3 for isothermal bainite formation at 380 °C. It should be noted that, along with ϕ values, the other model parameters should be assigned appropriate values in order to calculate the proportionality factor in Equation 3.26 and estimate the $(\mathrm{d}f/\mathrm{d}t)_v$ trends using the proposed model. In Figure 3.8 $(\mathrm{d}f/\mathrm{d}t)_v$ is calculated with $Q^*_{G\bar{X}}$ assumed to be $155\,\mathrm{kJ\,mol^{-1}}$ and $\Delta Q^*_{\bar{X}}$ to be $20\,\mathrm{kJ\,mol^{-1}}$. These assumed values are based on previously published data for the activation energy for bainite nucleation [5, 6, 31] in the literature. The X_b value is assumed to be $0.995 \times \bar{X}$ to simulate the limited carbon enrichment of austenite during bainite formation in Steel S3.

It can be seen in Figure 3.8 that the calculated trends are now much closer to the experimentally obtained $(\mathrm{d}f/\mathrm{d}t)_v$ curve in Figure 3.7(c). The non-linear increase in rate of bainite formation is predicted by the calculated trends when ϕ is not equal to 0. This clearly shows that ΔQ^* is a function of bainite fraction. These calculations validate the assumptions for ΔQ^* used in the proposed kinetic model.

The values for the model parameters obtained after comparison of the kinetic model with the experimentally obtained bainite formation kinetics in Steel S2 and Steel S3 at two different bainite formation temperatures is given in Table 3.5. It is observed that the ϕ parameter shows a negative value. Similar observations were noted in all other cases as well. This suggests that the activation energy for autocatalytic nucleation increases faster than the activation energy for grain-boundary nucleation as a function of bainite fraction.

In a physical sense, the rate at which bainite formation progresses can be estimated by calculating activation energies for both grain-boundary and autocat-

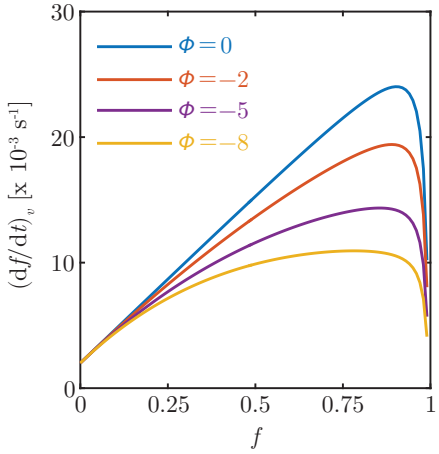

Figure 3.8: Calculated $(\mathrm{d}f/\mathrm{d}t)_v$ *vs* f in Steel S3 ($T = 380\,^{\circ}\mathrm{C}$) for varying ϕ values (in $\mathrm{kJ\,mol^{-1}}$) with $X_b = 0.99\bar{X}$.

Table 3.5: Values of fitting parameters obtained (95% Confidence Interval provided in parentheses).

Steel	T (°C)	$\bar{X}$ (wt%)	X_b (wt%)	$Q^*_{G\bar{X}}$ ($\mathrm{kJ\,mol^{-1}}$)	$\Delta Q^*_{\bar{X}}$ ($\mathrm{kJ\,mol^{-1}}$)	ϕ ($\mathrm{kJ\,mol^{-1}}$)
S2	370	0.3	0.22 (± 0.01)	164.7 (± 1.5)	20.5 (± 2.4)	-5.4 (± 2.3)
S3	380	0.2	0.199 (± 0.001)	164.5 (± 0.1)	23.6 (± 0.2)	-4.8 (± 0.1)

alytic nucleation. As discussed in already published literature, carbon enrichment of austenite leads to an increase in the activation energy for bainite nucleation, which leads to a decreasing rate of bainite formation as the bainite fraction increases. However, activation energy for grain-boundary nucleation increases at a different rate compared to the activation energy for autocatalytic nucleation. This suggests that the impact of carbon enrichment on autocatalytic nucleation and grain-boundary nucleation might be different. Also, other factors can lead to an increase in the activation energy for bainite formation, since the ability of austenite to transform into bainite is not just affected by its carbon enrichment during bainite formation. One other factor can be the plastic deformation of austenite that is associated with bainite formation [3, 16, 34]. These factors are accounted for by the parameter ϕ. It is also observed that ϕ can be affected by the grain size of the austenite in which the bainite formation occurs. Such behaviour can be due to the reducing volume of the austenite grains within which bainite formation can occur as the bainite fraction increases and to the stress state associated with this residual austenite volume (due to surrounding bainite). It can be, therefore, envisaged that as the bainite formation progresses, the austenite matrix in which the bainite formation occurs undergoes several changes, thereby affecting the bainite formation kinetics.

3.4. Conclusions

A model is proposed for the prediction of the isothermal bainite formation kinetics distinguishing the activation energy for grain-boundary nucleation and for autocatalytic nucleation. The model uses three physically relevant fitting parameters, namely carbon concentration in bainite which signifies the amount of carbon which does not participate in carbon enrichment of austenite, the activation energy for grain-boundary nucleation at the start of the transformation and the difference in activation energies for grain-boundary nucleation and autocatalytic nucleation at the start of the transformation. Furthermore, the model accounts for the variation in carbon content of austenite during the transformation. The model was tested for three different steels with different chemical compositions.

Based on the results of the experiments and model fitting, the traditional autocatalytic parameter may be expressed as a difference in activation energies related to the site of bainitic nucleation events. This essentially suggests that the autocatalytic parameter is a measure which indicates how much easier the autocatalytic nucleation is compared to the grain-boundary nucleation. This measure can be well represented as the activation energy for nucleation at an austenite grain boundary

being much higher than the activation energy for nucleation at the surface of a previously nucleated bainitic sub-unit. Comparison of the model with experimentally obtained kinetic data for bainite formation suggests that the carbon enrichment of austenite during bainite formation has a different influence on the activation energies for grain-boundary and autocatalytic nucleation. Furthermore, factors such as the momentary deformation state of the austenite and the momentary volume of the austenite grain can be expected to affect the bainite kinetics as well. From above discussions, it is clear that the bainite kinetics can be well predicted and interpreted with the help of this approach.

References

[1] A. Ravi, J. Sietsma, M. Santofimia, *Acta Materialia* **105**, 155 (2016).

[2] A. Ravi, J. Sietsma, M. Santofimia, *Scripta Materialia* **140**, 82 (2017).

[3] H. Bhadeshia, D. Edmonds, *Acta Metallurgica* **28**, 1265 (1980).

[4] G. Rees, H. Bhadeshia, *Materials Science and Technology* **8**, 985 (1992).

[5] S. van Bohemen, J. Sietsma, *International Journal of Materials Research* **99**, 739 (2008).

[6] S. van Bohemen, D. Hanlon, *International Journal of Materials Research* **103**, 987 (2012).

[7] M. Santofimia, F. Caballero, C. Capdevila, C. Garcia-Mateo, C. de Andres, *Materials Transactions* **47**, 1492 (2006).

[8] H. Bhadeshia, *Journal de Physique* **43**, 443 (1982).

[9] N. Chester, H. Bhadeshia, *J. Phys. IV France* **07**, 41 (1997).

[10] H. Bhadeshia, *Materials Science and Engineering: A* **273 - 275**, 58 (1999).

[11] H. Bhadeshia, *Bainite in Steels: Transformations, Microstructure and Properties*, Matsci Series (IOM Communications, 2001).

[12] S. Pati, M. Cohen, *Acta Metallurgica* **17**, 189 (1969).

[13] C. Magee, *Phase Transformation: Papers presented at a seminar of the American Society of Metals Oct 12 and 13, 1968* (1968).

[14] D. Koistinen, R. Marburger, *Acta Metallurgica* **7**, 59 (1959).

[15] H. Bhadeshia, *Acta Metallurgica* **29**, 1117 (1981).

[16] L. Fielding, *Materials Science and Technology* **29**, 383 (2013).

[17] R. Hehemann, K. Kinsman, H. Aaronson, *Metallurgical Transactions* **3**, 1077 (1972).

[18] H. Bhadeshia, D. Edmonds, *Metal Science* **17**, 411 (1983).

[19] S. van Bohemen, *Metallurgical and Materials Transactions A* **41**, 285 (2010).

[20] M. Herbig, D. Raabe, Y. Li, P. Choi, S. Zaefferer, S. Goto, *Phys. Rev. Lett.* **112**, 126103 (2014).

[21] Y. Li, D. Ponge, P. Choi, D. Raabe, *Ultramicroscopy* **159, Part 2**, 240 (2015).

[22] S. Singh, *Phase Transformations in Steels*, E. Pereloma, D. Edmonds, eds. (Woodhead Publishing, 2012), vol. 1 of *Woodhead Publishing Series in Metals and Surface Engineering*, pp. 385 – 416.

[23] S. van Bohemen, J. Sietsma, *Materials Science and Technology* **25**, 1009 (2009).

[24] D. Quidort, Y. Bréchet, *ISIJ International* **42**, 1010 (2002).

[25] C. García-Mateo, F. Caballero, H. Bhadeshia, *Microalloying for New Steel Processes and Applications* (Trans Tech Publications, 2005), vol. 500 of *Materials Science Forum*, pp. 495–502.

[26] G. Olson, M. Cohen, *Metallurgical Transactions A* **7**, 1897 (1976).

[27] G. Olson, M. Cohen, *Metallurgical Transactions A* **7**, 1905 (1976).

[28] G. Olson, M. Cohen, *Metallurgical Transactions A* **7**, 1915 (1976).

[29] M. Santofimia, F. Caballero, C. Capdevila, C. Garcia-Mateo, C. de Andres, *Materials Transactions* **47**, 2465 (2006).

[30] M. Kang, M.-X. Zhang, F. Liu, M. Zhu, *Materials Transactions* **50**, 123 (2009).

[31] D. San Martin, K. Aarts, P. Rivera-Diaz-del-Castillo, N. van Dijk, E. Bruck, S. van der Zwaag, *Journal of Magnetism and Magnetic Materials* **320**, 1722 (2008).

[32] S. Liu, G. Zhang, *Metallurgical Transactions A* **21**, 1509 (1990).

[33] H. Matsuda, H. Bhadeshia, *Proceedings of the Royal Society of London A: Mathematical, Physical and Engineering Sciences* **460**, 1707 (2004).

[34] E. Swallow, H. Bhadeshia, *Materials Science and Technology* **12**, 121 (1996).

4

The role of martensite/austenite interfaces during bainite formation

The cause is hidden; the effect is visible to all.

Ovid

Once I get on a puzzle, I can't get off.

Richard Feynman

The contents of this chapter have been submitted for publication in Acta Materialia under the title 'Influence of martensite/austenite interfaces on bainite formation in low-alloy steels below M_s'.

In Chapter 3, the influence of various factors such as carbon concentration of austenite and bainite formation temperature on the rate of bainite formation was discussed. In addition to these factors, the kinetics of bainite formation of steels depends on the overall heat treatment applied and can be affected by the presence of previously formed martensite. The literature review presented in Chapter 2 shows that several aspects regarding the effect of prior martensite on the kinetics of bainite formation are still unresolved. In order to further clarify these unresolved issues, it is important to analyse the common ground between the kinetics of bainite formation with and without prior martensite formation.

In this study, the formalism of the kinetic model proposed in Chapter 3 is modified and adapted to analyse the experimental results obtained for the kinetics of bainite formation both with and without prior martensite formation. The kinetic model considers that the evolution of bainite fraction is controlled by the nucleation of bainitic ferrite at austenite grain boundaries (γ/γ interfaces) and at bainite/austenite (α_b/γ) interfaces which form as bainite formation progresses. In principle, bainite nucleation would occur at γ/γ interfaces and α_b/γ interfaces even in the presence of pre-existing martensite. Therefore, the trends obtained for the model parameters during the comparison of experimental results with the proposed kinetic model must be applicable (and extrapolatable) to the entire range of temperatures at which bainite formation can occur. With the help of the analysis of the model parameters over a range of transformation temperatures for bainite formation, this chapter explores the interplay between different factors which affect the bainite formation kinetics in conditions both above and below M_s. Such an analysis sheds light on the role of prior martensite during bainite formation and its impact on bainite kinetics.

4.1. Kinetic model in presence of martensite

One of the most important factors which influences the kinetics of bainite formation is the transformation temperature at which bainite forms. The effect of transformation temperature is well accounted for using the kinetic model proposed in Chapter 3. However, during bainite formation below the M_s temperature, the presence of pre-existing martensite also affects the rate of bainite formation. Studies suggest that during treatments where austenite is quenched to form a certain fraction of martensite prior to bainite formation, martensite/austenite (α_m/γ) interfaces can also act as nucleation points for bainite formation [1–3]. Thus, the overall bainite formation rate at any given moment in the presence of pre-existing martensite can

then be given as

$$\frac{\mathrm{d}f}{\mathrm{d}t} = \left(\frac{\mathrm{d}f}{\mathrm{d}t}\right)_M + \left(\frac{\mathrm{d}f}{\mathrm{d}t}\right)_G + \left(\frac{\mathrm{d}f}{\mathrm{d}t}\right)_A \tag{4.1}$$

where $(\mathrm{d}f/\mathrm{d}t)_M$ gives the rate of bainite formation due to nucleation at α_m/γ interfaces, $(\mathrm{d}f/\mathrm{d}t)_G$ gives the rate of bainite formation due to nucleation at γ/γ interfaces and $(\mathrm{d}f/\mathrm{d}t)_A$ gives the rate of autocatalytic bainite formation.

Typically, bainite formation begins at γ/γ interfaces and then continues autocatalytically at α_b/γ interfaces. In the presence of pre-existing martensite, bainite can also nucleate at α_m/γ interfaces following which bainite nucleation can proceed autocatalytically at newly formed α_b/γ interfaces. This implies that the presence of α_m/γ interfaces can be source of additional autocatalytic nucleation sites and therefore can increase the rate of autocatalytic nucleation. Hence, $(\mathrm{d}f/\mathrm{d}t)_A$ in Equation 4.1 can be further expanded as,

$$\left(\frac{\mathrm{d}f}{\mathrm{d}t}\right)_A = \left(\frac{\mathrm{d}f}{\mathrm{d}t}\right)_{AM} + \left(\frac{\mathrm{d}f}{\mathrm{d}t}\right)_{AG} \tag{4.2}$$

where $(\mathrm{d}f/\mathrm{d}t)_{AM}$ gives the rate of bainite formation due to nucleation at α_b/γ interfaces which are formed due to bainite nucleation at α_m/γ interfaces and $(\mathrm{d}f/\mathrm{d}t)_{AG}$ gives the rate of bainite formation due to nucleation at α_b/γ interfaces which are formed due to bainite nucleation at γ/γ interfaces. In the absence of α_m/γ interfaces, $(\mathrm{d}f/\mathrm{d}t)_{AM}$ would be 0 and autocatalytic nucleation would be governed by $(\mathrm{d}f/\mathrm{d}t)_{AG}$ alone.

The rate of bainite formation is directly proportional to the density of potential nucleation sites which depends on the density of interfaces. As the bainite formation progresses, the nucleation sites are consumed at various interfaces. If the pre-existing martensite has an accelerating effect on the kinetics of bainite formation as observed in the literature [1, 2, 4], it can be postulated that bainite nucleation will take place at the α_m/γ interfaces when bainite formation occurs below the M_s temperature. Additionally, α_m/γ interfaces would be consumed quicker than γ/γ interfaces and autocatalytic nucleation sites under such circumstances. Once α_m/γ interfaces are consumed due to bainite formation in its vicinity, $(\mathrm{d}f/\mathrm{d}t)_M$ tends to zero and its influence on the overall bainite kinetics would diminish. Consequently, after a certain degree of bainite formation, the kinetics would be dominated primarily by autocatalytic and grain-boundary nucleation.

The kinetic model proposed in Chapter 3 is designed to capture the influence of autocatalytic bainite nucleation and grain-boundary bainite nucleation on the

rate of bainite formation. Based on the above discussion, the proposed kinetic model can therefore be compared with experimentally determined bainite kinetics obtained from later stages of bainite formation (when $(\mathrm{d}f/\mathrm{d}t)_M \approx 0$) where austenite to bainite transformation no longer occurs at α_m/γ interfaces. The analysis will give the specific values for the physical parameters (discussed in Chapter 3) used by the kinetic model. With the help of the parameters obtained, the contributions of $(\mathrm{d}f/\mathrm{d}t)_A$ and $(\mathrm{d}f/\mathrm{d}t)_G$ on the overall rate of bainite formation over the entire isothermal holding time for bainite formation can be calculated. Using these calculations and the experimentally obtained bainite formation kinetics, the influence of α_m/γ interface on the bainite formation ($(\mathrm{d}f/\mathrm{d}t)_M$) can be subsequently isolated using Equation 4.1 and Equation 4.2.

In order to determine the contributions of $(\mathrm{d}f/\mathrm{d}t)_G$ and $(\mathrm{d}f/\mathrm{d}t)_A$ when bainite formation occurs below the M_s temperature, the effect of pre-existing martensite fraction, f_m, on $(\mathrm{d}f/\mathrm{d}t)_G$ and $(\mathrm{d}f/\mathrm{d}t)_A$ should be incorporated into the model. It should be noted along with direct impact of f_m on the rate of bainite formation, as given by $(\mathrm{d}f/\mathrm{d}t)_M$, f_m also influences the available austenite fraction in which bainite formation can occur. As mentioned previously, the density of γ/γ interfaces and α_b/γ interfaces depends on the fraction of available austenite. Thus, it can be summarized that f_m has an effect on $(\mathrm{d}f/\mathrm{d}t)_G$ and $(\mathrm{d}f/\mathrm{d}t)_A$. The effect of f_m on the volume fraction of available austenite and on subsequent autocatalytic or grain-boundary bainite nucleation would be similar to the effect of the bainite fraction during typical bainite formation conditions above M_s (without any pre-existing martensite). Therefore, since f and f_m have a similar effect on the rate of bainite formation, the factor f in the kinetics model given in Chapter 3 can be replaced with $(f + f_m)$ in order to incorporate the effects of pre-existing martensite on the bainite kinetics. The presence of martensite would also affect the carbon enrichment of austenite since martensite can trap carbon either in form of carbides (tempered martensite) or as supersaturated martensitic ferrite (as shown in Section 4.3.4). As mentioned in Chapter 3, $T_0^{'}$, T_h and Q_G^* are a function of carbon concentration of austenite, X_γ, which varies as bainite formation progresses. It should be noted that if the factor f is replaced with $(f + f_m)$ while calculating X_γ in Equation 3.10, $T_0^{'}$, T_h and Q_G^* values will vary accordingly.

4.2. Experiments

Dilatometer studies carried out in [3] were used to validate the modified model proposed in this work. A steel with nominal composition Fe-0.2C-3.52Mn-1.52Si-

0.25Mo-0.04Al (in wt-%) (or, Fe-0.91C-3.49Mn-2.96Si-0.04Mo-0.08Al (in at-%)) was used in the study.

Dilatometer samples were first completely austenized at 900 °C for 4 min. The samples were then quenched to and isothermally held at temperatures ranging from 370 °C to 270 °C for 1 h. Finally, the samples were quenched to room temperature. The experimentally obtained M_s temperature of the steel is approximately 320 °C. It should be noted that during isothermal bainite treatments below the M_s temperature, a certain fraction of athermal martensite will have already formed prior to the start of bainite formation. The detailed experimental procedure is given in [3].

Optical microscopy and scanning electron microscopy were carried out to understand the microstructural evolution within the samples as a result of the heat treatments [3]. Microstructural studies revealed the possibility of macro-segregation of Mn within the steel used in this study (shown in Section 4.3.1). Electron probe microanalysis (EPMA) experiments were carried out to investigate the macro-segregation of Mn and to understand the distribution of alloying elements within the steel.

4.3. Results and discussion

The modified model was compared with experimentally obtained kinetic data for bainite formation both above and below M_s temperatures. The results inferred from this study are discussed in the following sections.

4.3.1. Experimental results

The experimentally determined evolution of bainite fraction under different isothermal conditions as a function of time is given in Figure 4.1. The detailed procedure for the calculation of the reported volume fraction of bainite as well as martensite formed prior to bainite formation is described in [3]. The martensite fractions prior to bainite formation and the experimentally obtained bainite fraction at the end of the isothermal steps are given in Table 4.1 as well.

Figure 4.1(a) shows the evolution of bainite fraction as a function of time in the absence of previously formed martensite, while Figure 4.1(b) shows the bainite formation kinetics in the presence of previously formed martensite. In Figure 4.1(b), the value on the y-axis at the start of the treatment gives the fraction of martensite formed prior to each isothermal treatment. The x-axis gives the holding time at the isothermal step during which bainite formation occurs. The isothermal step is

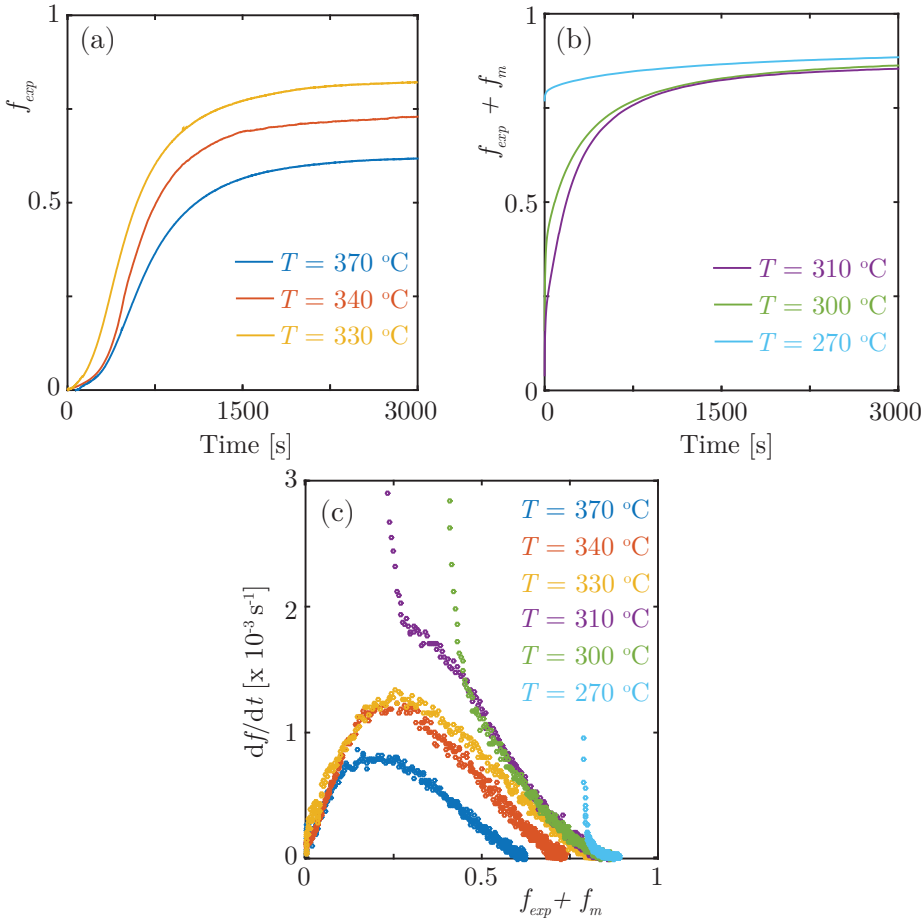

Figure 4.1: Experimentally obtained bainite fraction, f_{exp}, as a function of time (a) in the absence of any athermal martensite, i.e. above M_s conditions, and (b) in the presence of pre-formed athermal martensite, i.e. below M_s conditions. (c) Experimentally obtained rate of bainite formation, (df/dt), as a function of combined bainite-martensite ($f_{exp} + f_m$) fraction at different isothermal conditions. f_m is 0 when T>=320°C.

Table 4.1: Experimentally determined bainite fraction at the end of the isothermal treatment, f_{exp} and the martensite fraction, f_m, formed during the initial quench from austenitization temperature.

T [°C]	f_{exp}	f_m
370	0.62	0
340	0.74	0
330	0.83	0
320	0.84	0
310	0.82	0.04
300	0.71	0.16
270	0.12	0.77

considered to start (time = 0 on the x-axis) at the moment the prior cooling step, from the austenitization temperature, terminates. It should be noted that although dilatometer is programmed to terminate the aforementioned cooling step at the intended isothermal bainite formation temperature, this is not accurately realized during the experiments. A small undercooling (2-5 °C) below the intended isothermal temperature is usually observed. However, the sample temperature quickly stabilizes to the intended temperature (± 0.1 °C) within a couple of seconds.

Based on Figure 4.1(a) and Figure 4.1(b), the rate of bainite formation as a function of bainite evolution in the absence and in the presence of previously formed martensite is calculated in Figure 4.1(c). It should be stated that since Figure 4.1(c) is plotted as a function of combined bainite and martensite fractions, the rate of bainite formation curves are shifted depending on the fraction of previously formed martensite (Table 4.1). The rate of bainite formation due to bainite nucleation at γ/γ interfaces and α_b/γ interfaces is influenced by both bainite and martensite fraction when bainite forms in the presence of previously formed martensite as explained in Section 4.1. During bainite formation above M_s temperature, it can be seen from Figure 4.1(c) that the rate of bainite formation initially increases until a certain fraction of bainite is reached and then decreases as further bainite is formed. Furthermore, it can also be clearly seen that the presence of martensite fraction prior to bainite formation influences the rate of the bainite formation. During bainite formation below M_s, Figure 4.1(c) shows that the rate of bainite formation is relatively high in the early phases of bainite formation. The rate of bainite formation rapidly decreases after certain fraction of bainite is formed and then follows a trend similar to the one observed when bainite forms above M_s. In terms of absolute values, Figure 4.1(c) shows that the rate of bainite formation in the presence of martensite is typically higher almost throughout the bainite formation process. This can be seen especially in the case of bainite formation at 310 °C and 300 °C.

Based on Figure 4.1(c), a qualitative description for bainite formation process in the presence of previously formed martensite can be envisaged. When bainite forms below M_s, bainitic ferrite initially forms quickly, presumably at α_m/γ interfaces, resulting in the fast initial bainite kinetics. Once these interfaces are consumed, the bainite formation proceeds at a speed controlled by austenite grain-boundary bainite nucleation and autocatalytic bainite nucleation which peaks again until a certain bainite fraction is reached and then the rate of bainite formation slows down. This is similar to the trend seen when bainite forms above M_s where bainite forms only via grain-boundary nucleation and autocatalytic nucleation. This results in a peak (at $f_{exp} \approx 0.2$-0.3) as seen in Figure 4.1(c) (at all bainite formation temperatures above M_s where $f_M = 0$ and at 310 °C where $f_M = 0.04$). In case of bainite formation at 300 °C and 270 °C, the rate of bainite formation only slows down after initial fast kinetics due to the presence of α_m/γ interfaces since the combined bainite-martensite fraction is too high ($f_{exp} + f_M > 0.2$). These results are in line with the assumptions proposed in Section 4.1 suggesting that $(\mathrm{d}f/\mathrm{d}t)_M$ tends to zero after a certain fraction of bainite is formed. Furthermore, the higher overall rate of bainite formation in the presence of previously formed martensite even after $(\mathrm{d}f/\mathrm{d}t)_M$ tends to zero can be attributed to the increase in density of nucleation sites. The presence of α_m/γ interfaces leads to an increase in the rate of autocatalytic nucleation as discussed earlier (Equation 4.2). A further understanding of this trend is discussed in Section 4.3.2.

The results of the optical microscopy studies carried out on the samples obtained after various heat treatments is given in Figure 4.2. These results show a certain degree of inhomogeneity in the microstructural evolution depending on the transformation temperature at which bainite formation occurs. At relatively high bainite formation temperatures (above 340 °C), a banded microstructure can be observed (Figure 4.2(a)) where certain bands clearly show bainite while some bands appear to remain untransformed during the bainite formation stage. It must be noted that 2% Nital etchant was used to reveal the microstructures. Nital etches the bainitic regions while martensite and retained austenite regions remain unetched [5]. The banded microstructure is a result of inhomogeneous distribution of Mn within the steel as shown by EPMA results in Figure 4.2(d), which is due to macro-segregation of Mn introduced during the casting and rolling of the as-received steel. Thermodynamic calculations indicate that the driving force for both bainite nucleation and bainite growth decreases as the Mn content increases. Furthermore, comparing Figure 4.2(a) and Figure 4.2(b), it can be seen that the severity of the banded

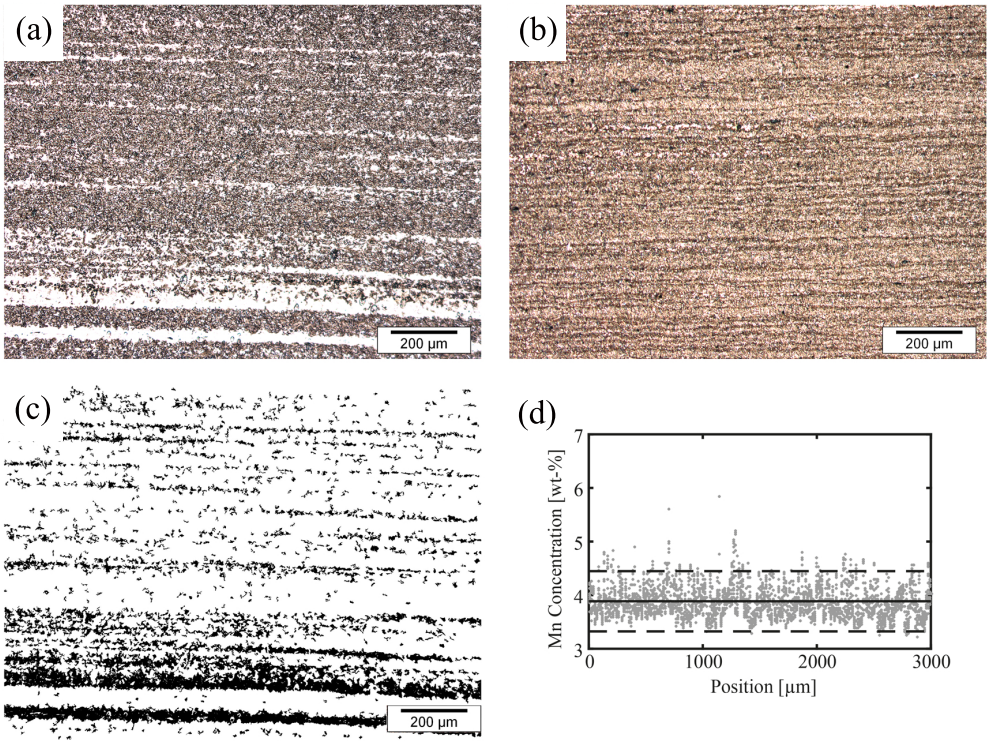

Figure 4.2: (a) Microstructural evolution following bainite formation treatment at 370 °C. Banded microstructure can be seen with bainite (etched; dark) and martensite/retained austenite (unetched; white) regions. (b) Microstructural evolution following bainite formation treatment at 310 °C. The severity of banding is reduced (fully etched; dark). (c) Areas indicating austenite fraction completely immune to bainite formation at 370 °C (black regions). This fraction of austenite is stabilized due to high Mn content in these regions. (d) EPMA results showing Mn distribution over a length of 3 mm within the steel used in the study.

microstructure, or in other words the resistance to bainite formation, decreases as the bainite formation temperature decreases. Such a trend can be attributed to increasing undercooling (or increasing driving force) for both bainite growth and bainite nucleation for a given Mn distribution in the steel.

It is evident from the above discussion that Mn segregation results in certain fraction of stable austenite which remains completely immune to bainite formation throughout the isothermal holding step, especially at higher bainite formation temperatures (as evidenced in Figure 4.2(a)). Furthermore, this stable austenite fraction decreases with decreasing bainite formation temperature since the undercooling increases. This implies that the experimentally obtained bainite fraction

Table 4.2: Adjusted fraction of bainite, f_{ad}, considering inhomogeneous Mn distribution. T is the bainite formation temperature, f_{exp} is the experimentally determined bainite fraction and $f_{\gamma Mn}$ gives the Mn-rich austenite fraction immune to bainite formation.

T [°C]	f_{exp}	$f_{\gamma Mn}$	f_{ad}
370	0.62	0.18	0.75
340	0.74	0.08	0.80
330	0.83	0.01	0.84
320	0.84	0.01	0.85
310	0.82	0	0.82
300	0.71	0	0.71
270	0.12	0	0.12

is underestimated since bainite formation only proceeds within a limited austenite matrix and the degree of this underestimation varies with bainite formation temperature. Thus, in order to compare bainite kinetics obtained at various temperatures, the total volume fraction of bainite formed at a given transformation temperature is thus adjusted by considering only the fraction of austenite where bainite formation occurs. Physically, this adjusted fraction of bainite formed, f_{ad}, signifies the fraction of bainite that would have formed if bainite formation was not restricted by inhomogeneities in Mn distribution and it can be given by

$$f_{ad} = \frac{f_{exp}}{1 - f_{\gamma Mn}} \tag{4.3}$$

where f_{exp} is the experimentally determined bainite fraction and $f_{\gamma Mn}$ is the Mn-rich austenite fraction which remains untransformed throughout the isothermal holding step. $f_{\gamma Mn}$ is analogous to $(f_\gamma)_u$ discussed in Chapter 3. $(f_\gamma)_u$ gives the austenite fraction which is stabilized as a result of carbon enrichment of austenite during bainite formation. $f_{\gamma Mn}$ was determined by image analysis of micrographs obtained. Using the banded structure seen in optical micrographs (Figure 4.2(a)), untransformed austenite bands during the isothermal bainite formation treatment can be isolated (black regions in Figure 4.2(c)). The volume fraction of these untransformed austenite bands, $f_{\gamma Mn}$, is assumed to be equal to the area fraction of the black regions in Figure 4.2(c). It should be noted that the untransformed austenite from the bainite formation stage partially transforms into martensite during final cooling leading to a retained austenite/untempered fresh martensite microstructure (which can be identified in the optical micrographs). The experimentally determined volume fraction of bainite and the volume fraction of bainite after adjusting for Mn distribution (Equation 4.3) are tabulated in Table 4.2.

Table 4.3: Values for the constants used in relating experimental observations with the bainite formation model.

Parameter	Value	Reference
$T_{h\bar{X}}$	821 K	Thermo-Calc
C_1	2271 K/at.fr.	Thermo-Calc
$T_{0\bar{X}}$	818 K	Thermo-Calc
C_2	7165 K/at.fr.	Thermo-Calc
K_Γ	130 J/mol K	[6]
m	0.018 /K	[7]

4.3.2. Comparison of experimental data with calculated kinetics

With the help of the modified kinetic model proposed in this work, the experimentally obtained bainite kinetics is compared with the model calculated bainite kinetics. The values for the various constants used for the model are given in Table 4.3. They were obtained using Thermo-Calc as well as different empirical equations [6, 7], as mentioned in [8]. The final bainite fraction given in Figure 4.3 is based on the adjusted bainite fraction, f_{ad}, as tabulated in Table 4.2.

Figure 4.3(a) and Figure 4.3(b) show the comparison between experimentally obtained and model derived bainite kinetics when the bainite formation temperature is above the M_s temperature. It can be seen that calculated and experimentally obtained kinetics agree well. It should be noted that the experimental kinetics was obtained using dilatometer experiments and over 7000 data points were recorded during the isothermal step where bainite formation occurs. Since the purpose of Figure 4.3 is to highlight the good correlation between the model and the experimental data, only a few, but a representative set, of the experimentally obtained data points is shown.

The modified kinetic model is derived based on the nucleation kinetics of bainite at γ/γ interfaces and α_b/γ interfaces only. However, at temperature below M_s, bainite formation can occur at α_m/γ interfaces as well which is not accounted for by the model. But, considering the results discussed in Section 4.3.1 and seen in Figure 4.1(c), only the kinetic data pertaining to the first few data points which show high rate of bainite formation is attributed to the bainite formation due to nucleation at α_m/γ interfaces. The rest of the kinetic data is controlled by bainite formation due to austenite grain-boundary and autocatalytic nucleation and thus, this partial experimental data set (see Figure 4.3(d)) is used to compare the experimentally obtained kinetics with the model when bainite is formed below M_s. The corresponding results are shown in Figure 4.3(c) and Figure 4.3(d). It can be

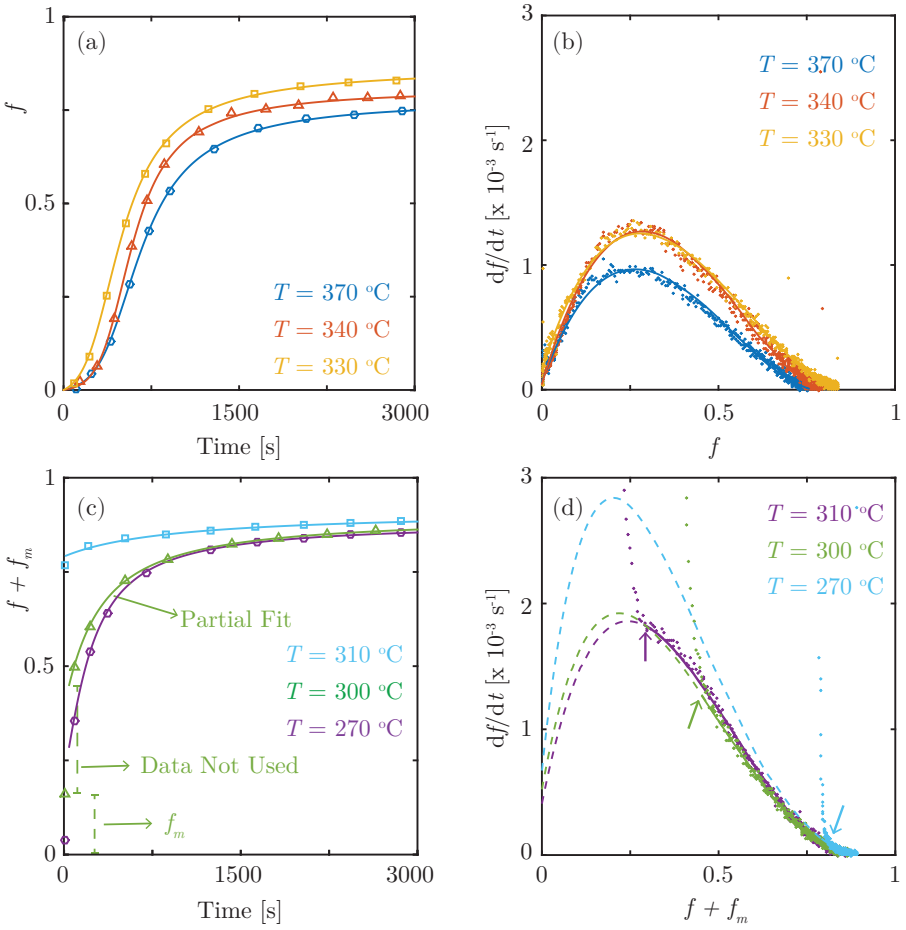

Figure 4.3: Comparison of bainite kinetics. f_{ad} (markers) and model derived (lines) bainite fraction as a function of time (a) in the absence of any martensite and (c) in the presence of previously formed martensite. Experimentally determined (dots) and model derived (solid lines) rate of bainite formation (b) in the absence of any martensite and (d) in the presence of previously formed martensite. In (c, d), a partial fit is used to compare the model with experimental data. In (c), the solid line (model based results) do not cover all markers (experimental data) showing the length of the partial fit. This is highlighted with text as well for T=300 °C case. Similar partial fit is used in all cases. In (d), the solid line shows the model calculated rate of bainite formation. Based on this fit, the rate of bainite formation is extrapolated to the entire data range to calculate the influence of autocatalytic and grain-boundary nucleation alone. The arrows in (d) indicate the end of extrapolation and start of partial fit.

seen that the kinetic model fits well when compared with the experimentally obtained data once the α_m/γ interfaces are consumed during bainite formation. In Figure 4.3(d), the dots give the experimentally obtained rate of bainite formation as a function of combined bainite-martensite fraction. The solid line gives the calculated rate of bainite formation estimated by the model when it is fitted to the partial experimental data set. The dashed line in Figure 4.3(d) shows the rate of bainite formation extrapolated over the entire time-scale of the bainite formation treatment based on the model parameters obtained using the partial fitting. Physically, this extrapolation gives the rate of bainite formation if it was only governed by autocatalytic nucleation and grain-boundary nucleation.

Based on results obtained in Figure 4.3, a few important conclusions can be derived. Firstly, the existing kinetic theory based on the displacive mechanism of bainite formation [8–12] and the formalism of kinetic model proposed in [8] can be used to accurately describe the bainite formation kinetics in the presence of pre-existing martensite once a certain fraction of bainite is formed. Similar analysis has been proposed recently by Samanta et al. [13]. Secondly, any effect of pre-existing martensite on the kinetics of bainite formation fades once the bainite formation progresses.

Both the complete fitting (for data obtained above M_s temperature) and the partial fitting (for data obtained below M_s temperature) of the experimentally determined data with the kinetic model yields corresponding model parameters. Figure 4.4(a) shows the variation in $Q^*_{G\bar{X}}$ parameter as a function of undercooling $(T_h - T)$. It can be seen that $Q^*_{G\bar{X}}$ decrease linearly with increasing undercooling. A linear trend compares well with similar results reported in the literature [12, 14]. Similar results were observed in Chapter 3 as well. It must be also noted in Figure 4.4(a) that the linear trend obtained for the variation in $Q^*_{G\bar{X}}$ as a function of undercooling can be extrapolated to the entire temperature range where austenite to bainite formation is possible, regardless of the presence of pre-existing martensite. The linear trend (dashed line in Figure 4.4(a)) is fit based only on $Q^*_{G\bar{X}}$ values obtained when bainite formation occurs above M_s and the $Q^*_{G\bar{X}}$ values obtained when bainite formation below M_s falls along this linear trend.

Figure 4.4(b) shows the variation in $Q^*_{A\bar{X}}$ as a function of undercooling $(T_h - T)$. Similar to Figure 4.4(a), $Q^*_{A\bar{X}}$ decreases linearly with increasing undercooling when bainite formation occurs above M_s. However, unlike Figure 4.4(a), the linear trend cannot be extrapolated to transformation temperatures where bainite formation occurs below the M_s. As seen in Figure 4.4(b), the calculated $Q^*_{A\bar{X}}$ values based on

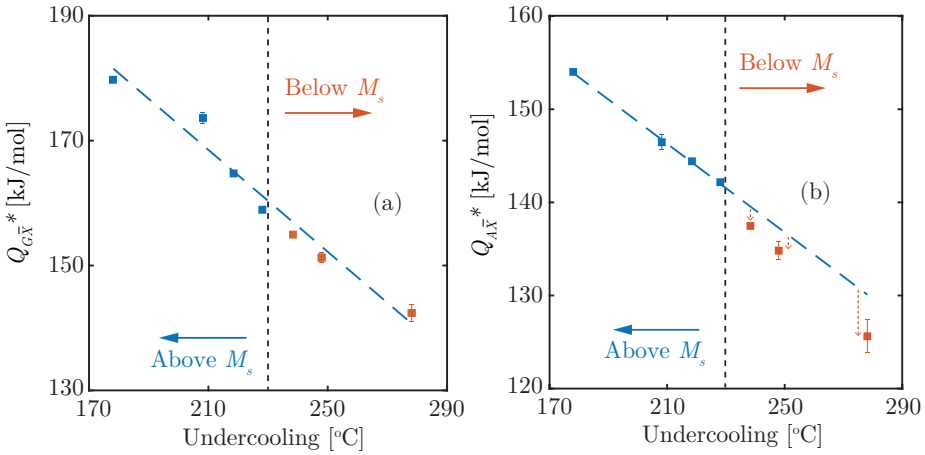

Figure 4.4: Variation of (a) $Q^*_{G\bar{X}}$ and (b) $Q^*_{A\bar{X}}$ as a function of undercooling ($T_h - T$). Square data points give the respective activation energy values derived from the model fitting parameters. The dashed line represents the linear fit considering only the activation energy values obtained when bainite formation occurs above M_s. The error bar gives the 95% confidence interval. In case the error bar is not visible, the margin of error is less than 1 kJ mol^{-1}.

the obtained kinetic data is slightly below predicted trend.

As mentioned earlier in Section 4.1, the presence of previously formed martensite leads to an increased rate of autocatalytic nucleation. On the other hand, bainite nucleation at α_m/γ interfaces would not have any effect on bainite nucleation at γ/γ interfaces and can be considered as two separate events which will proceed based on local conditions at the respective interfaces. These observations are corroborated by results seen in Figure 4.4. The variation in $Q^*_{G\bar{X}}$ as a function of undercooling (Figure 4.4(a)) shows that the activation energy for grain-boundary nucleation does not depend on the presence of previously existing martensite and only depends on transformation temperature. This also serves as a validation for the values of fitting parameters obtained based on the partial fitting of experimental data with the proposed kinetic model. Figure 4.4(b) shows that autocatalytic nucleation is however influenced by the presence of previously existing martensite. It should be noted that the kinetic model proposed in Chapter 3 and Section 4.1 is used to calculate the $Q^*_{G\bar{X}}$ and $Q^*_{A\bar{X}}$ given in Figure 4.4. As described previously, the model does not incorporate the influence of previously formed martensite and consequently does not account for increase in autocatalytic nucleation sites due to presence of α_m/γ interfaces. Thus, when compared with the experimental results, the model estimates a lower $Q^*_{A\bar{X}}$ when bainite forms below M_s to compensate for

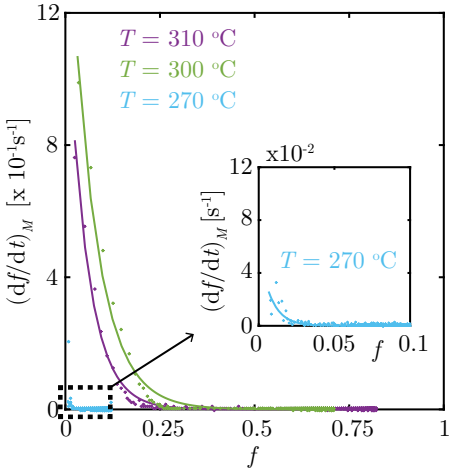

Figure 4.5: The rate of bainite formation at α_m/γ interfaces, $(\mathrm{d}f/\mathrm{d}t)_M$, which is calculated as the difference between the experimentally determined rate of bainite formation and the sum of $(\mathrm{d}f/\mathrm{d}t)_G$ and $(\mathrm{d}f/\mathrm{d}t)_A$. The dots give the calculated difference and the solid line represents an exponential fit of the calculated difference.

the underestimated autocatalytic nucleation sites and elucidate the increased rate of autocatalytic nucleation.

4.3.3. Impact of pre-existing martensite on bainite kinetics

Based on the results obtained in Section 4.3.1 and Section 4.3.2, it is clear that the presence of martensite prior to bainite formation accelerates its kinetics. This acceleration is due to bainite nucleation at α_m/γ interfaces as well as autocatalytic nucleation of bainite as result of α_b/γ interfaces created during bainite formation at α_m/γ interfaces (Equation 4.2).

Using Equation 4.1, the rate of bainite formation due to bainite nucleation at α_m/γ interfaces can be derived by estimating the difference between the experimentally obtained rate of bainite formation and the sum of $(\mathrm{d}f/\mathrm{d}t)_G$ and $(\mathrm{d}f/\mathrm{d}t)_A$. This difference is plotted as a function of bainite evolution in Figure 4.5 with the help of calculations reported in Figure 4.3(d). It should be noted that Figure 4.3(d) gives both the experimentally obtained overall rate of bainite formation as well as the model estimated sum of $(\mathrm{d}f/\mathrm{d}t)_G$ and $(\mathrm{d}f/\mathrm{d}t)_A$. Published results on the crystallography of bainite and martensite suggest that both the α_b/γ interface and the α_m/γ interface are typically a coherent or a semi-coherent interface and show a defined orientation relationship (near Kurdjumov-Sachs or near Nishiyama-Wasserman relationship) [15, 16]. Furthermore, at temperatures where bainite formation or

martensite formation occurs, partitioning of substitutional solute atoms does not occur [17, 18]. Thus, it can be assumed that the nucleation of bainite at a α_m/γ interface would be similar to the autocatalytic nucleation of bainite at a α_b/γ interface. This implies that the rate of bainite formation due to autocatalytic nucleation and due to the presence of α_m/γ interfaces can be compared with each other.

As already noted, the rate of bainite formation typically depends on two factors - activation energy for bainite nucleation and number density of nucleation sites. Based on the above mentioned similarities between α_b/γ interfaces and α_m/γ interfaces, it can be postulated that the activation energy for bainite nucleation would be similar in both cases. However, the number density of α_b/γ interfaces depends on the bainite fraction whereas the number density of α_m/γ interfaces depends on the previously formed martensite fraction. With the help of the above discussion and using Figure 4.5, the rate of bainite formation at α_m/γ interfaces can be given in terms of rate of bainite formation due to autocatalytic nucleation as

$$\left(\frac{\mathrm{d}f}{\mathrm{d}t}\right)_M = \frac{(\mathrm{d}f/\mathrm{d}t)_A}{(1-f)f}\left(\beta_1 \exp\left(-\beta_2 f\right)\right) \tag{4.4}$$

where β_1 and β_2 are constants. The factor $(1-f)f$ accounts for the number density of autocatalytic nucleation sites and the term $(\mathrm{d}f/\mathrm{d}t)_A/(1-f)f$ gives the rate of bainite formation due to autocatalytic nucleation per unit density of α_b/γ interfaces. $(\mathrm{d}f/\mathrm{d}t)_A$ can be calculated using the model and the model parameters obtained in Section 4.3.2. Using Equation 4.4 and Figure 4.5, the β_1 and β_2 are calculated for different bainite formation treatments carried out in the presence of previously formed martensite (Table 4.4). It can be noted that β_1 increases with increasing martensite fraction (decreasing bainite formation temperature). On the other hand, β_2 initially decreases with increasing prior martensite fraction (decreasing bainite formation temperature) and then increases when the martensite fraction is considerable (in this case $\approx 77\%$). These values indicate that the accelerating effect of α_m/γ interfaces is considerably high at the start of the bainite formation process and depends on the fraction of martensite present. This accelerating effect decreases exponentially as bainite formation continues. The exponential decay may be related to the availability of α_m/γ interfaces which initially increases with increasing martensite fraction and later decreases as a result of increasing austenite decomposition. Additionally, a higher initial martensite fraction implies that the subsequent carbon enrichment of austenite would be higher as well due to carbon partitioning from martensite to austenite during the isothermal step. This will increase the activation energy of bainite nucleation at α_m/γ interfaces resulting in

Table 4.4: β_1 and β_2 values obtained as a function of bainite formation temperature, T, when $T < M_s$.

T [°C]	f_m	β_1	β_2
310	0.04	10	15
300	0.16	18	10
270	0.77	73	131

slower kinetics. This implies that the impact of previously formed martensite on bainite kinetics depends on the fraction of martensite present which influences the density of nucleation sites where bainite can form and the carbon concentration of the austenite. These factors determine the acceleration of bainite formation.

Based on Equation 4.2, the total impact of pre-existing martensite on bainite kinetics can be quantified as the sum of $(\mathrm{d}f/\mathrm{d}t)_M$ and $(\mathrm{d}f/\mathrm{d}t)_{AM}$. Alternatively, the difference between the overall experimentally obtained rate of bainite formation and the sum of $(\mathrm{d}f/\mathrm{d}t)_G$ and $(\mathrm{d}f/\mathrm{d}t)_{AG}$ would give the impact of pre-existing martensite on bainite kinetics. The kinetic model described can be used to estimate the sum of $(\mathrm{d}f/\mathrm{d}t)_G$ and $(\mathrm{d}f/\mathrm{d}t)_{AG}$ terms. Figure 4.4 gives the variation of $Q^*_{G\bar{X}}$ and $Q^*_{A\bar{X}}$. It is self-evident that $Q^*_{G\bar{X}}$ determines $(\mathrm{d}f/\mathrm{d}t)_G$ and $Q^*_{A\bar{X}}$ determines $(\mathrm{d}f/\mathrm{d}t)_A$ (Chapter 3). Since $(\mathrm{d}f/\mathrm{d}t)_{AM}$ is 0 when bainite formation is carried out in the absence of α_m/γ interfaces, $Q^*_{A\bar{X}}$ determines $(\mathrm{d}f/\mathrm{d}t)_{AG}$ under such conditions. Figure 4.4(b) shows that $Q^*_{A\bar{X}}$ decreases linearly above M_s. Based on the above discussion, it can be postulated that if this linear trend based on above-M_s data points can be extrapolated, $Q^*_{A\bar{X}}$ predicted by this extrapolation can be used to determine $(\mathrm{d}f/\mathrm{d}t)_{AG}$ at a given temperature below M_s. This predicted $Q^*_{A\bar{X}}$ as well as the obtained $Q^*_{G\bar{X}}$ (Figure 4.4(b)) is used to recalculate the bainite kinetics using the model. Physically, the results give the sum of $(\mathrm{d}f/\mathrm{d}t)_{AG}$ and $(\mathrm{d}f/\mathrm{d}t)_G$ terms which is the rate of bainite formation assuming that there is no influence of martensite formation at all. Figure 4.6 gives a comparison between the predicted rate of bainite formation without any influence of pre-existing martensite and experimentally obtained kinetics when bainite forms below M_s temperatures.

4.3.4. Physical parameter X_b

Table 4.5 shows the variation of X_b as a function of bainite formation temperature. It can be seen in Table 4.5 that X_b is higher at lower bainite formation temperatures. Microstructural observations detailed in [3] show that when bainite formation occurs above 340 °C in the steel studied in this work, cementite precipitation is completely suppressed. However, as bainite formation temperature decreases, the possibility of

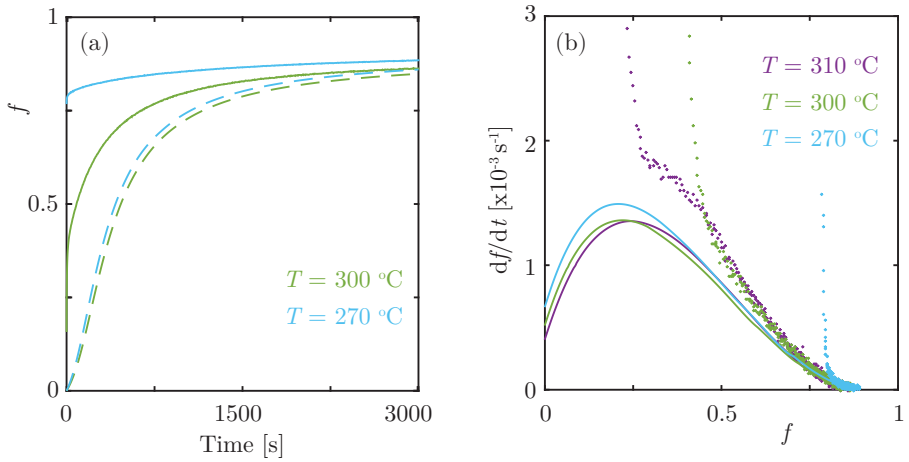

Figure 4.6: (a) Experimentally determined (solid line) bainite evolution in the presence of previously formed martensite and model predicted (dashed line) bainite evolution excluding the influence of previously formed martensite on bainite kinetics. (b) Experimentally determined (dots) rate of bainite formation during below M_s conditions and calculated (lines) rate of bainite formation excluding the influence of previously formed martensite.

lower-bainite formation increases. Furthermore, as the bainite formation temperature drops below the M_s temperature, austenite also decomposes into martensite prior to bainite formation. The X_b values shown in Table 4.5 are in line with these results. If cementite formation is completely suppressed, the amount of carbon trapped within bainite would be relatively low and more carbon would be available for carbon enrichment of surrounding austenite. Therefore, the X_b value would be relatively low as well. As the probability of lower-bainite formation increases and/or as more martensite formation occurs, the amount of carbon available for carbon enrichment of the austenite will be lower since more carbon would become trapped within the bainitic or martensitic regions. This would result in a higher X_b value.

4.4. Conclusions

The studies carried out in this work show that the existing kinetic theory for displacive bainite formation can be used to describe grain-boundary and autocatalytic bainite formation in conditions both above and below M_s. Using the existing kinetic theory for bainite formation, the role of α_m/γ interfaces on the overall rate of bainite formation is isolated and quantified in detail. An equation to describe the rate of bainite nucleation at α_m/γ interfaces has been proposed in this work.

The results indicate that bainite formation in the presence of previously formed

Table 4.5: X_b values obtained as a function of bainite formation temperature, T ($\bar{X} = 0.91$ at%). The calculated standard error of the X_b values is less than 0.03 at%.

T [°C]	X_b [at%]
370	0.164
340	0.187
330	0.405
320	0.466
310	0.433
300	0.489
270	0.520

martensite begins at both γ/γ interfaces as well as α_m/γ interfaces. The rate of bainite formation at α_m/γ interfaces does not affect bainite formation at γ/γ interfaces. However, bainite formation at α_m/γ interfaces leads to the creation of α_b/γ interfaces which can facilitates autocatalytic nucleation. The role of the α_m/γ interfaces on the rate of bainite nucleation is closely dependent on the fraction of the pre-existing martensite. The fraction of pre-existing martensite can affect both the number density of nucleation sites and carbon enrichment of austenite. As the pre-existing martensite fraction increases, the rate at which bainite formation starts, increases. However, the overall rate of bainite formation decreases quickly as the available α_m/γ interfaces are consumed and carbon enrichment of austenite increases due to carbon partitioning from martensite to austenite.

References

[1] H. Vetters, J. Dong, H. Bornas, F. Hoffmann, H.-W. Zoch, *International Journal of Materials Research* **97**, 1432 (2006).

[2] W. Gong, Y. Tomota, S. Harjo, Y. Su, K. Aizawa, *Acta Materialia* **85**, 243 (2015).

[3] A. Navarro-López, J. Sietsma, M. Santofimia, *Metallurgical and Materials Transactions A* **47**, 1028 (2016).

[4] H. Kawata, M. Takahashi, K. Hayashi, N. Sugiura, N. Yoshinaga, *THERMEC 2009* (Trans Tech Publications, 2010), vol. 638 of *Materials Science Forum*, pp. 3307–3312.

[5] B. Bramfitt, A. Benscoter, *Metallographer's Guide: Practice and Procedures for Irons and Steels* (ASM International, 2001).

[6] S. van Bohemen, *Metallurgical and Materials Transactions A* **41**, 285 (2010).

[7] S. van Bohemen, J. Sietsma, *Materials Science and Technology* **25**, 1009 (2009).

[8] A. Ravi, J. Sietsma, M. Santofimia, *Acta Materialia* **105**, 155 (2016).

[9] G. Rees, H. Bhadeshia, *Materials Science and Technology* **8**, 985 (1992).

[10] M. Santofimia, F. Caballero, C. Capdevila, C. Garcia-Mateo, C. de Andres, *Materials Transactions* **47**, 1492 (2006).

[11] H. Bhadeshia, *Journal de Physique* **43**, 443 (1982).

[12] S. van Bohemen, J. Sietsma, *International Journal of Materials Research* **99**, 739 (2008).

[13] S. Samanta, P. Biswas, S. Singh, *Scripta Materialia* **136**, 132 (2017).

[14] H. Bhadeshia, *Bainite in Steels: Transformations, Microstructure and Properties*, Matsci Series (IOM Communications, 2001).

[15] N. Takayama, G. Miyamoto, T. Furuhara, *Acta Materialia* **60**, 2387 (2012).

[16] G. Miyamoto, N. Takayama, T. Furuhara, *Scripta Materialia* **60**, 1113 (2009).

[17] H. Bhadeshia, A. Waugh, *Acta Metallurgica* **30**, 775 (1982).

[18] F. Caballero, M. Miller, S. Babu, C. Garcia-Mateo, *Acta Materialia* **55**, 381 (2007).

5

Impact of austenite grain boundaries and ferrite nucleation on bainite kinetics

It doesn't matter how beautiful your theory is,
it doesn't matter how smart you are.
If it doesn't agree with experiment, it's wrong.

Richard Feynman

The mere observation of a phenomenon
inevitably changes that phenomenon.

Observer Effect

The contents of this chapter have been submitted for publication in Acta Materialia under the title 'Impact of austenite grain boundaries and ferrite nucleation on bainite kinetics'.

The influences of the composition of the steel and the temperature at which the bainite formation occurs on isothermal bainite formation kinetics is discussed in detail in Chapter 3. Additionally, the overall heat treatment which is applied prior to the bainite formation process influences the kinetics of bainite formation. For instance, parent austenite grain size, prior martensite formation and prior ferrite formation have all been shown to influence the rate of subsequent bainite formation [1–11]. The influence of martensite/austenite (α_m/γ) interfaces on bainite formation is discussed in Chapter 4. The effect of parent austenite grain size and prior ferrite formation on bainite kinetics is, although, still under debate. Some studies show that these parameters accelerate the bainite formation kinetics [3, 4, 10] while other studies show the contrary [5, 6, 11]. It must be pointed out that studies regarding the effect of ferrite formation prior to bainite formation are very scarce in the literature. Such studies are nevertheless essential for efficient development of multi-phase microstructures where ferrite formation may precede bainite formation.

In addition to phase transformations prior to bainite formation, the austenite grain boundary condition, i.e., presence of interface precipitates or segregation of alloying elements to the austenite grain boundaries, affects the rate of bainite formation. Umemoto et al. [12] showed that precipitation of cementite or FeS at austenite grain boundaries can act as preferential nucleation sites and can lead to an acceleration of bainite kinetics. Furthermore, the elemental distribution of alloying elements in the vicinity of interfaces (such as austenite grain boundaries) will be determined in the prior heat treatments and can affect bainite formation. It should be noted that austenite grain boundaries, which act as sites for bainite nucleation, are regions of defects in a material and solute segregation occurs to these interfaces [13]. The heat treatment affects the transport of solute atoms to these interfaces, both thermodynamically and kinetically. The grain boundary segregation can influence the activation energy for bainite nucleation at austenite grain boundaries and consequently affect rate of bainite formation. Nonetheless, little attention has been paid to understanding the influence of chemical composition in the vicinity of austenite grain boundaries on the rate of bainite formation in the literature.

In this work, a series of heat treatments is carried out to systematically investigate the influence of the overall heat treatment on the rate of bainite formation in a low-carbon silicon-containing steel. The effect of ferrite formation prior to bainite formation as well as the effect of chemical composition at and in the vicinity of austenite grain boundaries is the primary focus of this work. Isothermal bainite formation treatments are carried out directly after complete austenitization treatment

as well as following an intermediate soaking treatment at different temperatures for varying holding times. The intermediate soaking treatment employed prior to the bainite formation step is an isothermal heat treatment at a temperature between the austenitization temperature and the bainite formation temperature. The intermediate soaking treatment affects the austenite grain boundary condition via elemental segregation and/or austenite decomposition into ferrite near the austenite boundaries. It was observed that the kinetics of bainite formation can be influenced by the intermediate soaking treatment. These experiments provide insight into nucleation mechanism of bainitic ferrite at austenite boundaries. Furthermore, with the help of the results obtained from this work, strategies to control the kinetics of bainite formation will be proposed.

5.1. Experiments

A hot rolled steel with a nominal composition of Fe-0.2C-3Mn-2Si (in wt-%) was used in this study. 10 mm long cylindrical dilatometer samples with a diameter of 3.5 mm were machined from the hot-rolled plate. The samples were subjected to various heat treatment conditions in a Bähr DIL805A/D Dilatometer. The detailed time-temperature parameters used during various heat treatments are given in Figure 5.1(a). Some samples were cooled to 400 °C for isothermal bainite formation directly after complete austenitization, while other samples were subjected to an intermediate soaking treatment at different temperatures prior to the isothermal bainite treatment. The experimentally determined A_{c3} temperature of the steel used in this study is approximately 895 °C when a heating rate of 5 °C/s is employed.

In order to further understand the dilatometer results obtained after the heat treatments, the samples were subjected to a series of selected characterization techniques. Microstructural evolution during bainite formation was observed using optical microscopy and Scanning Electron Microscopy (SEM) techniques. Site-specific Atom Probe Tomography (APT) experiments were carried out to study the austenite grain boundary condition in terms of local chemical composition and nano-scale austenite decomposition at the austenite grain boundaries prior to bainite formation. An additional set of heat treatments was employed to produce samples for this APT study. Firstly, the as-received and machined dilatometer samples were homogenized at 1250 °C for 48 h to eliminate any artefacts related to chemical composition as a result of macro-segregation of Mn in the steel. In order to ensure that the samples were not subjected to decarburization during homogenization, the samples were sealed within a quartz tube under argon atmosphere prior to the homogenization

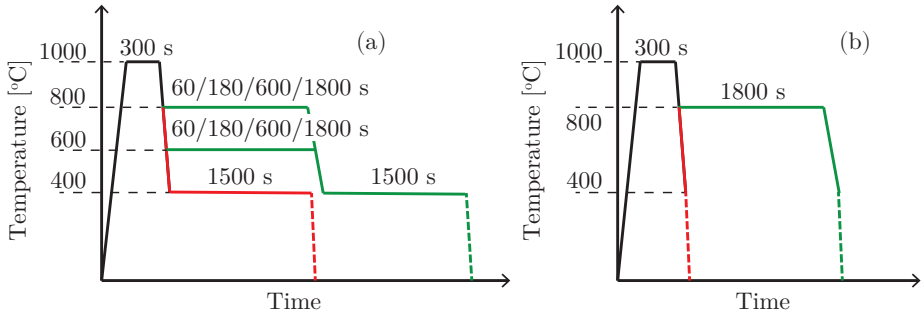

Figure 5.1: (a) Schematic of heat treatment profiles used for understanding the effect of austenite grain boundary pre-conditioning on bainite formation kinetics. (b) Schematic of heat treatment profiles used prior to APT sample preparation. Heating was carried out at a rate of 5 °C/s while all the cooling steps prior to the isothermal bainite treatment were performed at -40 °C/s. After the bainite formation treatment, the samples were cooled to room temperature at a rate of almost -400 °C/s (dashed line).

treatment. Following homogenization, the samples were heat treated according to the thermal profile given in Figure 5.1(b), where some samples were subjected to an intermediate soaking treatment while others were cooled directly to 400 °C similar to the earlier heat treatments. It should be noted that the samples were immediately quenched at a rate of -400 °C/s from 400 °C. Considering such a high cooling rate, it can be assumed that the diffusion processes would not occur during cooling and the solute atoms would be frozen at their respective locations. Thus, the chemical composition observed at the austenite grain boundaries after these heat treatments will provide quantitative information regarding interfacial composition at the austenite grain boundaries prior to the start of the bainite formation at 400 °C.

The site-specific studies were carried out following the steps described in already published works such as [14–16]. Electron Backscatter Diffraction (EBSD) analysis with a step size of 100 nm was carried out on the heat treated samples prepared for APT analysis to understand the crystallography of the microstructures obtained after different heat treatment conditions. EBSD data analysis was performed using TSL OIM software. ARPGE software [17] was employed to perform the prior austenite reconstruction using the EBSD data. With the help of the prior austenite reconstruction analysis, the sites for APT analysis in all samples, namely locations on a general high angle austenite grain boundary, were extracted. The misorientation angles of the isolated general high angle austenite grain boundaries lie within a narrow range of 40° - 45° in order to ensure that results obtained from the APT

measurements on different samples is comparable.

APT specimens were prepared from these isolated grain boundaries via Focused Ion Beam (FIB) milling according to the procedure described in [18]. APT analyses were then performed using a Local Electrode Atom Probe (LEAP 3000XHR, Cameca Instruments). The data obtained from the APT experiments were reconstructed and analyzed using the IVAS software developed by Cameca Instruments. The reconstruction parameters were estimated using the technique described in [19].

5.2. Results

The experimental observations are illustrated in detail in the following sections.

5.2.1. Dilatometer results

Figure 5.2 shows the kinetics of bainite formation at 400 °C in terms of change in length of the sample following complete austenitization and various intermediate soaking treatments. The degree of sample expansion corresponds with the volume fraction of bainite formed [20, 21]. Bainite formation kinetics at 400 °C without any prior intermediate soaking treatment is also plotted in Figure 5.2 (blue lines in Figure 5.2(a)-(d) indicated by intermediate soaking time equal to 0). Figure 5.2(a) and Figure 5.2(b) show change in length of the sample as a function of time while Figure 5.2(c) and Figure 5.2(d) show the corresponding rate of change in length of the dilatometer sample as a function of its length expansion. Since the change in length of the sample is determined by the volume fraction of bainite formed, Figure 5.2(c) and Figure 5.2(d) essentially give the rate of bainite formation as the fraction of bainite increases. Figure 5.2 shows that the soaking time and the soaking temperature used during the intermediate treatment play a role in the acceleration of the subsequent bainite formation. An increase in the intermediate soaking time and/or a decrease in the intermediate soaking temperature increases the degree of acceleration of bainite formation.

Figure 5.3 gives insight into the effect of intermediate soaking time-temperature parameters on the degree of acceleration of bainite formation kinetics. This degree of acceleration, Γ_{200}, is calculated as

$$\Gamma_{200} = \Delta L_{I200} / \Delta L_{O200} \tag{5.1}$$

ΔL_{I200} is the observed change in length of the sample after 200 s from the start of bainite formation treatment following a particular intermediate soaking treatment

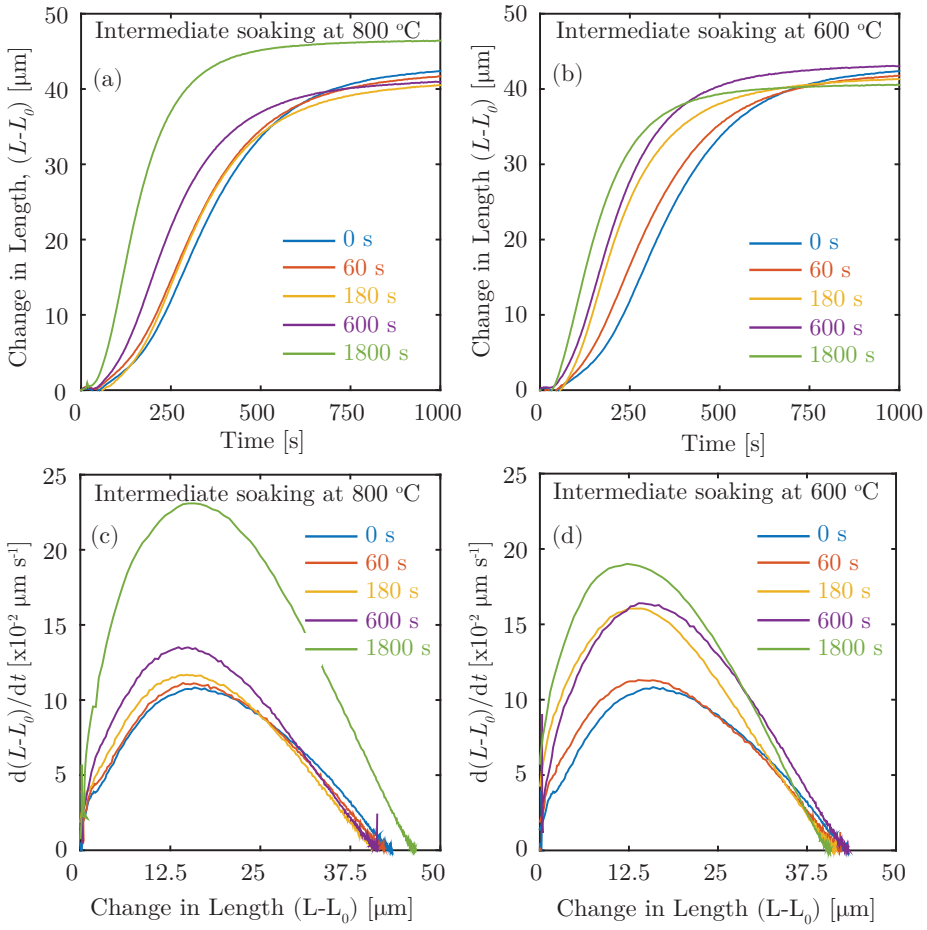

Figure 5.2: Change in length of the sample during bainite formation treatment at 400 °C after intermediate soaking treatment (a) at 800 °C and (b) at 600 °C for varying holding times. Corresponding rate of change of length w.r.t sample length change after intermediate soaking treatment (c) at 800 °C and (d) at 600 °C for varying holding times. In all figures, holding time of 0 seconds represents bainite formation treatment without any intermediate soaking treatment (blue lines).

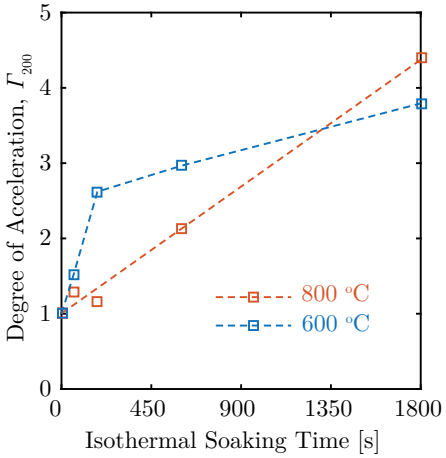

Figure 5.3: Degree of acceleration of bainite formation kinetics, Γ_{200}, as a function of holding time during various intermediate soaking treatments.

and ΔL_{O200} is the corresponding change in length of the sample during bainite formation without intermediate soaking treatment. Γ_{200} is greater than 1 when the intermediate soaking treatment results in the acceleration of bainite formation kinetics. Figure 5.3 shows that, within the range of the experiments performed, Γ_{200} increases linearly with increasing intermediate soaking time when the intermediate soaking temperature is 800 °C. In case of an intermediate soaking at 600 °C, Γ_{200} increases quickly when the intermediate soaking time is short. However, for longer soaking times, Γ_{200} increases at a lower rate. The possible reasons behind these trends are further discussed in Section 5.3.

Thermo-Calc calculations indicate that there is a chemical driving force for austenite to ferrite transformation below 812 °C, which implies that the intermediate soaking treatment can lead to ferrite formation. Figure 5.4 shows the dilatometer results pertaining to the change in the length of the sample during intermediate soaking treatment at 800 °C and 600 °C. Similar to austenite to bainite transformation, ferrite formation leads to an expansion of the sample. Figure 5.4 shows that dilatometry gives no indication of ferrite growth during intermediate soaking treatment at 800 °C while austenite decomposition is indicated to continuously occur during intermediate soaking treatment at 600 °C. Similar results are observed during microstructure analysis and APT experiments as shown in Section 5.2.2 and Section 5.2.3 respectively. It should be noted that in Figure 5.4, the change in length of the sample observed within the first 200 s is related to an instrument error which

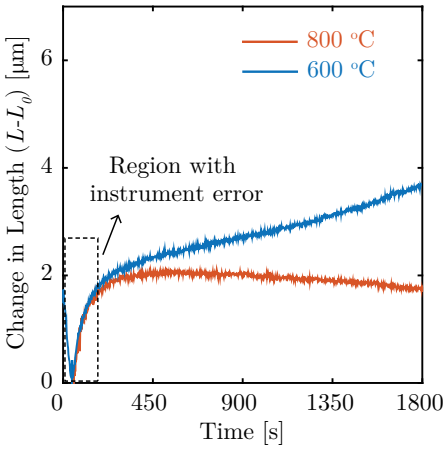

Figure 5.4: Change in length of the sample during intermediate soaking treatment.

is caused due to change in atmosphere within the dilatometer. The cooling step before the intermediate soaking treatment was carried out using a controlled flow of He gas while the isothermal soaking treatment was carried out in vacuum. The time required for the evacuation of the chamber during the intermediate soaking treatment following He injection during the previous cooling step led to the instrumental error seen during the initial 200 s of the intermediate soaking treatment. Figure 5.4 shows that this change in length due to instrumental error is around 2 µm and is independent of annealing temperature. It can be postulated that this instrumental error occurs during bainite formation at 400 °C as well. However, Figure 5.2 shows that the change in length at 400 °C is higher than 2 µm in all cases in the first 200 s of the bainite-formation treatment. Therefore, the recorded sample dilatation during the first 200 s could be attributed to both bainite formation and instrumental error. The instrumental error will influence the calculation of Γ_{200}. However, since this error is constant and independent of annealing temperature (Figure 5.4), trend observed for Γ_{200} in Figure 5.3 would not be affected.

5.2.2. Microstructural evolution

Figure 5.5 sheds light on the microstructural evolution of bainite without and with intermediate soaking treatment. Figure 5.5(a) shows a bainitic microstructure with martensite/austenite islands (formed during final quenching) which is expected to be obtained after a bainite treatment without any intermediate soaking. By comparing the microstructures shown in Figure 5.5 to previously published results [22], it can

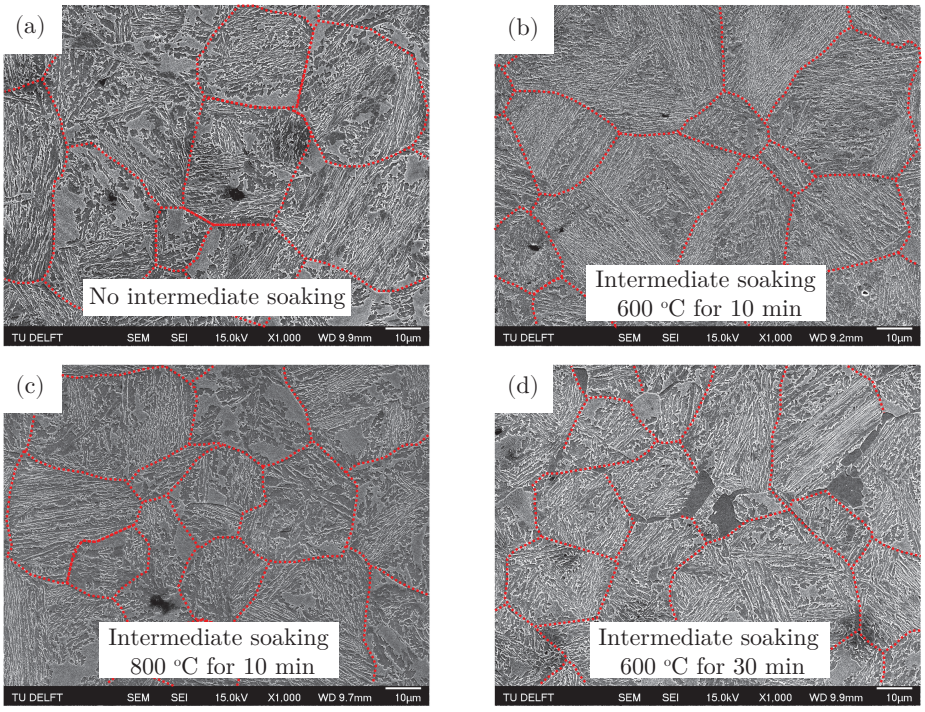

Figure 5.5: Microstructures obtained (a) after bainite treatment without intermediate soaking treatment, (b) after bainite treatment with intermediate soaking treatment at 600 °C for 10 min, (c) after bainite treatment with intermediate soaking treatment at 800 °C for 10 min and (d) after bainite treatment with intermediate soaking treatment at 600 °C for 30 min. Figures (a) - (d) are obtained via SEM analysis. In all figures, needle-shaped regions are bainite while lightly etched or unetched regions are martensite/austenite islands. Also, red dashed lines indicate prior austenite boundaries. In Figures (d), large dark etched islands denote ferrite formed during intermediate soaking treatment. The ferrite islands are observed in the vicinity of prior austenite boundaries.

be postulated that upper bainite forms during the isothermal treatment at 400 °C. Figure 5.5(b) and Figure 5.5(c) give the microstructure obtained when bainite formation treatment was carried out after an intermediate soaking treatment at 600 °C and 800 °C for 10 min. They show that the obtained microstructures are almost identical in spite of the different heat treatment routes. Similar microstructure is obtained when bainite treatment is carried out after an intermediate soaking treatment at 800 °C for 30 min. Unlike these figures, Figure 5.5(d) shows a mixed microstructure where both ferrite and bainite are present. This microstructure was obtained after bainite treatment following an intermediate soaking treatment at 600 °C for 30 min. Based on the image analysis of the obtained optical micrographs, a maximum of 5% ferrite is formed during intermediate soaking treatment at 600 °C for 30 min. These results correspond well with the results presented in Section 5.2.1 where ferrite formation was observed only during the intermediate soaking treatment at 600 °C. Comparing the dilatometer results and the microstructural studies, it can be argued that when a holding time of less than 10 min is employed during intermediate soaking treatment at 600 °C, the fraction of ferrite formed may be too small to be detected via microscopy, while a holding time greater than 10 min leads to observable ferrite growth.

5.2.3. Site specific APT studies

Since dilatometer and microstructural studies did not reveal any ferrite growth during intermediate treatment at 800 °C, site-specific APT studies were carried out as a higher resolution experiment to explore the reasons behind the accelerating effect of these treatments on subsequent bainite kinetics. APT studies can reveal any local chemical composition variation in the vicinity of parent austenite boundaries as well as any nano-scale ferrite growth as a result of intermediate soaking treatment.

In Figure 5.6, the APT results based on the site-specific investigations carried out in the vicinity of parent austenite boundaries are compiled. Figure 5.6 (a)-(e) show the results from samples which were directly quenched without any prior intermediate soaking treatment (red line in Figure 5.1(b)) while Figure 5.6 (f)-(j) show the results from samples which were quenched after a prior intermediate soaking treatment at 800 °C for 30 min (green line in Figure 5.1(b)). Figure 5.6(a) and Figure 5.6(f) give the location from which the atom probe tips were lifted out for the APT study. In order to calculate the variation in local chemical composition at the interface, a cuboid shaped region of interest (ROI) with dimensions of 45 nm × 20 nm × 20 nm with the longest axis normal to the parent austenite boundary was

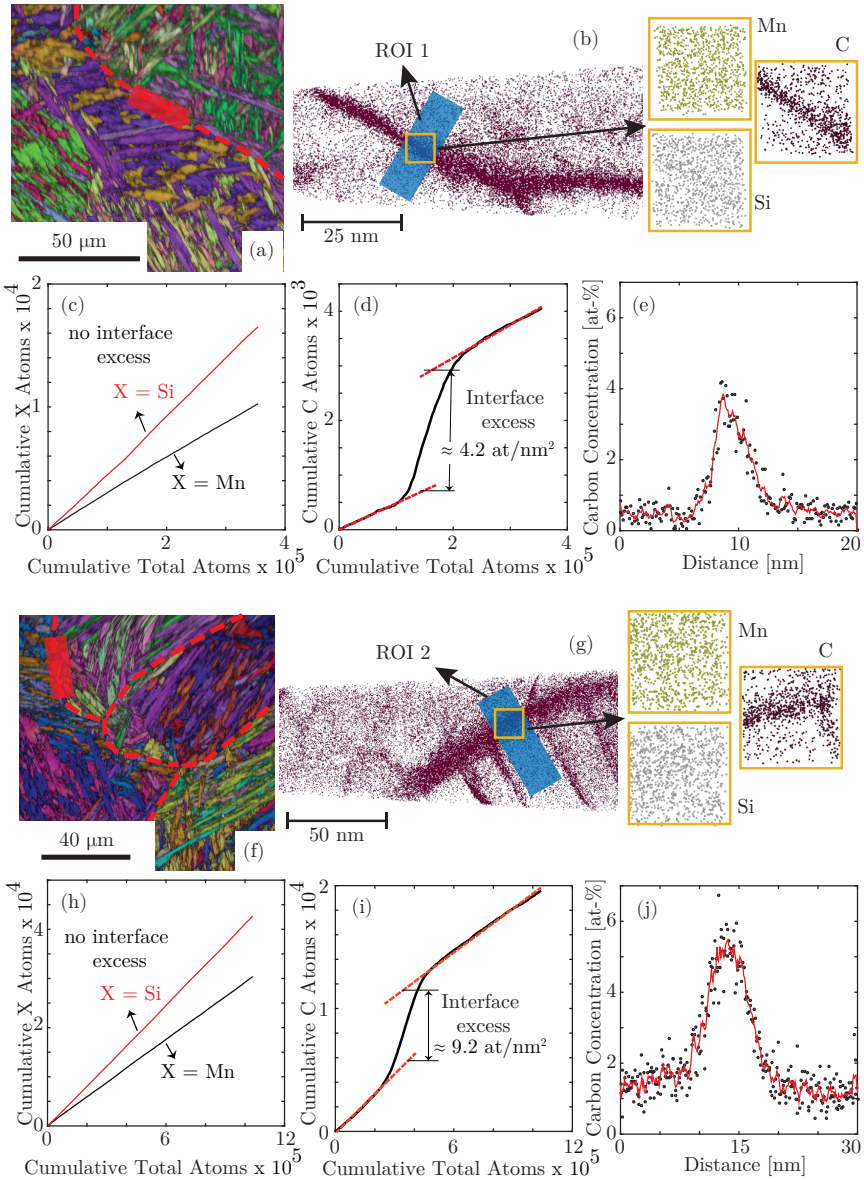

Figure 5.6: APT results in samples which were directly quenched from 400 °C without any holding at this temperature. Figures (a)-(e) show the results in samples without any prior intermediate soaking treatment while Figures (f)-(j) show the results in samples with a prior intermediate soaking treatment at 800 °C for 30 min. (a) and (f) give the combined inverse pole figure and image quality map showing the prior austenite boundary (red dashed line) used for atom probe tips lift-out (red shaded rectangles). (b) and (g) give the reconstructed APT image showing overall C distribution along with atom maps of elements near the grain boundary regions (yellow squares). Blue shaded regions in the vicinity of the grain boundaries indicate the ROIs used to calculate the local compositional variations. (c) and (h) provide the ladder GIE plot of Mn and Si in ROI 1 and ROI 2 respectively whereas (d) and (i) show the ladder GIE plot of C in ROI 1 and ROI 2 respectively. (e) and (j) provide the carbon distribution across the grain boundary in ROI 1 and ROI 2 respectively. Dots shows the actual amount of carbon while red line shows the smoothed trend. The analysis for the ladder plot calculation and carbon distribution was carried out perpendicular to the respective grain boundary.

chosen. The elemental distributions in and around the ROI are shown in Figure 5.6(b) and Figure 5.6(g). Based on the elemental distribution, Gibbs Interface Excess (GIE) plots were calculated within the ROI (Figure 5.6(c)-(d) and Figure 5.6(h)-(i)). GIE plots give the number of atoms of a given element as compared to the total number of atoms within the volume of the ROI along its longest axis [23]. The slope of the GIE plot represents the concentration of a given atom along the length of the ROI. It is evident that the GIE plot would be linear if there is no difference in composition along the length of the ROI and the slope of the GIE plot will be a constant. A change in slope indicates a difference in elemental distribution along the ROI.

APT results show no signs of segregation of Mn and Si to the parent austenite grain boundaries prior to bainite formation irrespective of the use of intermediate soaking during the heat treatments. Unlike Mn and Si, Figure 5.6(d) and Figure 5.6(i) shows that carbon segregation to austenite boundaries prior to bainite formation does occur. Based on the APT results, the degree of carbon segregation to the austenite grain boundaries is observed to be higher when an intermediate soaking treatment is employed. Using the GIE plots, the interfacial carbon excess at the prior austenite grain boundaries after the intermediate soaking treatment at 800 °C for 30 min is measured to be 9.2 atoms per nm^2 while the interfacial carbon excess at the prior austenite boundaries without any intermediate soaking is 4.2 atoms per nm^2. The interfacial carbon excess was calculated using the procedure described in [23].

It is important to point out that further statistical data regarding such carbon segregation as a result of intermediate soaking treatment would strengthen the argument, but could unfortunately not be achieved during this work. Moreover, Herbig et al. [24] noted that the crystallography of the grain boundaries has an effect on the degree of carbon segregation. Thus, it is important to confirm if the observed carbon segregation is a result of the character of the grain boundaries or the intermediate soaking treatment. However, as pointed out in the experimental section, all the parent austenite boundaries used for site-specific APT analysis in this work are high angle grain boundaries and have a misorientation angle between 40° - 45°. Such a criterion for site selection for APT studies was adopted to alleviate the effects of the character of grain boundaries on carbon segregation.

APT studies do not reveal any ferrite growth along the parent austenite grain boundaries at 800 °C. It should be noted that the low solubility of carbon in ferrite would have been highlighted in the APT results if ferritic regions were present during

APT studies. It can be seen in Figure 5.6 that the carbon concentration on either side of parent austenite grain boundaries is about 0.92 at%, which is equal to the bulk carbon concentration of the steel. This indicates the presence of martensite which is expected to form upon cooling without any bainite formation. (Figure 5.6(e) and Figure 5.6(j)). This is consistent with the dilatometer and microstructural results seen above.

5.3. Discussion

Based on the results illustrated in the above sections, in-depth inferences regarding the effect of overall heat treatment on rate of bainite formation can be derived.

5.3.1. Bainite formation kinetics

The results described in Section 5.2.1 clearly show that the use of an intermediate soaking treatment prior to isothermal bainite treatment leads to an acceleration of bainite formation kinetics. In order to understand these results further, the underlying rate determining factors are explored in this section. The influence of intermediate soaking treatment at 600 °C and 800 °C on these underlying factors is discussed in Section 5.3.2 and Section 5.3.3.

The kinetics of bainite formation is dependent on the rate of bainite nucleation [25–27]. In Chapter 3, it was presented that the overall rate of bainite formation, $\mathrm{d}f/\mathrm{d}t$, can be given in terms of rate of bainite nucleation at austenite grain boundaries and rate of autocatalytic bainite nucleation. It should be noted that bainite nucleation typically occurs at available interfaces and the rate of bainite nucleation depends on the type of the interface at which nucleation occurs [26]. With the approach given in Chapter 3, $\mathrm{d}f/\mathrm{d}t$ can be given as

$$\frac{\mathrm{d}f}{\mathrm{d}t} = \kappa_p \left[\exp\left(\frac{-Q_G^*}{kT}\right) + \exp\left(\frac{-Q_A^*}{kT}\right) f \right] \tag{5.2}$$

where k is Boltzmann constant, T is the bainite formation temperature and f is the bainite fraction. Q_G^*, according to [26], gives the activation energy for bainite nucleation at austenite grain boundaries and Q_A^* is the activation energy for autocatalytic bainite nucleation at bainite/austenite (α_b/γ) interfaces. During bainite formation from a completely austenitic matrix, austenite grain boundaries are initially the only available interfaces. As bainite formation progresses, α_b/γ interfaces are created and become available for further bainite formation. However, in the presence of an intermediate annealing treatment involving ferrite formation, bai-

nite nucleation can occur at ferrite/austenite (α/γ) interfaces as well [11]. In such cases, Q_G^* is the effective activation energy for bainite nucleation at any previously existing interfaces of two different characters. The combination of austenite grain boundaries and α/γ interfaces is referred to as previously existing interfaces in this paper. In Equation 5.2, κ_p is the pre-exponential factor and mainly accounts for the influence of the number density of initial nucleation sites, N, available at previously existing interfaces prior to bainite formation. According to [26], κ_p can be given as

$$\kappa_p \propto \frac{kT}{h} N \tag{5.3}$$

where h is Planck constant. N depends on factors such as density of interfaces available and bainite formation temperature. Based on Equation 5.2 and Equation 5.3, the rate of bainite formation under isothermal conditions depends on N, Q_G^* and Q_A^*.

Any influence of the intermediate soaking treatment on Q_A^* can be categorically ruled out due to two reasons. Firstly, Q_A^* affects the rate of bainite formation if bainite nucleation occurs at α_b/γ interfaces. These interfaces are only created during the isothermal treatment at 400 °C and not during any prior treatment. Equation 5.2 shows that Q_A^* is coupled with f which is 0 prior to the isothermal treatment at 400 °C. Secondly, the activation energy for bainite nucleation is dependent on the carbon concentration of austenite matrix in the vicinity of the interface at which the nucleation occurs [26, 28]. APT results show that the intermediate soaking treatment at 800 °C only influences the carbon concentration at austenite grain boundaries while the carbon concentration within the bulk of the austenite remains practically unaffected. Additionally, microstructural results (Section 5.2.2) show that the maximum ferrite fraction formed during the intermediate soaking treatment at 600 °C is around 5%. Although ferrite formation is typically accompanied by carbon enrichment of surrounding austenite, such a low ferrite fraction will not influence the average carbon concentration of austenite significantly. Thus, it can be postulated that the carbon concentration of the austenite near the α_b/γ interfaces, and consequently Q_A^*, would be similar regardless of the intermediate soaking treatment since the initial bulk composition of austenite grain is unaffected by it. This implies that the experimentally observed acceleration of bainite formation kinetics is due to either a decrease in Q_G^* or an increase in N, or both.

In order to understand the influence of Q_G^* and N on the rate of bainite formation, $\mathrm{d}f/\mathrm{d}t$ is computed for various Q_G^* and κ_p values using Equation 5.2 (Figure 5.7). It should be noted that since κ_p is directly proportional to N (Equation 5.3),

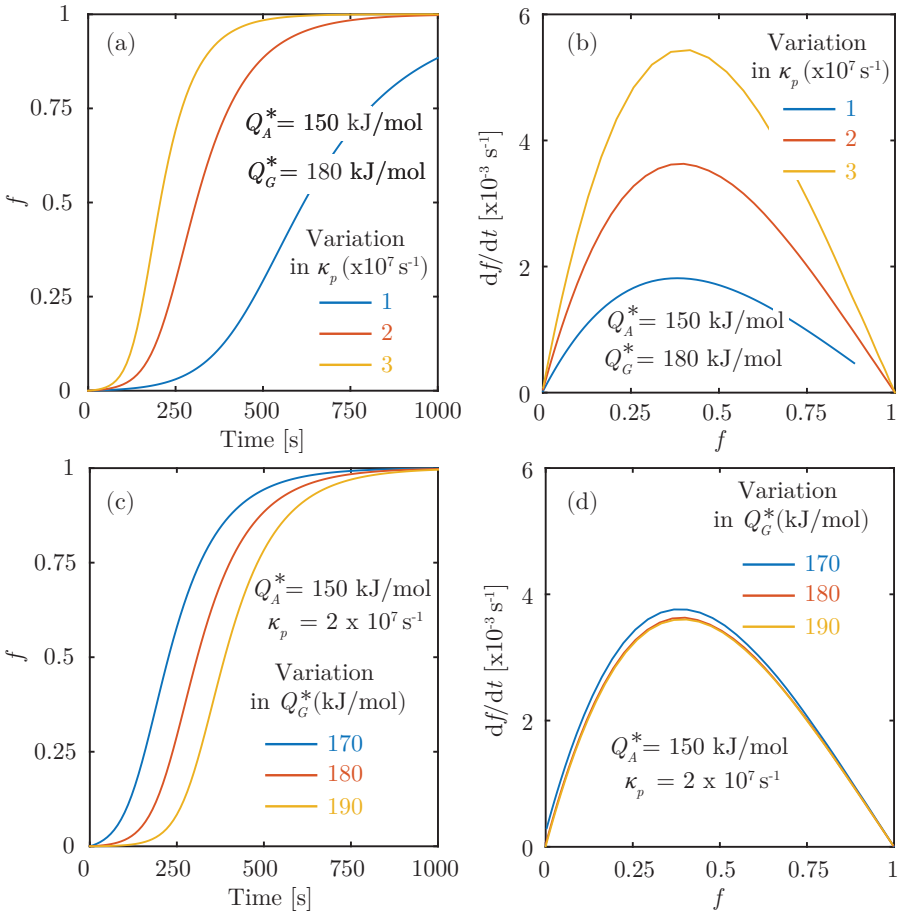

Figure 5.7: Bainite evolution at 400 °C as a function of time with variation in (a) κ_p and (c) Q_G^*. Corresponding $\mathrm{d}f/\mathrm{d}t$ values as a function of bainite fraction, f with variation in (b) κ_p and (d) Q_G^*. Increase in κ_p implies an increase in the number density of bainite nucleation sites.

the effect of κ_p and N on $\mathrm{d}f/\mathrm{d}t$ would be similar. Q_A^* is assumed to be a constant (150 kJ/mol, based on results in literature [26, 29]) in these calculations. This assumption does not affect the conclusions of this work since it does not play a role in accelerating bainite kinetics during the experiments carried out in this work. Using $\mathrm{d}f/\mathrm{d}t$, the bainite evolution over time can be calculated (Figure 5.7). The values for Q_G^* and κ_p are chosen such that the calculated time required for the complete bainite formation is around 750 s - 1000 s. This value is comparable with the experimentally observed time required for the cessation of bainite formation given in Figure 5.2.

Figure 5.7(c) shows that the overall time required for bainite formation decreases as Q_G^* decreases. However, Q_G^* does not have any significant influence on the instantaneous rate of bainite formation as the bainite fraction increases (Figure 5.7(d)). On the other hand, as κ_p (i.e., N) increases, the overall time required for bainite formation decreases (Figure 5.7(a)) and the instantaneous rate of bainite formation increases (Figure 5.7(b)). These trends can be explained by the mechanism of bainite formation. Since bainite formation begins at previously existing interfaces, a reduction in Q_G^* for a constant N implies that the bainite formation begins earlier in time. However, once the bainite formation begins, its formation rate is mainly controlled by nucleation at α_b/γ interfaces where Q_G^* does not play a role. This is highlighted in Figure 5.7(c) and Figure 5.7(d). Unlike Q_G^*, N influences the rate of bainite nucleation at α_b/γ interfaces as well as at austenite grain boundaries and α/γ interfaces. The above discussion suggests that the nucleation at previously existing interfaces is a precursor for autocatalytic nucleation at α_b/γ interfaces. Thus, an increase in N results in the increase of the rate of autocatalytic nucleation as the density of autocatalytic nucleation sites increases. Since N influences both the rate of bainite formation at previous existing interfaces and at α_b/γ interfaces, κ_p affects the instantaneous rate of bainite formation and the overall time required for bainite formation (Figure 5.7(a) and Figure 5.7(b)).

Figure 5.7 can be compared with experimental results observed in Figure 5.2. Experimental results show that the intermediate annealing treatment has an effect on both the overall time required for bainite formation and the instantaneous rate of bainite formation as a function of bainite fraction. This implies that the acceleration of bainite formation kinetics as a result of the applied intermediate annealing treatment is mainly due to the increase in N.

5.3.2. Effect of ferrite growth on bainite kinetics

As observed in Section 5.2, the intermediate soaking treatments sometimes lead to observable ferrite growth while ferrite growth is undetected in other cases. Furthermore, results in Section 5.2.1 clearly show that the rate of bainite formation is influenced to a certain degree by the presence of a prior intermediate soaking treatment regardless of observable ferrite growth. In this section, bainite formation following intermediate soaking treatments which leads to observable ferrite growth is discussed. Additionally, the effect of intermediate soaking treatments on ferrite growth itself is also explored in this section. In Section 5.3.3, bainite formation following intermediate soaking treatments which does not lead to observable ferrite growth is discussed.

The results shown in earlier sections show that ferrite growth is detected only during intermediate soaking treatment at 600 °C with soaking times longer than 10 min. Thermo-calc calculations for the steel composition used in this study suggest that there is a driving force for ferrite formation below 812 °C. However, it must be realized that, although ferrite formation may be thermodynamically feasible, kinetic constraints need to be overcome for ferrite growth to occur. Literature reports suggest that the mode of the austenite to ferrite phase transformation is controlled by the prevailing thermodynamic conditions as well as the diffusivities of the alloying elements [30, 31]. In general, the austenite to ferrite transformation may occur in different ways - (i) with complete redistribution of alloying elements and the austenite and ferrite fraction in full equilibrium (ortho-equilibrium) (ii) with partitioning of substitutional alloying elements (or elements which diffuse slowly) between austenite and ferrite, and the interface in full local equilibrium condition (*Partitioning Local Equilibrium*, PLE); (iii) with negligible partitioning of substitutional alloying elements between austenite and ferrite, and the interface in full local equilibrium condition (*Negligible Partitioning Local Equilibrium*, NPLE) and (iv) without any redistribution of substitutional alloying elements (para-equilibrium) [30].

The mode of austenite to ferrite transformation can be estimated using the equilibrium phase diagram. Figure 5.8 shows the isothermal section (at 600 °C and 800 °C) through the Fe-C-Mn-2 wt% Si phase diagram with NPLE/PLE transition line. It can be seen in Figure 5.8 that for the composition of the steel used in this study, the austenite to ferrite transformation at 600 °C occurs under NPLE conditions while ferrite formation at 800 °C occurs at PLE conditions. Typically, PLE conditions for ferrite growth are characterized by sluggish kinetics due to redistribution of substitutional alloying elements during ferrite growth, while under NPLE con-

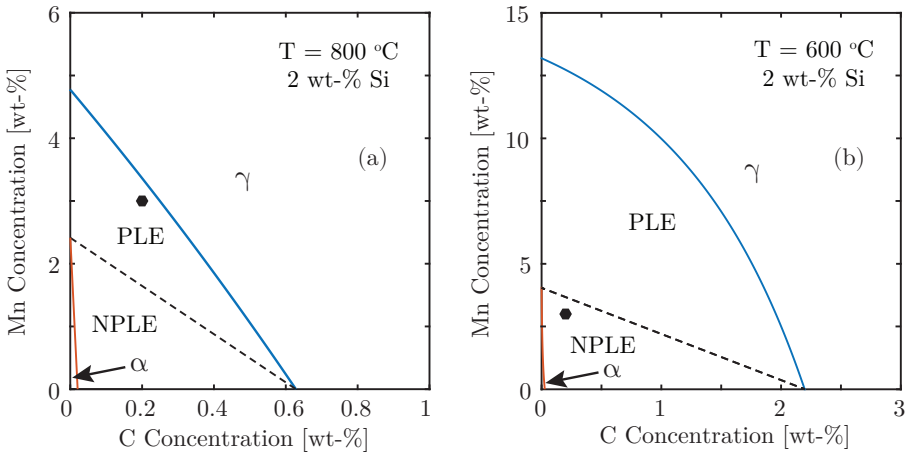

Figure 5.8: Isothermal section through the Fe-C-Mn-2Si phase diagram (a) at 800 °C and (b) at 600 °C. The blue shows the $\gamma/(\alpha+\gamma)$ phase boundary and the red line shows the $\alpha/(\alpha+\gamma)$ phase boundary. The dashed line shows the NPLE/PLE transition in the dual-phase $\alpha+\gamma$ region. The dot gives the composition of the steel used in this study.

ditions ferrite growth is considerably faster. These kinetic restrictions can explain the differences in the fraction of ferrite observed during the intermediate soaking treatment.

In Section 5.3.1, it was derived that the acceleration of bainite formation after an intermediate soaking treatment was due to an increase in number density of initial bainite nucleation sites, N. Ferrite growth prior to bainite treatment has a direct influence on the density of interfaces (consequently, N) available for bainite formation. Ferrite growth leads to the creation of α/γ interfaces. This implies that additional interfaces within the prior austenite grains are created and the total density of interfaces available for bainite nucleation increases.

Zhu et al. reported that the presence of α/γ interfaces retards the kinetics of subsequent bainite formation since the driving force for bainite nucleation at these interfaces is lower than the driving force for bainite nucleation at prior austenite grain boundaries [10]. Such a retarding effect is mainly due to partitioning of carbon into austenite during ferrite growth. Zhu et al. suggested that the partitioning of alloying elements leads to higher elemental concentration near the α/γ interfaces. Additionally, it is evident that the partitioning of carbon into austenite during ferrite formation increases the chemical stability of austenite and thus, the driving force for subsequent bainite formation following ferrite formation during intermediate soaking treatment will be lower. However, the impact of carbon partitioning on

the reduction of the driving force for bainite formation is not significant when the ferrite fraction is small [10], as is the case in the experiments in this work. Quidort et al. [11] postulated that the formation of around 10% of grain boundary ferrite can stimulate subsequent bainite formation.

5.3.3. Carbon segregation and its effect on bainite nucleation sites

During the intermediate soaking treatment at 800 °C as well as at 600 °C for soaking times less than 10 min, experimental results do not show any ferrite growth. However, this cannot be unequivocally claimed as complete absence of ferrite formation during these intermediate soaking treatments, especially since austenite transformation into ferrite is thermodynamically possible at these temperatures. But, based on the experimental results, it can be suggested that if ferrite formation does occur during these soaking treatments, the ferrite grains would be nano-scale in size and they would be sparsely located along the parent austenite grain boundaries. Ferrite grains larger than 100 nm would have been detected during SEM/EBSD analysis. Additionally, if the ferrite grains were not sparsely located, they would have been detected during APT analysis as low carbon regions near parent austenite grain boundaries due to low solubility of carbon in ferrite. Such small and sparsely located ferrite grains will not have any considerable impact on the total density of interfaces. Thus, it can be argued that the acceleration of bainite formation kinetics in the presence of intermediate soaking treatment at 800 °C as well as during intermediate soaking treatment at 600 °C for shorter soaking times is not due to creation of α/γ interfaces, unlike as seen in Section 5.3.2. Under these circumstances, acceleration of bainite formation alludes to a different mechanism in play. This fits well with results given in Figure 5.3 which shows that the rate of acceleration of bainite formation, Γ_{200}, changes when significant ferrite growth is observed during longer prior intermediate soaking treatment at 600 °C.

APT results presented in Section 5.2.3 show that the carbon segregation to austenite grain boundaries is higher when an intermediate soaking treatment is used prior to bainite formation compared to when bainite formation occurs without any intermediate soaking. These results are in line with previously published experimental results [32–34]. Abe et al. carried out a two-step heat treatment in order to understand the segregation behavior of carbon and phosphorus in medium carbon steels [32]. In their study [32], samples were austenized at 1100 °C, followed by isothermal holding at temperatures between 800 °C and 1000 °C for 10 - 1000 seconds. The samples were then cooled to room temperature. Such a treatment is

similar to the austenitization and intermediate soaking treatment (Figure 5.1(b)) used in this study. Abe et al. also observed that the use of a step treatment (or intermediate soaking treatment) led to increased carbon segregation at the austenite grain boundaries compared to samples directly cooled from the austenitization temperature (which would be the starting condition for bainite formation without intermediate soaking treatment) [32]. These results compare well with results presented in this work. In addition, Abe et al. suggested that the degree of carbon segregation during the intermediate soaking treatment increases with increasing holding time as well as with decreasing intermediate soaking temperature [32]. The role of such an increased carbon segregation to austenite grain boundaries as a result of intermediate soaking treatment in accelerating subsequent bainite formation kinetics can be explained using the discussion below.

Several previously published studies have hypothesized that solute segregation to grain boundaries during isothermal holding can lead to solute-rich and solute-poor areas within the austenite matrix [33–36]. Kang et al. studied the distribution of carbon near the vicinity of the austenite grain boundaries after short isothermal holding at 300 °C in several high carbon steels [33]. They observed that the isothermal holding led to carbon enrichment of the austenite grain boundaries as well as to the creation of carbon-depleted zones in near vicinity of the austenite grain boundary (upto a distance of 200 nm from the grain boundary) [33]. In a separate study, Zhang et al. reported similar results [34]. These results are in good agreement with the APT results presented in this work which show that intermediate soaking treatment (which is an isothermal holding step at an elevated temperature) leads to carbon segregation in the vicinity of austenite grain boundaries. Furthermore, comparing the published results in [33, 34] with the APT results observed in this study, it can be postulated that the increased carbon segregation during intermediate soaking treatment would consequently lead to similar carbon-rich and carbon-poor areas. Kang et al. suggest that the formation of carbon-rich and carbon-poor areas during isothermal holding is a result of stress fields associated with the dislocations and grain boundaries [33]. Kang et al. argue that clustering of carbon atoms occurs within the tensile zones near the dislocations and grain boundaries and carbon depletion occurs in the regions under compressive stress during isothermal holding [33]. The formation of carbon-rich and carbon-poor areas is referred to as pre-bainitic phenomenon by Kang et al. Furthermore, it is suggested that the low-carbon regions assist in the bainite nucleation process since the driving force for bainite formation increases with decrease in the carbon concentration of the austenite matrix. How-

ever, Bhadeshia argues that the formation of carbon-depleted regions does not affect the kinetics of bainite formation since an equal number of carbon-rich regions would be created in the process which would counter-balance the effects of carbon-poor areas [22]. The longevity and thickness of carbon-depleted regions observed has also been questioned by certain researchers [36, 37]. As mentioned previously, carbon segregation to austenite grain boundaries occurs in order to reduce their interfacial free energy [13]. Aaronson et al. argue that carbon-depleted regions in the immediate vicinity of austenite grain boundaries would exist only for a limited time until the chemical potential of carbon in the austenite grain boundary is the same as in the bulk [36]. Using the McLean model for kinetics of solute segregation [38], Umemoto et al. estimate that the carbon segregation to austenite grain boundaries should be instantaneous due to the high diffusion rate of carbon and near equilibrium segregation is expected to be achieved even during quenching [3]. Therefore in order to explain results seen by Kang et al. [33], Aaronson et al. [36] suggest that presence of extensively carbon-enriched regions and corresponding depleted regions during isothermal holding is indicative of austenite decomposition into phases with low carbon solubility, for instance ferrite.

The above hypothesis from Aaronson et al. [36] fits the experimental results observed in this study and forms the basis for the theory explaining the observation of accelerated bainite kinetics as a result of intermediate soaking treatment. It can be argued that carbon segregation to austenite grain boundaries leads to fluctuations in carbon composition in its vicinity. These carbon fluctuations can result in the formation of stable ferrite nuclei during the intermediate soaking treatment especially since there is a driving force for ferrite formation at the soaking temperatures used in this study. However, kinetic constraints as seen in Section 5.3.2 will restrict the diffusional growth of these ferrite grains. If the intermediate soaking treatment already leads to body-centered cubic (BCC) ferrite nuclei with low carbon content in the vicinity of the austenite grain boundaries which grow into bainite once the isothermal bainite formation temperature is reached, the initiation time for bainite formation via grain-boundary nucleation is reduced. This leads to acceleration of bainite kinetics. It can be argued that, during intermediate soaking treatment, the number of BCC ferrite nuclei increases with increasing soaking time and with decreasing soaking temperature (since chemical driving force for austenite to ferrite transformation increases).

The above discussion explains the results observed in Figure 5.3, which shows that the rate of bainite formation increases with increasing soaking time in the

presence of an intermediate soaking treatment at 800 °C where no austenite to ferrite formation is detected. Additionally, the rate of bainite formation increases at a much higher rate in the presence of an intermediate soaking treatment at 600 °C when short soaking times are used. However, during longer soaking times at 600 °C, the BCC nuclei would grow to form ferrite rendering the nuclei formed during the intermediate soaking treatment unavailable for subsequent bainite formation. Under such circumstances, the rate of bainite formation is controlled by the increase in total density of interfaces as a result of formation of α/γ interfaces. It should be further pointed out that an increase in the number of BCC ferrite nuclei directly increases N which was determined as the primary rate controlling factor in Section 5.3.1.

During the experiments carried out in this work, the carbon-poor areas were not detected. However, it must be pointed out that these are difficult to detect via APT measurements since fast cooling to room temperature after intermediate soaking treatment leads to martensite formation in the low carbon steel used in this study. This leads to additional interfaces and defects within the austenite matrix into which carbon segregation can further occur. Additionally, if ferrite nuclei form during the intermediate soaking treatment, their location would be difficult to isolate. It must be noted that, due to the composition of the steels in the studies of Kang et al. [33] and Zhang et al. [34], the room temperature microstructure obtained after a short isothermal holding at an elevated temperature and quenching is entirely austenitic. However, in the present study the carbon-rich areas along the austenite grain boundaries due to carbon segregation are immediately visible (Figure 5.6) which can be extrapolated as indirect evidence for the fluctuation of carbon composition in the vicinity of austenite grain boundaries (bainitic nucleation sites) during intermediate soaking treatment.

Based on the evidence presented here, it can be postulated that carbon segregation during intermediate soaking treatment plays a role in the rate of subsequent bainite formation. Typically, without any intermediate soaking treatment, carbon segregation would occur at the bainite formation temperature. An intermediate soaking treatment assists to start the primary stages of bainite nucleation, and thus reducing the time required for overall bainite formation during subsequent treatment.

5.4. Conclusions

The effect of different heat treatment routes on the rate of bainite formation has been studied in this work with the help of a customized set of heat treatments. The

results of this work show that the rate of bainite formation in low-carbon steels can be accelerated mainly via two mechanisms.

A small fraction of ferrite (less than 5%) formed prior to bainite formation increases the number density of interfaces available for bainite nucleation and consequently, leads to an increase in the rate of bainite formation. It is important to note that the rate of bainite formation increases only as long as the nucleation rate increases which is when the fraction of ferrite formed prior to bainite formation is small. As the fraction of ferrite formed increases, the activation energy for subsequent bainite formation increases due to elemental partitioning from ferrite to austenite and this, in extreme cases, can slow down the kinetics of the bainite formation. Furthermore, a short isothermal holding between the bainite formation and austenitization temperatures leads to increased carbon segregation to austenite grain boundaries prior to the start of bainite formation as compared to bainite formation without such treatment. The increased carbon segregation plays an important role in the acceleration of bainite kinetics as well.

Based on the results obtained, it can be further hypothesized that the rate of bainite formation can be manipulated by controlling the overall heat treatment route. In this study, intermediate soaking treatments are used for acceleration of bainite formation. Another energy-efficient route for introducing secondary nucleation sites is via appropriately choosing the austenitization temperature or a proper cooling rate. For instance, an austenitization temperature just below the A_{c3} temperature would create both the primary nucleation sites (austenite grain boundaries) and the secondary interfaces (α/γ interfaces) in the same heat treatment step. Such an austenitization temperature would automatically lead to an almost fully austenitic matrix with a minute fraction of ferrite at the interfaces. The small fraction of ferrite nestled within the austenite matrix would not affect the chemical composition of the austenite matrix for subsequent bainite formation. Furthermore, a tailored cooling rate can influence the carbon segregation at austenite grain boundaries as well as austenite decomposition into ferrite.

References

[1] C. Garcia-Mateo, F. Caballero, H. Bhadeshia, *ISIJ International* **43**, 1821 (2003).

[2] T. Sourmail, V. Smanio, *Acta Materialia* **61**, 2639 (2013).

[3] M. Umemoto, K. Horiuchi, I. Tamura, *Transactions ISIJ* **22**, 854 (1982).

[4] S.-J. Lee, J.-S. Park, Y.-K. Lee, *Scripta Materialia* **59**, 87 (2008).

[5] F. Hu, P. Hodgson, K. Wu, *Materials Letters* **122**, 240 (2014).

[6] G. Xu, F. Liu, L. Wang, H. Hu, *Scripta Materialia* **68**, 833 (2013).

[7] H. Vetters, J. Dong, H. Bornas, F. Hoffmann, H.-W. Zoch, *International Journal of Materials Research* **97**, 1432 (2006).

[8] A. Navarro-López, J. Sietsma, M. Santofimia, *Metallurgical and Materials Transactions A* **47**, 1028 (2016).

[9] H. Kawata, M. Takahashi, K. Hayashi, N. Sugiura, N. Yoshinaga, *THERMEC 2009* (Trans Tech Publications, 2010), vol. 638 of *Materials Science Forum*, pp. 3307–3312.

[10] K. Zhu, H. Chen, J.-P. Masse, O. Bouaziz, G. Gachet, *Acta Materialia* **61**, 6025 (2013).

[11] D. Quidort, Y. Bréchet, *Acta Materialia* **49**, 4161 (2001).

[12] M. Umemoto, T. Furuhara, I. Tamura, *Acta Metallurgica* **34**, 2235 (1986).

[13] D. Raabe, M. Herbig, S. Sandlöbes, Y. Li, D. Tytko, M. Kuzmina, D. Ponge, P.-P. Choi, *Current Opinion in Solid State and Materials Science* **18**, 253 (2014).

[14] Y. Li, D. Ponge, P. Choi, D. Raabe, *Ultramicroscopy* **159, Part 2**, 240 (2015).

[15] Y. Li, D. Ponge, P. Choi, D. Raabe, *Scripta Materialia* **96**, 13 (2015).

[16] M. Herbig, M. Kuzmina, C. Haase, R. Marceau, I. Gutierrez-Urrutia, D. Haley, D. Molodov, P. Choi, D. Raabe, *Acta Materialia* **83**, 37 (2015).

[17] C. Cayron, *Journal of Applied Crystallography* **40**, 1183 (2007).

[18] K. Thompson, J. Sebastian, S. Gerstl, *Ultramicroscopy* **107**, 124 (2007).

[19] S. Suram, K. Rajan, *Ultramicroscopy* **132**, 136 (2013).

[20] A. Matsuzaki, H. Bhadeshia, *Materials Science and Technology* **15**, 518 (1999).

[21] Y. Xu, G. Xu, X. Mao, G. Zhao, S. Bao, *Metals* **7** (2017).

[22] H. Bhadeshia, *Bainite in Steels: Theory and Practice* (Maney Publishing, 2015), third edn.

[23] B. Krakauer, D. Seidman, *Phys. Rev. B* **48**, 6724 (1993).

[24] M. Herbig, D. Raabe, Y. Li, P. Choi, S. Zaefferer, S. Goto, *Phys. Rev. Lett.* **112**, 126103 (2014).

[25] H. Bhadeshia, *Journal de Physique* **43**, 443 (1982).

[26] A. Ravi, J. Sietsma, M. Santofimia, *Acta Materialia* **105**, 155 (2016).

[27] M. Santofimia, F. Caballero, C. Capdevila, C. Garcia-Mateo, C. de Andres, *Materials Transactions* **47**, 1492 (2006).

[28] S. van Bohemen, *Metallurgical and Materials Transactions A* **41**, 285 (2010).

[29] M. Kang, M.-X. Zhang, F. Liu, M. Zhu, *Materials Transactions* **50**, 123 (2009).

[30] H. Farahani, W. Xu, S. van der Zwaag, *Metallurgical and Materials Transactions A* **46**, 4978 (2015).

[31] Z.-Q. Liu, G. Miyamoto, Z.-G. Yang, T. Furuhara, *Acta Materialia* **61**, 3120 (2013).

[32] T. Abe, K. Tsukada, H. Tagawa, I. Kozasu, *ISIJ International* **30**, 444 (1990).

[33] M. Kang, Y. Yang, Q. Wei, Q. Yang, X. Meng, *Metallurgical and Materials Transactions A* **25**, 1941 (1994).

[34] M.-X. Zhang, P. Kelly, *Materials Characterization* **40**, 159 (1998).

[35] K. Tsuzaki, K. Fujiwara, T. Maki, *Materials Transactions, JIM* **32**, 667 (1991).

[36] H. Aaronson, J. Hirth, *Scripta Metallurgica et Materialia* **33**, 347 (1995).

[37] H. Aaronson, G. Shiflet, *Materials Characterization* **54**, 177 (2005).

[38] P. Lejcek, *Grain Boundary Segregation in Metals* (Springer-Verlag Berlin Heidelberg, 2010).

6

The role of grain-boundary cementite during bainite formation

"We rely on sight to confirm the existence of things.
So how do we know that No-see-ums exist?
Verification is ruled out by definition.
It's an ontological quandary".

Calvin

"Hold still a moment."

Hobbes

"Ooh, I itch."

Calvin

"Glad I could help."

Hobbes

The contents of this chapter have been submitted for publication in Scripta Materialia under the title 'The role of grain-boundary cementite during bainite formation in high-carbon steels'.

The thickness of bainitic laths depends on the bainite formation temperature and they tend to become finer as the transformation temperature decreases [1–3]. This implies that low-temperature austenite to bainite transformation leads to highly grain refined microstructures resulting steel grades with improved strength and toughness properties [2, 4]. The lowering of austenite to bainite transformation temperature, however, leads to extremely slow bainite formation kinetics, especially in high carbon steels with total transformation times ranging from few hours to over several days [5, 6]. Therefore, in order to fully utilize the potential of bainite formation at low-temperatures in an efficient manner, it is important to develop strategies to accelerate the low-temperature bainite formation kinetics. In Chapter 4, the effect of previously formed martensite on the rate of bainite formation was discussed while in Chapter 5, the effect of ferrite formation on the rate of subsequent bainite formation was discussed. In case of high-carbon steels, the strategies discussed in Chapter 4 and Chapter 5 pose certain challenges. The formation of grain-boundary ferrite is thermodynamically not feasible in high-carbon steels. Additionally, bainite formation in the presence of pre-existing martensite is typically carried out at temperatures higher than the quenching temperature required to form an initial martensite fraction. This implies that an additional heating step is necessary [7, 8] which may be hard to achieve in industrial lines [6]. Furthermore, compared to a fully bainitic microstructure, mechanical properties of martensite/bainite microstructures can be vastly different [9, 10] if the morphology and distribution of bainite is markedly different from that of the surrounding martensite [9].

In this work, an alternative strategy based on the decoration of austenite grain boundaries (γ/γ interfaces) with cementite precipitates is proposed for the acceleration of bainite formation kinetics in high-carbon steels. Such a strategy results in an almost fully bainitic microstructure without any need of additional heat treatment steps. Although large networks of grain-boundary cementite can act as crack initiation and propagation sites [11], published results suggest that small isolated regions of grain-boundary cementite are not detrimental to the mechanical properties [12]. In this work, it is observed that a small fraction of isolated cementite precipitates can increase the rate of subsequent bainite formation significantly. The fundamental reasons behind such a trend are also discussed in this work.

6.1. Experiments

The composition of the high-carbon steel used in the present work is given in Table 6.1. The kinetics of bainite formation and the effect of grain-boundary cementite

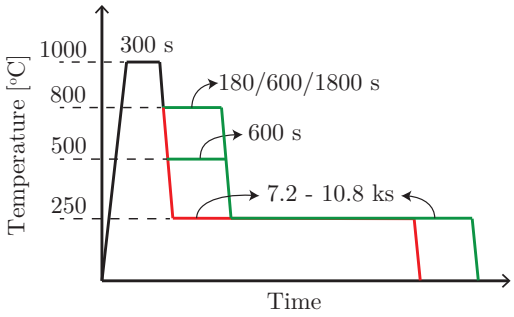

Figure 6.1: Schematic of heat treatment profiles used for understanding the effect of grain-boundary cementite precipitation on bainite formation kinetics. The heating rate used during the heat treatments is 5 °C/s while the all cooling steps are carried out at -40 °C/s.

Table 6.1: Chemical compositions of steels used for study (values in wt%).

C	Mn	Si	Cr	Cu	Mo	Ni	V
1.05	0.274	0.278	1.67	0.030	0.012	0.042	0.016

on the rate of bainite formation was studied with the help of a Bähr DIL805A/D dilatometer. Dilatometer samples with dimensions of 10 mm × 4 mm × 2 mm were used in this study. The samples were first fully austenized at 1000 °C for 5 min. The bainite formation treatment was carried out at 250 °C. The samples were held isothermally at this temperature for 2-3 hours. It should be noted that the A_{c3} temperature is estimated to be 927 °C based on Thermo-Calc calculations while the experimentally determined M_s temperature is approximately 150 °C. Similar to the experiments in Chapter 5, some samples were isothermally treated at different intermediate temperatures for different soaking times prior to bainite formation treatment. The intermediate temperatures were chosen such that the austenite grain boundary could be decorated with a small fraction of cementite based on Thermo-Calc calculations. The time-temperature parameters used during various heat treatments are given in Figure 6.1. During the heat treatments, all heating steps were carried out at a constant heating rate of 5 °C/s while all the cooling steps were performed at -40 °C/s. In order to understand the obtained dilatometer results, a detailed microstructural study of all heat treated samples was carried out. The samples were etched using 2% Nital solution to reveal the microstructure and studied using optical microscopy and scanning electron microscopy (SEM) techniques.

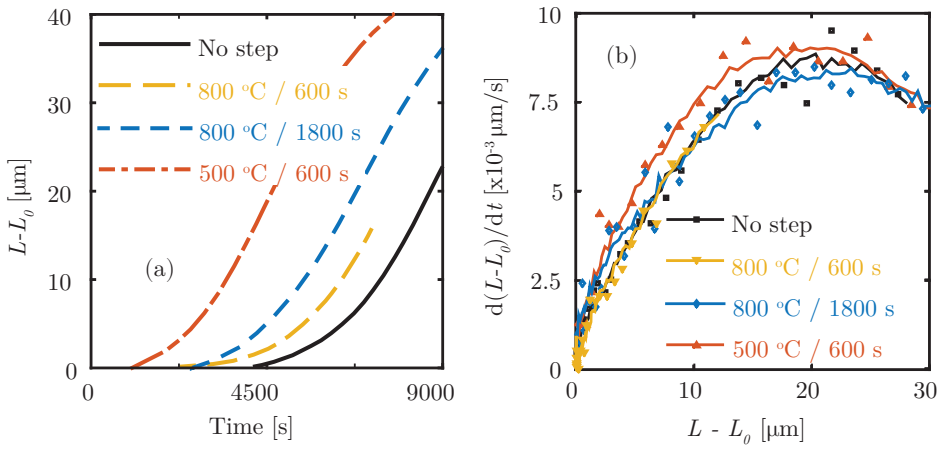

Figure 6.2: (a) Bainite evolution obtained via different heat treatment routes represented in terms of change in length of the sample during isothermal holding at 250 °C. (b) Corresponding rate of change of length of sample as a function of sample expansion during isothermal holding at 250 °C. No step refers to the heat treatment where intermediate soaking was not applied prior to bainite formation. The rest of the curves were obtained after an intermediate soaking treatment was employed. The time and temperature of the intermediate soaking treatment is mentioned in the legend. In (b), the dots give the experimental data points while the line gives the smoothed average of the experimental data points.

6.2. Results and discussion

The kinetics of bainite formation during the different heat treatments are compiled in Figure 6.2. In Figure 6.2(a), bainite formation as a function of time is represented in terms of change in length of the sample as a function of time during the isothermal holding at 250 °C. Similar procedures for evaluating the kinetics of bainite formation have been used by previously published reports [13, 14] as well as in Chapter 5.

Figure 6.2(a) shows that the bainite formation is accelerated when a prior intermediate soaking treatment is applied. Moreover, the degree of acceleration of bainite formation can be observed to increase as the intermediate soaking treatment temperature decreases. Similarly, the time required for bainite formation at 250 °C also decreases as holding time during the intermediate soaking treatment increases. This is similar to the results seen in Chapter 5 in the case of low-carbon steels.

Figure 6.2(b) shows the rate of change of the dilatometer sample length as a function of change in sample length during bainite formation at 250 °C after various intermediate soaking conditions. Since the change in length of the sample represents the volume fraction of bainite formed, Figure 6.2(b) essentially gives the rate of

bainite formation as the bainite fraction increases. It is interesting to see that, although the overall time for bainite formation decreases when an intermediate soaking treatment is employed, the instantaneous rate of bainite formation as a function of bainite evolution is nearly similar in all cases. This implies that the overall time required for bainite formation after an intermediate soaking treatment is lower since the onset of bainite formation takes place earlier in time compared to when bainite forms without an intermediate soaking treatment. However, after the transformation has begun, the bainite formation rate is similar in all cases.

Figure 6.3 shows the results obtained from the microstructural studies. Figure 6.3(a) shows that a lower-bainite and martensite/retained austenite microstructure is obtained after a low-temperature bainite formation treatment at 250 °C without any prior intermediate soaking treatment. It should be noted that the nital etch used to reveal the microstructure selectively etches bainitic regions while fresh martensite and retained austenite remain unetched. Dilatometry results show that the austenite to bainite transformation is not yet completed during the time frame of the experiment (2-3 h isothermal holding at 250 °C) and the residual austenite partially transforms into fresh martensite upon cooling to room temperature. This is evident in the obtained microstructure. Figure 6.3(b) and Figure 6.3(c) show the resultant microstructure when bainite formation is carried out following intermediate soaking treatments for 10 min at 800 °C and 500 °C respectively. These figures also show a lower bainite and martensite/retained austenite microstructure. Additionally, it is observed that the parent austenite grain boundaries are decorated with grain-boundary cementite when an intermediate soaking treatment is used. The fraction of the grain-boundary cementite precipitates is higher when the intermediate soaking treatment is carried out at 500 °C than at 800 °C.

Based on these results, it can be concluded that the grain-boundary cementite formed during the intermediate soaking treatment decreases the time required for the onset of bainite formation and leads to faster overall bainite formation kinetics in high carbon steels. Umemoto et al. also reported that cementite precipitation leads to faster bainite formation kinetics in medium carbon steels [15]. However, they did not indicate if such faster kinetics is result of earlier onset of bainite formation as seen in this work. Additionally, the fundamental reason behind such a trend is not studied in their work. However, understanding the mechanism is essential to effectively use grain-boundary cementite to accelerate bainite formation kinetics. In subsequent paragraphs, the underlying reason behind the decrease in the time required for the onset of bainite formation in the presence of grain-boundary

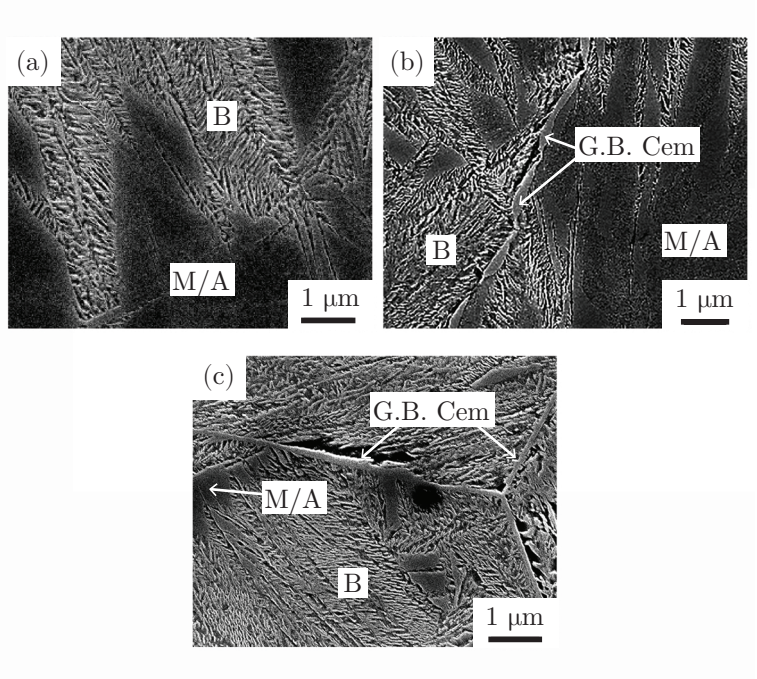

Figure 6.3: SEM micrographs obtained after bainite formation treatment when it is preceded by (a) no intermediate soaking treatment, (b) intermediate soaking treatment at 500 °C for 10 min and (c) intermediate soaking treatment at 800 °C for 10 min. Microstructure studies revealed Bainite (B), Martensite/Retained austenite (M/A) islands and grain-boundary cementite (G.B. Cem) depending on the corresponding treatment route.

cementite is investigated.

The rate of bainite formation depends on the nucleation kinetics of bainite [16, 17] which is determined by the *activation energy required for the nucleation process* and the density of nucleation sites [16–23]. Since bainite nucleation mainly proceeds at interfaces [16, 21], the density of bainite nucleation sites depends on the *density of available interfaces*. Thus, it can be postulated that the acceleration of bainite kinetics due to the formation of grain-boundary cementite can be attributed to one or both of the above mentioned factors (written in italics). The effect of grain-boundary cementite on each of these factors is discussed below.

The *activation energy for bainite nucleation* depends on the chemical conditions at nucleation sites. The precipitation of grain-boundary cementite affects the carbon concentration in the vicinity of the cementite/austenite (θ/γ) interface. Figure 6.4 shows the distribution of carbon during cementite formation in austenite for various times at 800 °C and 500 °C. The carbon profile was calculated using multi-component diffusion simulations performed with DICTRA. 1-D isothermal holding simulations at 800 °C and 500 °C were carried out to replicate the intermediate soaking treatment. A rectangular cell assuming an initial austenite size of 60 µm and a cementite size of 1 nm was used for the simulations. It should be noted that the austenite grain size after the austenitization treatment used in this study was observed to be around 60 µm. Simulations were carried out in a system with a composition identical to the steel composition given in Table 6.1 with the exception of Cu since the exceptionally low solubility of Cu [24] in cementite led to convergence problems. Simulations excluding Cu are not expected to affect the results since studies suggest that Cu does not affect the formation of cementite [24]. Wasynczuk et al. suggest that Cu partitions out of cementite during its formation and precipitates as ϵ-Cu at θ/γ interfaces [24]. Additionally, published results indicate that the θ/γ interface is faceted and Cu precipitates only along the partially coherent and immobile facets of the θ/γ interface [24, 25]. This implies that the Cu precipitation does not impede the migration of mobile regions of θ/γ interfaces and thus the kinetics of cementite precipitation is not influenced by the presence of Cu [24].

Figure 6.4 shows that a higher cementite fraction is formed at 500 °C than at 800 °C. The steep drop in carbon concentration in Figure 6.4 indicates the position of the θ/γ interface, which gives insight into the growth of cementite precipitates during intermediate soaking treatments. It should be noted that during 1-D DICTRA simulations, the thickness of the cemenite given in Figure 6.4 in comparision with the overall size of the simulation cell can be extrapolated as the fraction of cementite

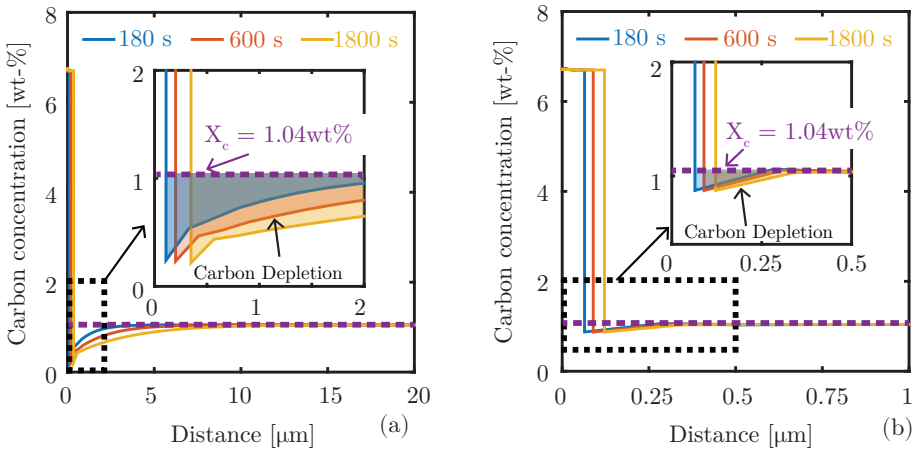

Figure 6.4: Variation in carbon concentration in the vicinity of θ/γ interface as a result of cementite precipitation after isothermal holding at (a) 500 °C and (b) 800 °C for different times based on DICTRA calculations simulating intermediate soaking treatments. Shaded regions indicate the carbon depleted regions. Simulations indicate moving θ/γ interface during the time-scale of the intermediate soaking treatment as well as a higher fraction of cementite formation during intermediate soaking treatment at 500 °C.

formed. These results are in line with the experimental results which suggest a higher fraction of grain-boundary cementite precipitates when the intermediate soaking treatment temperature is lower. Figure 6.4 suggests that cementite precipitates continue to grow within the time scale of the intermediate soaking treatments used in this work. Furthermore, it can be seen in Figure 6.4 that the precipitation of cementite leads to depletion of carbon in the austenite matrix in the vicinity of the θ/γ interface. This trend can be explained by the partitioning growth of carbon-rich cementite which leads to local decrease in carbon concentration in the vicinity of θ/γ interfaces at the austenite front. The activation energy for bainite nucleation depends on the carbon concentration of the austenite matrix and it decreases with decreasing carbon content [21–23]. This implies that the activation energy for bainite nucleation at θ/γ interfaces would be lower than the activation energy for bainite nucleation at γ/γ interfaces without grain-boundary cementite. The increase in the rate of bainite formation with increased fraction of cementite along the γ/γ interfaces as a result of an intermediate soaking treatment at 500 °C compared to 800 °C is also consistent with the above discussion.

Figure 6.2(b) shows that the rate of bainite formation as a function of bainite fraction remains constant regardless of the presence of grain-boundary cementite and the overall acceleration of bainite formation is only due to faster onset of bai-

nite formation as a result of an intermediate soaking treatment (and cementite precipitation). As explained in earlier chapters, bainitic sub-units nucleate and grow initially at already existing interfaces (typically γ/γ interfaces [16, 26] and in this case, θ/γ interfaces as well [27]). This leads to the creation of bainite/austenite (α_b/γ) interfaces. Bainite formation then continues autocatalytically at these newly created α_b/γ interfaces [16, 26]. Figure 6.4 shows that the degree of carbon depletion within the austenite matrix decreases as the distance from the θ/γ interfaces increases. Thus, the activation energy for autocatalytic bainite nucleation, which is dependent on the carbon concentration of austenite in the vicinity of α_b/γ interfaces, would be similar regardless of the presence of grain-boundary cementite during bainite formation. Furthermore, θ/γ interfaces and γ/γ interfaces only assist in the initiation of bainite formation. Upon the onset, bainite formation only occurs autocatalytically. This correlates well with Figure 6.2(b) where the instantaneous rate of bainite formation is similar in the presence and absence of grain-boundary cementite. However, the onset of bainite formation is controlled by the activation energy for bainite nucleation at γ/γ interfaces and θ/γ interfaces. In the presence of θ/γ interfaces, the activation energy for bainite nucleation at these interfaces is lower and thus, the onset of bainite formation is quicker.

As mentioned previously, the rate of bainite formation can be influenced by the *density of interfaces available*. The total density of interfaces present prior to bainite formation depends on both the density of γ/γ interfaces and the density of θ/γ interfaces when bainite formation occurs in the presence of pre-existing grain-boundary cementite. Considering the microstructural evidence, a significant increase in the number density of interfaces due to grain-boundary cementite precipitation is unlikely. Grain-boundary cementite precipitation leads to the creation of θ/γ interfaces. However, during cementite precipitation, it is evident that the γ/γ interfaces would be annihilated. Furthermore, since grain-boundary cementite is precipitated only along the parent austenite grain boundaries and does not grow into the austenite grain (Figure 6.3), it can be envisaged that the newly formed θ/γ interfaces mainly replaces the annihilated γ/γ interfaces. Thus, it can be argued that the overall density of interfaces does not increase with increasing fraction of grain-boundary cementite.

6.3. Conclusions

Summarizing the above results, it can be concluded that grain-boundary cementite precipitation accelerates the kinetics of bainite formation due to faster onset of

bainite formation. Such an acceleration is mainly attributed to the decrease in the activation energy for bainite nucleation at θ/γ interfaces which can be achieved even with a small fraction of grain-boundary cementite. In terms of heat treatment design, controlled grain-boundary cementite precipitation can be achieved even during cooling from the austenitization temperature and thus eliminating the necessity of additional heat treatment steps to accelerate the low-temperature bainite formation kinetics in high-carbon steels.

References

[1] I. Timokhina, H. Beladi, X. Xiong, Y. Adachi, P. Hodgson, *Acta Materialia* **59**, 5511 (2011).

[2] C. Garcia-Mateo, F. Caballero, *ISIJ International* **45**, 1736 (2005).

[3] S. Singh, H. Bhadeshia, *Materials Science and Engineering: A* **245**, 72 (1998).

[4] H. Bhadeshia, *Science and Technology of Advanced Materials* **14**, 014202 (2013).

[5] C. Garcia-Mateo, F. Caballero, H. Bhadeshia, *ISIJ International* **43**, 1821 (2003).

[6] T. Sourmail, V. Smanio, *Acta Materialia* **61**, 2639 (2013).

[7] W. Gong, Y. Tomota, S. Harjo, Y. Su, K. Aizawa, *Acta Materialia* **85**, 243 (2015).

[8] H. Kawata, M. Takahashi, K. Hayashi, N. Sugiura, N. Yoshinaga, *THERMEC 2009* (Trans Tech Publications, 2010), vol. 638 of *Materials Science Forum*, pp. 3307–3312.

[9] Y. Tomita, K. Okabayashi, *Metallurgical Transactions A* **16**, 73 (1985).

[10] P. Abbaszadeh, S. Kheirandish, H. Saghafian, M. Goodarzy, *Materials Research* **21** (2017).

[11] H. Bhadeshia, *Bainite in Steels: Transformations, Microstructure and Properties*, Matsci Series (IOM Communications, 2001).

[12] K. Han, D. Edmonds, G. Smith, *Metallurgical and Materials Transactions A* **32**, 1313 (2001).

[13] A. Matsuzaki, H. Bhadeshia, *Materials Science and Technology* **15**, 518 (1999).

[14] Y. Xu, G. Xu, X. Mao, G. Zhao, S. Bao, *Metals* **7** (2017).

[15] M. Umemoto, T. Furuhara, I. Tamura, *Acta Metallurgica* **34**, 2235 (1986).

[16] M. Santofimia, F. Caballero, C. Capdevila, C. Garcia-Mateo, C. G. de Andres, *Materials Transactions* **47**, 1492 (2006).

[17] H. Bhadeshia, *Journal de Physique* **43**, 443 (1982).

[18] D. Quidort, Y. Bréchet, *ISIJ International* **42**, 1010 (2002).

[19] G. Rees, H. Bhadeshia, *Materials Science and Technology* **8**, 985 (1992).

[20] N. Chester, H. Bhadeshia, *J. Phys. IV France* **07**, 41 (1997).

[21] A. Ravi, J. Sietsma, M. Santofimia, *Acta Materialia* **105**, 155 (2016).

[22] D. Quidort, Y. Bréchet, *Scripta Materialia* **47**, 151 (2002).

[23] S. van Bohemen, *Metallurgical and Materials Transactions A* **41**, 285 (2010).

[24] J. Wasynczuk, R. Fisher, G. Thomas, *Metallurgical Transactions A* **17**, 2163 (1986).

[25] F. Khalid, D. Edmonds, *Metallurgical Transactions A* **24**, 781 (1993).

[26] S. van Bohemen, J. Sietsma, *International Journal of Materials Research* **99**, 739 (2008).

[27] M. Umemoto, K. Horiuchi, I. Tamura, *Transactions ISIJ* **22**, 854 (1982).

7

Conclusions and recommendations

Science is a wonderful thing
if one does not have to earn one's living at it.

Albert Einstein

also if one does...

Jilt Sietsma

The main objective of this doctoral thesis is to understand the fundamental principles governing the kinetics of bainite formation. In this work, the effect of the initial austenite condition on the overall rate of bainite formation in steels is discussed in detail. Additionally, the effect of dynamically evolving austenite matrix as a result of progressive bainite formation on bainite kinetics is also studied. As given in Chapter 1, the studies in this work are carried out assuming that bainite growth occurs under displacive and diffusionless conditions. Based on the various studies compiled in Chapters 3-6, the following conclusions can be derived.

7.1. General conclusions

1. The rate of bainite formation can be well described using the displacive and diffusionless theory. Based on the microstructural evidence, the displacive and diffusionless theory suggests that bainite nucleation occurs at interfaces (Chapter 2). Furthermore, the displacive and diffusionless theory suggests that the rate of bainite nucleation is determined by the nature of the interface at which nucleation occurs and it controls the rate of bainite formation. The experimental results obtained throughout this work are consistent with these underlying phenomena.

2. The rate of bainite nucleation depends on the number density of bainite nucleation sites at a given interface and the activation energy for bainite nucleation at the specific interface (Chapter 3). Bainite formation in a completely austenitic matrix begins at austenite grain boundaries (γ/γ interfaces) and then continues at newly formed bainite/austenite (α_b/γ) interfaces. Using this experimentally observed evidence, a novel physically based kinetic description of bainite formation is developed in this work and validated using various sets of kinetic data. According to this kinetic description, the rate of bainite formation can be expressed as the sum of the rate of bainite nucleation at γ/γ interfaces and the rate of bainite nucleation at α_b/γ interfaces. Such an approach provides a physical basis for understanding the autocatalytic bainite nucleation (nucleation at α_b/γ interfaces).

3. It is noted that the rate of bainite formation process becomes progressively slower as the total fraction of bainite formed increases (Chapter 3). Such a decrease in the bainite formation rate can be attributed to the increase in activation energy for bainite nucleation at both γ/γ interfaces and α_b/γ interfaces. The activation energy for bainite nucleation varies with increasing

bainite fraction due to associated changes in the austenite matrix with respect of carbon concentration of austenite and dislocation density. The experimentally obtained kinetic data indicates that the degree of influence of bainite fraction on the activation energy for bainite nucleation at γ/γ interfaces is lower than its corresponding influence on the activation energy for bainite nucleation at α_b/γ interfaces. It should be pointed out that such trends could be isolated only because of the novel description of the kinetic model proposed in this work using which the effects of nucleation at specific interfaces can be studied separately.

4. In addition to bainite formation within a completely austenitic matrix, the influence of partial decomposed austenite on bainite formation is investigated in this work. Studies given in Chapters 4-6 show that, depending on the type of interface at which bainite nucleation occurs, both the density of nucleation sites and the activation energy for bainite nucleation can be influenced. This understanding of the influence of specific interfaces on overall rate of bainite formation is vital for the efficient development of multi-phase microstructures. Currently available kinetic models only account for the influence of γ/γ and α_b/γ interfaces while calculating the rate of bainite formation. They do not include the effects of other interfaces, such as martensite/austenite (α_m/γ), cementite/austenite (θ/γ) and ferrite/austenite (α/γ) interfaces. Considering its implications in multi-phase microstructure development, a more complete and physically rigorous description to calculate the rate of bainite formation including the effects of other interfaces is essential. In order to tackle this issue, it is proposed that the kinetic description of bainite formation developed in this work can be expanded to include the influence of bainite nucleation at various previously existing interfaces. Chapter 4 gives an insight into the use of the kinetic model developed in this work to understand the influence of martensite/austenite interface on the overall bainite formation kinetics.

5. Results in Chapter 5 indicate that an isothermal holding of a completely austenitic microstructure at a temperature above bainite formation temperature and below A_{c3} without any observable phase transformation followed by a bainite formation treatment leads to an acceleration of bainite kinetics. Such a trend could be attributed to the formation of stable nano-scale ferrite nuclei during the isothermal holding prior to bainite formation. These nuclei grow into bainitic plates once bainite growth is thermodynamically feasible. Further

studies need to be carried out to confirm the presence of the nano-scale ferrite nuclei. These results can potentially open up new avenues for acceleration of bainite formation kinetics via controlling the heat treatment prior to bainite formation.

6. Chapters 4-6 show that the presence of α_m/γ interfaces, θ/γ interfaces and α/γ interfaces prior to bainite formation lead to an acceleration of bainite formation within the scope of the experiments performed. However, the underlying phenomenon determining the kinetics is different in each case. The presence of α_m/γ and α/γ interfaces provide additional nucleation sites for bainite formation to begin. It also affects the rate of autocatalytic bainite nucleation. α_m/γ interfaces have an accelerating effect on bainite formation regardless of density of the interfaces. However in case of α/γ interfaces, it is expected that the rate of bainite formation would decrease as the density of α/γ interfaces increases. It should be noted that the fraction of ferrite (and carbon enrichment of austenite) prior to bainite formation increases along with an increase in the density of α/γ interfaces. In the presence of θ/γ interfaces, the acceleration of bainite formation is due to a decrease in activation energy for bainite formation at θ/γ interfaces. Such a decrease in activation energy is due to formation of low carbon areas in the vicinity of θ/γ interfaces as a result of carbon-partitioning controlled growth of cementite.

7.2. Unresolved issues

One of the major unresolved issues concerning the kinetics of bainite formation which requires immediate attention is related to the "Incomplete Reaction Phenomenon". In Chapter 2, it was discussed that experimental observations during bainite formation show that, depending on the chemical composition of the steels, austenite to bainite formation in steels prematurely halts temporarily, i.e. a transformation stasis occurs, before the entire austenite is consumed. According to the proposition that austenite to bainite formation in steels is a displacive and diffusionless process, $T_0^{'}$ theory is used to describe the incomplete reaction phenomenon. This theory is also used in the proposed kinetic model (Chapter 3) as a thermodynamic condition to determine the termination of bainite formation. As described in Chapter 3 as well as in several already published papers, the end of bainite formation can be well described by the $T_0^{'}$ theory in most cases [1–3]. However, during some in-house experiments carried out during the course of this research work, it is observed that

bainite formation comes to an end even before the thermodynamic limit prescribed by the $T_0^{'}$ theory. Such results are observed mainly when bainite formation is taking place in Fe-0.2C-3Mn-2Si (wt-%) steel at temperatures above 420 °C. Similar results have been observed previously as well [4, 5]. Inaccurate estimations of the transformation stasis can severely compromise the development of a predictive model to describe the kinetics of bainite formation. It also calls into question the validity of the $T_0^{'}$ theory and consequently the principles of displacive and diffusionless mechanism of bainite formation [4].

A possible reason for the observed discrepancies between experimental results and $T_0^{'}$ theory predictions may be related to an improper estimation of carbon distribution within the austenite matrix. According to the $T_0^{'}$ theory, bainite formation would cease if the driving force for bainite growth is below a certain thermodynamic limit [6]. The continuous carbon enrichment of austenite during bainite formation leads to a decrease in the driving force for bainite growth [7]. Experimental observations published in the literature suggest that the carbon distribution within the residual austenite as a result of its carbon enrichment during bainite formation is not uniform [8–10]. However, such a non-uniform distribution of carbon is not accounted for in any of the displacive-theory based kinetic models describing bainite formation published till date in the author's knowledge. Typically, it is assumed that the carbon concentration in austenite is uniform while predicting the achievable bainite fraction based on $T_0^{'}$ theory. Similar assumption is used in this work as well (Chapter 3) where a simple mass balance approach is used to compute the carbon content in residual austenite during bainite formation. However, based on the experimental observations of non-uniform carbon enrichment of austenite [8–10], a mass balance approach would be ineffective. An inhomogeneous carbon distribution would indicate that the carbon enrichment of austenite in the vicinity of at the bainite/austenite interfaces would be much higher compared to the austenite region further away. An indication of local composition variations is observed during the APT analysis shown in Chapter 5. This can significantly affect the driving force for bainite growth at these interfaces and thus, the final volume fraction of bainite.

The effect of strain energy, which is required to accommodate bainite within the austenite matrix, on the driving force for austenite to bainite transformation is another issue to be carefully reviewed. According to published literature, the stored energy of bainite is usually considered to be a constant regardless of the composition of austenite in which bainite formation occurs or the temperature at which the bainite formation occurs. Theoretical considerations suggest that the

strain energy required to accommodate bainite is dependent on the strength of the austenite which would be affected by conditions at which bainite formation takes place. Similar concerns have been raised by other researchers as well [4].

7.3. Possible new lines of investigation

The results obtained in the course of this work opens up possibilities for new lines of investigation. A brief description of these avenues is given below.

1. *Carbon redistribution at interfaces during initial stages of austenite decomposition* – Austenite decomposition into product phases such as ferrite and bainite begins via nucleation of these phases in the vicinity of austenite grain boundaries. Although nucleation of new product phases is one of the fundamental steps during austenite decomposition (or any phase transformation process), a thorough experimental investigation into the mechanism of nucleation is often very difficult due to the size of the nuclei. However, with the advances in atom probe analysis in the recent years, site-specific APT experiments combined with austenite grain boundary character analysis using EBSD technique can be used for an in-depth analysis of ferrite and bainite nucleation mechanism. In Chapter 5, the interfacial carbon composition in the vicinity of austenite interfaces prior to bainite formation was analyzed. This study can be followed up based on the experimental scheme given below to understand the nucleation mechanism during austenite decomposition into bainite. In Chapter 5, APT samples were quenched immediately from bainite formation temperature without any isothermal holding. However, a short isothermal holding at this stage will allow for nucleation of bainite to begin at the austenite grain boundaries. Thus, if samples are quenched after a short isothermal holding with varying holding times, various stages of bainite nucleation at the austenite grain boundaries can be captured. Site-specific APT analysis of the austenite boundaries from these samples would provide insight into the elemental redistribution behaviour during bainite nucleation. It should be noted that since ferrite and bainite have a body centered cubic structure, the solid solubility of carbon within ferrite and bainite is low compared to the solid solution of carbon in austenite. Thus, low carbon regions within the APT samples can be identified as bainite nuclei. If the samples are quenched after a short isothermal holding, it is likely that only a small number of bainite nuclei form during the isothermal holding and the rest of the

austenite fraction transforms into martensite. Moreover, it can be postulated that martensite retains the carbon concentration of the austenite matrix and thus appears as high carbon regions during APT analysis. The EBSD analysis of the austenite grain boundaries would provide information regarding the character of the grain boundary. Based on analysis of both chemical composition and grain boundary character, the ability of specific grain boundary to act as a bainite nucleation site can be determined. Similar experiments can be carried out in the case of ferrite nucleation. Furthermore, based on these studies, the differences and similarities between bainite and ferrite nucleation can be identified. It should however be considered that bainite or ferrite nuclei formed during short isothermal holding at a specific temperature may not be detected via SEM which is typically used to isolate sites for specific analysis. So, multiple random sites from a general austenite boundary must be chosen for APT analysis with the expectation that some may contain the required regions of interest. The existence of nuclei can only be confirmed based on low carbon regions observed during APT analysis. Thus, these experiments have a certain degree of trial and error. But, the results from these studies can be extremely useful in understanding nucleation mechanism of different phases in steels.

2. *Comparison of proposed kinetic model results with results based on diffusional theory of bainite formation* – The kinetic model proposed in this work is developed using the principles of diffusionless and displacive theory for bainite formation. Results in Chapter 3 and Chapter 4 show that the experimentally obtained kinetic data during austenite to bainite formation correlates extremely well with the model calculated kinetics.

   However, as discussed in Chapter 2, a competing theory based on the diffusional mechanism of bainite growth is also proposed in the literature. If it is assumed that bainite does not form according to the displacive and diffusionless theory, it would be interesting to understand the interpretation of the model and the model parameters according to the diffusional theory given the fact that the model calculated kinetics mathematically fit very well to the experimental results. Furthermore, it should be noted that the mathematical description of the kinetic model based on the diffusional approach [11] also uses two separate exponential functions similar to the approach proposed in Chapter 3. This implies that the underlying mathematical description of the kinetic model in both cases is the same and only the interpretation of the

model parameters differs.

3. *Mechanical characterization of bainite microstructures formed via accelerated route* – In Chapters 4-6, different heat treatment strategies to accelerate the bainite formation kinetics in steels are discussed. In order to utilize these strategies, it is important to compare the mechanical properties of bainite microstructures obtained via these heat treatment routes to bainite microstructures obtained via typical routes without any intermediate treatments. Some studies regarding the effect of martensite formation prior to bainite formation on the tensile properties of the final microstructures are already underway. However, the effect of other heat treatment strategies such as ferrite formation or cementite formation prior to bainite formation on the final mechanical properties of the steel should also be studied.

References

[1] F. Caballero, C. Garcia-Mateo, M. Santofimia, M. Miller, C. de Andres, *Acta Materialia* **57**, 8 (2009).

[2] F. Caballero, M. Miller, C. Garcia-Mateo, J. Cornide, *Journal of Alloys and Compounds* **577, Supplement 1**, S626 (2013).

[3] L. Fielding, *Materials Science and Technology* **29**, 383 (2013).

[4] Y. Xia, G. Miyamoto, Z. Yang, C. Zhang, T. Furuhara, *Acta Materialia* **91**, 10 (2015).

[5] H. Chen, K. Zhu, L. Zhao, S. van der Zwaag, *Acta Materialia* **61**, 5458 (2013).

[6] H. Bhadeshia, *Acta Metallurgica* **29**, 1117 (1981).

[7] A. Ravi, J. Sietsma, M. Santofimia, *Acta Materialia* **105**, 155 (2016).

[8] C. Garcia-Mateo, F. Caballero, M. Miller, J. Jimenez, *Journal of Materials Science* **47**, 1004 (2012).

[9] M.-X. Zhang, P. Kelly, *Materials Characterization* **40**, 159 (1998).

[10] Z. Lawrynowicz, *Materials Science and Technology* **18**, 1322 (2002).

[11] D. Quidort, Y. Bréchet, *ISIJ International* **42**, 1010 (2002).

Acknowledgements

The research work compiled in this thesis is a collaborative effort. The author would like to take a moment to acknowledge the people involved in the process. It should be noted that an informal style is used to write the contents of this section. The author believes that such an informal tone is necessary to convey the author's emotions.

Firstly, I whole-heartedly thank Maria and Jilt. They have been absolutely incredible as promotors. They believed in me, supported me, gave me the freedom to develop my own scientific path and pushed me when they felt I could do more. The confidence I have in my abilities as an independent researcher (which is quite high as of today) is a testament to their mentorship.

Secondly, I thank the wonderful researchers who directly contributed to the work presented in this thesis along with my promotors – Michael, Ankit and Alfonso. Your support during the process was phenomenal. I want to specially thank Ankit for pulling off consecutive all-nighters to finish the APT experiments.

I also express my gratitude towards the sponsors of this work. The research leading to the results in the work has received funding from the European Research Council under the European Union's Seventh Framework Programme (FP/2007-2013)/ERC Grant Agreement n. [306292]. I also want to add that Michael acknowledges the funding by the German Federal Ministry of Education and Research (Bundesministerium für Bildung und Forschung) through grant 03SF0535.

I want to give a shout out to Nico, Sander, Kees, Richard and Hans for helping me with my experiments. They have also been great gate-keepers of the experimental/research facilities at TU Delft. I thank Max-Planck-Institut für Eisenforschung in Düsseldorf for letting me use their experimental facilities as well. I also want to thank my colleagues at the MSE department. The entire PhD process would not have been the same if not for the people I interacted with on a daily basis. Pina, Anand, Muru, Gautam, Constantinos, Bij-Na, Xin, Jun, Zaloa, Carola, Javier, Behnam - Thank you. Special thanks to Stefan from TATA Steel as well! The interactions with you during my PhD was extremely helpful.

Finally, I want to express my deepest and sincerest gratitude to the people who have always stood by me - my family and my friends. Some of them deserve a special mention for their part during the PhD process. Prashanth, Wilco, Siddharth and Danilo - thanks for being there. Ann-Sophie - thank you for being my support system. Mythri - thanks for being my biggest cheer leader! Appa and Amma - thank you for everything you have done for me.

Curriculum Vitæ

Ashwath Maniam RAVI

28-05-1988 Born in Palo Alto, California, United States of America.

Education

2005–2009 Bachelors in Metallurgical Engineering
Malaviya National Institute of Technology

2009–2012 European Masters in Materials Science
Universidade de Aveiro
Technische Universität Hamburg
Aalborg Universitet

2013– PhD. Materials Science and Engineering
Technische Universiteit Delft
Thesis: Understanding bainite formation in steels
Promotor: Prof. dr. M.J. Santofimia
Prof. dr. ir. J. Sietsma

Experience

2017– Principal Researcher
TATA Steel Europe

Scholarships

2009 Erasmus Mundus Scholarship awarded by the European Commission

List of Publications

6. **A.M. Ravi**, J. Sietsma, M.J. Santofimia, *The role of grain-boundary cementite during bainite formation in high-carbon steels*, Submitted to Scripta Materialia.

5. **A.M. Ravi**, A. Kumar, M. Herbig, J. Sietsma, M.J. Santofimia, *Impact of austenite grain boundaries and ferrite nucleation on bainite formation in steels*, Submitted to Acta Materialia.

4. **A.M. Ravi**, A. Navarro-López, J. Sietsma, M.J. Santofimia, *Influence of martensite/austenite interfaces on bainite formation in low-alloy steels below M_s*, Submitted to Acta Materialia.

3. **A.M. Ravi**, J. Sietsma, M.J. Santofimia, *Bainite formation kinetics in steels and the dynamic nature of the autocatalytic nucleation process*, Scripta Materialia, **140**, 82-86 (2017).

2. **A.M. Ravi**, J. Sietsma, M.J. Santofimia, *Exploring bainite formation kinetics distinguishing grain-boundary and autocatalytic nucleation in high and low-Si steels*, Acta Materialia, **105**, 155-164 (2016).

1. **A.M. Ravi**, J. Sietsma, M.J. Santofimia, *Effect of prior austenite grain size on bainite formation: Faster or Slower Kinetics?*, Proceedings of the International Conference on Solid-Solid Phase Transformations in Inorganic Materials, (2015).

List of Conferences

4. **A.M. Ravi**, J. Sietsma, M.J. Santofimia, *Bainite formation: Influence of Strain Energy and Chemical Inhomogeneity*, Oral presentation in MSE Congress 2016 - Materials Science and Engineering Congress (2016).

3. **A.M. Ravi**, J. Sietsma, M.J. Santofimia, *Understanding the role of prior austenite grain size in isothermal bainite formation kinetics*, Poster presentation in THERMEC 2016 - International Conference on Processing and Manufacturing of Advanced Materials: Processing, Fabrication, Properties, Application (2016).

2. **A.M. Ravi**, J. Sietsma, M.J. Santofimia, *Isothermal bainite kinetics based on grain boundary nucleation kinetics and autocatalytic nucleation kinetics*, Oral presentation in Euromat 2015 - European Congress and Exhibition on Advanced Materials and Processes (2015).

1. **A.M. Ravi**, J. Sietsma, M.J. Santofimia, *Effect of prior austenite grain size on bainite formation: Faster or Slower Kinetics?*, Poster presentation in PTM 2015 - International Conference on Solid-Solid Phase Transformations in Inorganic Materials, (2015).